Biological evaluation of an L-dideoxy Bicyclic Nucleoside Analogue active against measles virus

A thesis submitted for the degree of Philosophiae Doctor in Cardiff University

by

Rohan Narayan

March 2019

Cardiff School of Pharmacy and Pharmaceutical Sciences

Cardiff University

Abstract

Measles wild-type virus (MeV) is the etiological agent of measles, a highly contagious life-threatening disease. We previously reported that a novel L-chiral dideoxy bicyclic pyrimidine nucleoside analogue ($_{L}$-ddBCNA),hereby named cf2642, inhibited both MeV and vaccinia virus (VACV) infection in vitro, with a structure activity relationship indicating a host target. The aim of this project was to elucidate the mechanism of action by which cf2642 inhibits the MeV life cycle, focusing on endocytosis and particularly macropinocytosis that has recently been demonstrated to be exploited by this virus to gain cell entry.

Initial cytotoxicity analysis of cf2642 in HeLa and Vero cells stably expressing the human Signalling Lymphocyte Activation Molecule (SLAM) receptor for MeV (VeroSLAM) demonstrated cell line dependent toxicity. The drug caused the generalized peripheral scattering of early and late endosomes/lysosomes in both cell lines, but did not affect traffic from the plasma membrane to lysosomes of the fluid phase/macropinocytosis probe dextran. MeV induced syncytia and autophagy in VeroSLAM cells was also inhibited by cf2642, indicating that another cellular target(s) was being affected.

Given that cf2642 may have a cell-target(s), and that MeV and VACV use macropinocytosis as a mode of cell entry, the relationship between these two was tested. MeV stimulated macropinocytosis in VeroSLAM cells and this effect was abrogatedrapidly and completely by cf2642. In an attempt to

mimic the effects of MeV activation of SLAM receptors a non-infectious setting, a SLAM clustering model was developed using anti-SLAM antibodies to cluster these receptors. This caused a significant stimulation in macropinocytosis that was abolished by cf2642. Confocal microscopy highlighted both MeV and SLAM clustering induced effects on actin morphology that were also abrogated by cf2642. A virus entry/spread assay using MeV expressing GFP in combination with time of addition assays highlighted the inhibitory effect of the drug on virus spread and illustrated that a cellular target(s) that was important during the entire virus life cycle was targeted.

Overall, the data indicates that cf2642 renders its antiviral activity by inhibiting MeV spread and possibly virus entry occurring via macropinocytosis. This is postulated to be via a general mechanism on plasma membrane and internal membranes that are critical for the virus life cycle.

Dedicated To

My beloved parents

Harish Govind, Hilda Harish

& sister *Rhea Mary Harish*

Acknowledgements

First and foremost, I would like to sincerely thank my principal supervisor Prof. Arwyn Jones for his unwavering support, motivation and patience throughout the course of my PhD research. I am very grateful for his continuous motivation and immense knowledge in the field of cell biology, which has helped me to complete this research project.

I would also like to thank our collaborator, Dr. Joachim Bugert at the Bundeswehr Institute for Microbiology in Munich, for making his laboratory available for my research work. His expert knowledge in virology, and guidance, especially during the first year of my PhD, has helped me immensely. I also thank Prof. Lothar Zöller and Dr. Heiner von Buttlar for their continuous support, Daniela Friese for her technical assistance, and all other staff and students for making my tenure in Munich, a wonderful experience.

I would like to offer special thanks to late Prof. Chris McGuigan who synthesized the L-ddBCNA cf2642, without which none of this work would have been possible.

I also thank my co-supervisor Dr. Peter Watson and members of his laboratory, whose comments and troubleshooting suggestions during routine group meetings has helped me improvise my research work.

Many thanks to all past and present members of Lab 1.14, namely Dr. Edward Sayers, Dr. Jennifer Wymant, Dr. Hope Dalton, Dr. Lin He, Jared Whitehead and Saeed Tayeb for their support, friendship, technical assistance and most importantly, for being such wonderful colleagues.

Thanks to Prof. Andrea Brancale and his lab members for synthesising and making available the drug cf2642 that was used in my research. I also thank Dr. Fabrizio Pertusati and Dr. Michaela Serpi for their support.

Special thanks to Ser-Cymru Life Science Research Network Wales for funding my PhD project and for being so supportive during the entire course of my studies.

Finally, my deep and sincere gratitude to my family for their unparalleled love and support. Hilda Harish and Rhea Mary Harish, you are the best!

Declaration

This work has not been submitted in substance for any other degree or award at this or any other university or place of learning, nor is being submitted concurrently in candidature for any degree or other award.

Signed (candidate)  ……

Date ……31-03-2019……

STATEMENT 1

This thesis is being submitted in partial fulfilment of the requirements for the degree of PhD.

Signed (candidate)  ……

Date ……31-03-2019……

STATEMENT 2

This thesis is the result of my own independent work/investigation, except where otherwise stated.

Other sources are acknowledged by explicit references. The views expressed are my own.

Signed (candidate)  ……

Date ……31-03-2019……

STATEMENT 3

I hereby give consent for my thesis, if accepted, to be available online in the University's Open Access repository and for inter-library loan, and for the title and summary to be made available to outside organisations.

Signed (candidate)  ……

Date ……31-03-2019……

Table of contents

List of figures and tables

List of figures

List of tables

Abbreviations

1. AMPK- Adenosine monophosphate activated protein kinase
2. ATCC- American Tissue Culture Collection
3. APS- Ammonium Persulphate
4. ATG- Autophagy related
5. BODIPY- boron-dipyrromethene
6. BSA- Bovine Serum Albumin
7. BSC-1 Grivet monkey kidney epithelial cells
8. CD150- Cluster of differentiation 150
9. CD63- Cluster of differentiation 63
10. CME- Clathrin Mediated Endocytosis
11. DAPI- 4′,6-diamidino-2-phenylindole
12. $_{L}$-ddBCNA- dideoxy Bicyclic Nucleoside Analogue with $_{L}$-chirality
13. Dextran488- Dextran Alexa Fluor488
14. DNA- Deoxyribonucleic acid
15. DMSO- Dimethyl sulphoxide
16. DMEM- Dulbecco’s modified Eagle medium
17. DTT- Dithiothreitol
18. EEA1- Early Endosomal Antigen 1
19. EBSS- Earle’s Balanced Salt Solution
20. ER- Endoplasmic reticulum
21. EDTA- Ethylenediaminetetraacetic acid
22. EGF- Epidermal Growth Factor
23. FBS- Fetal Bovine Serum

24. FITC- Fluorescein Isothyocyanate
25. IC_{50}- Half maximal inhibitory concentration
26. EE- Early Endosomes
27. EIPA 5-(N-ethyl-N-isopropyl) amiloride
28. F- Fusion
29. GFP- Green Fluorescent Protein
30. H- Hemagglutinin
31. HSV1/2- Herpes Simplex Virus type1/2
32. IF- Immunofluorescence assay
33. IRGM- Immunity regulated GTPase family M protein
34. LC3B- Microtubule-associated proteins 1A/1B light chain 3B
35. LDL- Low Density Lipoprotein
36. LE- Late Endosomes
37. MeV Ed- Measles vaccine Edmonston strain
38. MeV- Measles virus wild-type strain
39. mTOR- mechanistic target of Rapamycin
40. min- minute
41. MOI- Multiplicity of Infection
42. PAS- pre-autophagosomal structure
43. PI3K- Phosphoinositide 3-kinase
44. PIP3- Phosphatidylinositol (3,4,5)-trisphosphate
45. PBS- Phosphate Buffered Saline
46. PBST- Phosphate Buffered Saline supplemented with 0.025% Tween20
47. pi- Post infection
48. PFU- Plaque Forming Units

49. PFA- Paraformaldehyde
50. PVLR4- Poliovirus receptor-related 4
51. PVDF- Polyvinylidene difluoride
52. RSV- Respiratory Syncytial Virus
53. rpm- Rotations per minute
54. RNA- Ribonucleic acid
55. RK13- Rabbit Kidney epithelial cell line
56. ROI- Region of interest
57. SLAM- Signalling lymphocyte activation molecule
58. SAR- Structure Activity Relationship
59. SSPE- Subacute Sclerosing Panencephalitis
60. TCID50- Median tissue culture infectious dose
61. TEMED- Tetramethylethylenediamine
62. ToA- Time of addition
63. Tf- Transferrin
64. Tfr- Transferrin receptor
65. ULK1- Unc-51-like kinase 1
66. FIP200- Focal adhesion kinase family interacting protein of 200 kDa
67. VACV- Vaccinia virus
68. VeroSLAM- Vero cells expressing the human signalling lymphocytic activation molecule
69. VZV- Varicella zoster virus

Chapter 1 - Introduction

1.1. Background - Summary of previous studies by Dr. Laura Farleigh

Preliminary studies involving the analysis of L-ddBCNA antiviral activity was performed by Dr. Laura Farleigh as part of her PhD research parts of which were pubished in 2014(Farleigh, 20140). A brief summary of her findings is given below.

Initial experiments studying the effects of L-ddBCNA against VACV expressing luciferase demonstrated antiviral activity at an early (2 hr) time point. However, this was not due to the effects on viral entry or early transcription, as demonstrated by experiments using fluorescent VACV particles and *in vitro* virus transcription assays respectively. Time of addition assays showed that L-ddBCNAs inhibited VACV even when added at 8 hr post infection, meaning that a cellular process utilized by the virus during its entire life cycle was being targeted. Further evidence for a cellular target for L-ddBCNAs was provided by cell-range assays wherein varying levels of antiviral activity against VACV and measles virus was observed across a broad range of cell lines tested.

Based on the notion that cell-targeting effects of L-ddBCNAs may not be limited to VACV alone, the activity of these drugs was also tested against a few other enveloped and non-enveloped DNA and RNA viruses namely herpes simplex virus type 1 and 2 (HSV 1/2), adenovirus, measles wild-type strain (MeV) and influenza virus. Antiviral activity was observed only against MeV, which demonstrated that a cellular process that is crucial for both VACV and MeV was being affected.

To assess whether chemical modifications of the drugs has any role in their antiviral activity, a structure activity relationship (SAR) study was done by testing the effects of different L-ddBCNAs against both MeV and VACV. The results demonstrated that the antiviral activity of these compounds was dependent on the length of their lipophilic side chain, and the lead compound cf2642 with a 5 C side chain length inhibited both VACV and MeV at IC_{50} of 0.2 µM and 7.5µM respectively. The SAR study was performed using three different biological assays namely 2 hr VACV luciferase assay, 4 days VACV plaque assay and 48 hr MeV TCID50 (median tissue culture infectious dose) assay and since all these assays involved intracellular transport and membrane trafficking, it was speculated that ddBCNAs was likely affecting cellular membrane compartments crucial for both VACV and MeV.

Treatment with L-ddBCNAs resulted in varying degrees of cytotoxicity across a range of cell lines and the cells remained viable even up to 4 days post treatment if the tissue culture medium was replaced at regular intervals. This was attributed to the fact that L-ddBCNAs resulted in acidic pH of extracellular medium. More importantly, it was shown that the antiviral activity was not the direct result of drug induced cytotoxicity.

Bringing together the findings from this research project, it was hypothesized that the antiviral activity of L-ddBCNAs/cf2642 may be attributed to their cell-targeting activity that in turn affects both VACV and MeV. Since the effect against VACV was observed at an early (2 hr) time point, this was speculated to be a result of effects on early viral DNA transcription sites within cells, or membrane compartments involved therein.

During early stages of virus infection, MeV induces a cellular process called autophagy which in turn leads to syncytia formation. Since L-ddBCNAs/cf2642 inhibited MeV induced syncytia formation, it was hypothesized that the anti-MeV activity could due to effects on autophagy-related membrane compartments (Farleigh, 2014).

1.2. Measles

Measles, one of the most contagious diseases known to man, is caused by infection with MeV. The disease is characterized by fever and a maculopapularrash, often accompanied by cough, coryza and conjunctivitis. MeV is a single-stranded negative-sense RNA virus belonging to the family *Paramyxoviridae*, genus *Morbillivirus*(Yanagi et al., 2006). The long incubation period of 10-14 days and airborne route of transmission allows the virus to infect large populations with high efficiency (Rima and Duprex, 2006).

Despite the overall decrease of measles related deaths between 2000 and 2007 because of efficient vaccination strategies, the disease later reached epidemic proportions in several parts of Europe (Plemper and Snyder, 2009). Measles contributed to an estimated 100,000 deaths globally in 2017, with the highest mortality rate observed among children under the age of five. (Alya Dabbagh, 2018). A 95% vaccination rate within a given population is often required to maintain herd immunity against measles (Farrugia and Quinti, 2018). The recent measles outbreaks in the US during January-April 2019 resulted in a total of 704 positive cases and was mostly associated with unvaccinated U.S residents returning after international travel (Manisha Patel, 2019). In such cases, measles spreads rapidly

among the unvaccinated individuals, resulting in sporadic outbreaks. The lack of a specific antiviral against measles only adds to the problem (Hopkins Tanne, 2019).

1.1.1. Classification

MeV is an enveloped, single-stranded, non-segmented, negative-sense RNA virus belonging to the order *Mononegavirales*, family *Paramyxoviridae* (Yanagi et al., 2006). Members of this group are characterized by their typical pleomorphic morphology when viewed under an electron microscope. The order *Mononegavirales* that also includes other virus families namely *Rhabdoviridae, Bornaviridae and Filoviridae*, includes all non-segmented negative strand RNA viruses.

The family *Paramyxoviridae* is further divided into two subfamilies namely *Pneumovirinae* which includes notable viruses like respiratory syncytial virus (RSV), metapneumovirus, avian pneumovirus; and *Paramyxovirinae*, whichis in turn divided into five different genera. MeV belongs to the genus *Morbillivirus*that also contains animal viruses like canine distemper virus, rinderpest virus and pestes de petits ruminants virus among others. The other genera include the genus *Respirovirus* which includes Sendai virus and human parainfluenza virus types 1 and 3; genus *Rubulavirus*which includes the type speciesmumps virus; genus *Avulavirus*containingavian paramyxoviruses and Newcastle disease virus and finally the genus *Henipah* which includes the Hendra and Nipah viruses which are associated with fatal encephalitis in infected people (Rima and Duprex, 2011a). Among the members of genus *Morbillivirus*, both canine distemper virusand MeV

have high affinity for lymphocytes and can spread rapidly from the lymphoid organs to epithelial cells. This in turn enables these viruses to establish immunosuppression in their hosts, often lasting for years' post infection (Krumm et al., 2014).

1.1.2. Structureand genome organization

MeV is a pleomorphic enveloped virus ranging in size from 100 to 300 nm. The envelope is a lipid bilayer containing the viral transmembrane glycoproteins hemagglutinin (H) and fusion (F) that are derived from host cells upon the release of infectious virions. The H and F proteins together constitute the virus fusion complex. The matrix (M) proteins lies beneath the envelope and the viral negative sense RNA genome is packaged within the particle in the form of a helical nucleocapsid (N). The nucleocapsid is associated with the phosphoprotein (P) and large polymerase protein (L) which together constitute the ribonucleoprotein (RNP) complex. (Fig 1.1) (Bhella et al., 2004). Apart from these six structural proteins, two non-structural proteins namely the V and C proteins are also produced by translation of the P gene at alternate start codons. The 186 amino acid (aa) C protein (MeV-C) is known to aid MeV replication by inhibiting host mediated type-1 interferon responses (Shaffer et al., 2003). In addition, the MeV-C protein has also been implicated in autophagy induction by both Measles vaccine Edmonstonstrain (MeVEd) and MeV(Richetta et al., 2013). The RNA genome is bound by 2649 copies of the N protein, meaning that each N protein associates with exactly six nucleotides (rule of six) of the genomic RNA (Calain and Roux, 1993).

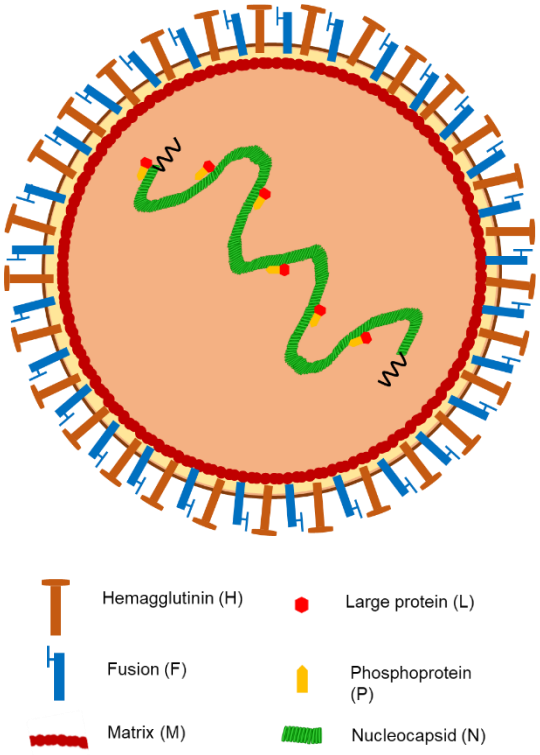

Fig 1.1 Structure of MeV. Measles virus structure showing hemagglutinin and Fusion glycoproteins on their surface and matrix protein within the particle. The helical single stranded RNA genome is bound by the nucleocapsid protein and phosphoprotein. The large polymerase is the RNA dependent RNA polymerase enzyme.

1.1.3. MeV entry

MeV entry into cells occurs via the fusion of virus and the plasma membrane of the host cell. This membrane fusion-mediated virus entry pathway involves interactions between the virus H, F proteins and a specific cellular receptor called SLAM/CD150 (Moss and Griffin, 2012). The virion initially binds to the cell surface via the virus H protein - cell receptor interaction that causes the virus particle to be closely juxtaposed to the cell membrane. This causes the F protein to undergo conformational changes which initiates fusion of the two membranes, resulting in release of the viral RNP complex into the cell.

The F protein is an integral type 1-membrane protein and is a homotrimer. The precursor F0 is first cleaved by the host cell protease furin to form two subunits F1 and F2 that are held together by disulphide bonds. The highly hydrophobic N-terminal region of the F1 subunit protrudes out from the virus envelope and forms the fusion peptide which is in turn inserted into the cell membrane to initiate the fusion process (S.J Flint, 2008). Fusion occurs directly with the plasma membrane at neutral pH and not in endocytic vesicles. This is unlike few other enveloped viruses like Influenza that are known to utilize CME to gain cell entry (Luo, 2012). A direct consequence of MeV fusion process is the formation of multinucleated giant cells, a typical cytopathic effect (CPE) of MeV infection (Yanagi et al., 2006).

In addition to the above mentioned membrane fusion-mediated entry, some research groups have speculated the possibility that MeV may also use a macropinocytosis-like pathway to gain cell entry (Crimeen-Irwin et al., 2003, Frecha et al., 2011). Indeed, two different groups have recently provided experimental evidence to support this (Delpeut et al., 2017)(Goncalves-Carneiro et al., 2017). This is discussed in detail in section 1.4.

Two major cell entry receptors have been identified for measles viruses, CD46 (cluster of differentiation 46) and CD150/SLAM (Signaling Lymphocyte Activation Molecule). MeV-Ed uses the CD46 receptor for cell entry and can also bind to SLAM (Naniche et al., 1993). CD46 is a transmembrane protein that is expressed on all nucleated cells in humans and protect cells from complement mediated lysis by binding to the complement proteins c3b and c4b (Riley-Vargas et al., 2004). On the other hand, MeV can only bind to the CD150/SLAM for entry. SLAM is a member of the immunoglobulin superfamily and is expressed mainly in immature thymocytes, memory T cells, macrophages and mature dendritic cells and mitogen activated B and T lymphocytes. The SLAM receptor is described in details in Section 1.2.1.

MeV also uses a yet another receptor called Nectin4, an adherens junction protein that is expressed on the basolateral side of epithelial cells. Nectin-4 is not used for cell entry but for release/transmission of the virus, mainly because this receptor cannot be accessed by MeV from the apical surface of epithelial cells. Instead, MeV infected lymphocytes or dendritic cells transmits the virus to epithelial cells expressing the Nectin4 receptor, thereby enabling translocation to the airways and transmission via respiratory secretions/droplets (de Vries et al., 2012, Racaniello, 2011). The different types of cellular receptors used by measles viruses are shown in Table 1.1.

Table 1.1 Cellular receptors for measles virus

Receptors	Representative cell type	Comments	References
SLAM/CD150	Activated T and B lymphocytes, mature dendritic cells, macrophages	Used by both MeV and MeV-Ed	(Berger et al., 2010b, Tatsuo et al., 2000)
CD46	Ubiquitous cell surface receptor	Used by MeV-Ed and laboratory adapted MeV strains	(Dorig et al., 1993, Santiago et al., 2010)
Nectin-4/PVLR4 (poliovirus receptor-related 4	Expressed in several tissues including primary airway epithelial cells.	Used by all measles virus strains	(Mühlebach et al., 2011, Noyce and Richardson, 2012a)
C-type lectins: DC-SIGN, Langerin	Dendritic cells and Langerhans cells	Used as attachment receptors for all measles virus strains.	(de Witte et al., 2006, van der Vlist et al., 2011)

Apart from cell entry receptors, MeV also utilize two C-type lectins namely DC-SIGN (Dendritic Cell-Specific Intercellular adhesion molecule-3-

Grabbing Non-integrin) and Langerin as cell attachment receptors. DC-SIGN is used for transmission of MeV from infected dendritic cells to T lymphocytes and Langerin has been shown to aid in antigen presentation by Langerhans cells to CD4+ T-lymphocytes (de Vries et al., 2012).

1.1.4. Replication

Fusion of the virus envelope with cellular plasma membrane during entry, results inrelease of virus RNP complex into the cytoplasm. MeV replication occurs within cytoplasmic inclusion bodies or viral factories which are primarily located in the perinuclear regions, especially during early stages of replication (Zhou et al., 2019). Initially, transcription of the MeV negative sense RNA genome is carried out by virus encoded RdRpcomplex to produce positive sense mRNAs (Figure 1.2). Transcription is essentially guided by short conserved polyadenylation signals that flank each transcriptional element and follows a characteristic “stopstart” pattern by which genes near the 3’ end are transcribed more abundantly, compared to the 5’ end(Harrison et al., 2010, Whelan et al., 2004).Translation of virus proteins then occur using the host cell machinery. MeV genomic RNA replication occurs via a two-step process wherein the genomic RNA is first used to produce positive-sense antigenomes which is then used as a template to produce further negative-sense genomic RNA that subsequently gets incorporated in the RNP complex of mature virus particles(Rima and Duprex, 2009, Lamb, 2006). This is followed by the RNP assembly which occurs in the cytoplasm and is tightly linked to viral RNA synthesis. After

assembly, the RNP complex is released by budding at specific sites in the cell plasma membrane, thereby incorporating the virus envelope proteins(Griffin, 2007). Infectious MeV particles are formed only after the assembly of all structural and non-structural proteins of the virus, including viral glycoproteins and RNPs, are assembled at designated sites near the cell plasma membrane. The assembly process is initiated by the virus M protein that directly bind to the plasma membrane and interacts with RNP complex and viral glycoproteins via their cytoplasmic tail(Harrison et al., 2010).

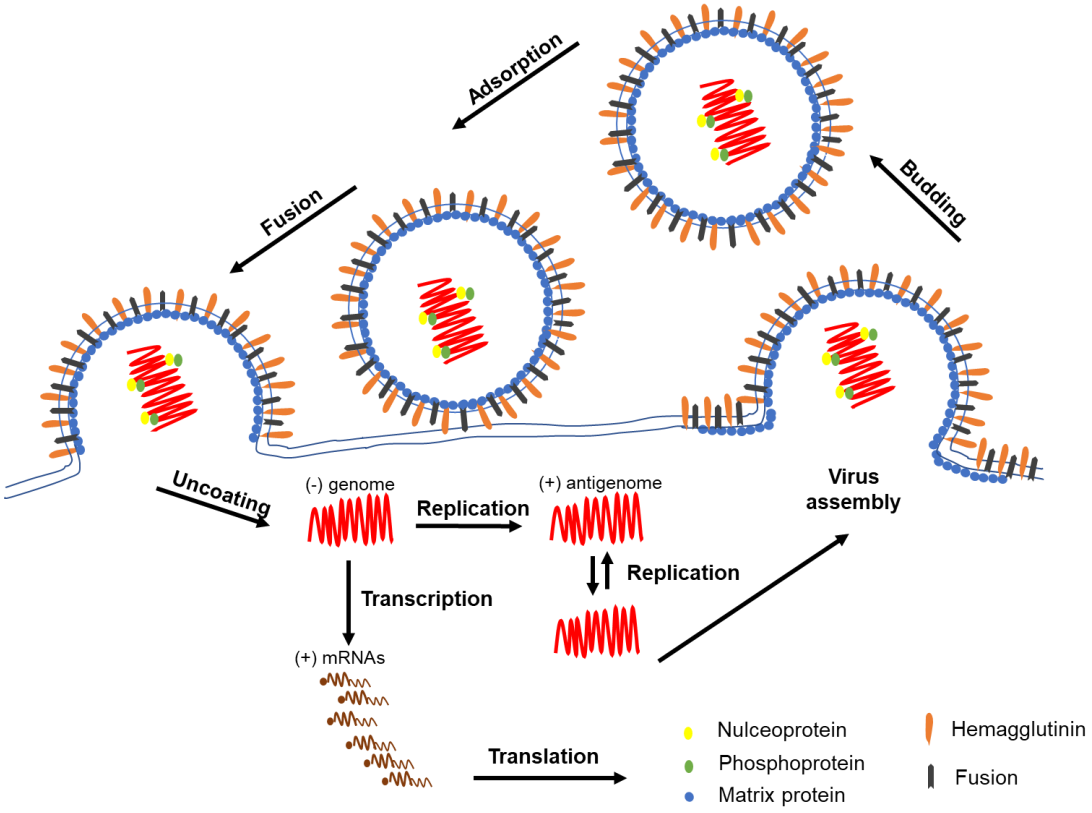

Fig 1.2 MeV life cycle. Upon entry of MeV particles into the cell via membrane fusion, the virus genome is transcribed by a virus encoded RdRp enzyme and the virus proteins are translated by host cell machinery. Replication of viral genome occurs using the positive-sense viral RNA as a template. Post virus assembly near the plasma membrane, the MeV particles are release by budding, which then proceed to infect new cells.

1.1.5. Pathogenesis and clinical symptoms

Transmission of MeV occurs via respiratory droplets that are mainly produced during coughing or sneezing by infected individuals. Small-particle aerosols may also contribute to transmission since they can remain suspended in the air for long durations. The incubation period (time between exposure to the virus and appearance of symptoms) of measles ranges from 10-14 days. Infected individuals start shedding virus during this period and continue for many days after the onset of rash. This facilitates measles spread well before the onset of symptoms, thereby affecting quarantine measures (Moss and Griffin, 2012).

Upon the transmission of MeV via aerosols, the virus is first exposed to mucosa of the respiratory tract in susceptible hosts. This is followed by virus entry into circulating SLAM positive alveolar macrophages and dendritic cells, which ferry the virus across the epithelial barrier (Lemon et al., 2011). These infected dendritic cells/macrophages then transport the virus to the draining lymph nodes, leading to the infection of B and T lymphocytes, thereby establishing primary viremia. Virus dissemination occurs through the BALT (bronchus-associated lymphoid tissue) and spreads to the thymus, spleen and other secondary lymphoid organs, culminating in secondary viremia and acute immunosuppression (Ludlow et al., 2010). This is followed by virus spread to the skin, kidneys, liver, gastrointestinal tract and within the entire respiratory tract. Virus shedding occurs when MeV infects primary airway epithelial cells of the upper respiratory tract that express the Nectin-4 receptor on their basolateral surface. MeV particles are thought to be transported to these sites within infected lymphocytes and myeloid cells

that are decorated with MeV glycoproteins on their surface. Once, MeV gains entry into the airway epithelial cells, a final round of virus amplification occurs which then facilitates virus shedding via aerosols (Noyce and Richardson, 2012b).

Measles complications include secondary bacterial infections that occur due to prolonged periods of immunosuppression and also neurological diseases like acute demyelinating encephalomyelitis (ADEM), measles inclusion body encephalitis (MIBE) and subacute sclerosing pan encephalitis (SSPE) (Yanagi et al., 2006). SSPE is a lethal late complication that usually occurs years after the initial infection. Other complications include bacterial otitis media and bronchopneumonia (Plemper and Snyder, 2009).

1.1.6. Diagnosis

Pattern recognition of measles symptoms can be made by considering patients presenting with Koplik's spots, which is the pathognomonic for this disease. This is often accompanied by fever, a generalized rash and sometimes clinically compatible symptoms like cough, coryza and conjunctivitis (Gans et al., 2018). People presenting with such symptoms are often considered for measles diagnosis, especially when the disease is currently circulating in the area or if the patients have recently travelled to measles endemic areas (Moss and Griffin, 2012). Serological tests are often used for laboratory confirmation of measles. This may include either a positive test for measles IgM or a 4-times rise in measles specific IgG antibodies between acute and convalescent sera. Other tests include MeV

isolation from clinical samples and detection of MeV RNA using real-time reverse transcriptase PCR (Bellini and Helfand, 2003).

1.1.7. Antigenicity

RNA viruses are prone to have high mutation rates due to their error prone RNA dependent RNA polymerase activity (Sanjuán et al., 2010). Yet MeV are antigenically monotypic and do not undergo antigenic drift as other RNA viruses like Influenza. This is partly because the MeV H and F proteins are essentially unable to tolerate significant mutations due to evolutionary constraints (Fulton et al., 2015). The public health significance of this is that, neutralizing antibodies that are produced upon measles vaccination or wild type measles infections offer lifelong protection against all MeV genotypes (Moss and Griffin, 2012).

1.3. Signalling Lymphocyte Activation Molecule (SLAM/CD150)

The human SLAM immunoglobulin superfamily comprises nine (SLAMF1 - F9) different leucocyte cell-surface proteins that are involved in the activation and differentiation of T lymphocytes, natural killer cells (NK cells) and antigen presenting cells (macrophages and dendritic cells). They serve as costimulatory molecules for immune cells in the adaptive immune system and also aid in lineage-commitment of thymocytes to CD4+/CD8+ T cells and NK cell development (Sintes and Engel, 2011). SLAM is involved mainly in IL-2 independent T cell expansion and IFN production by activated T cells.

1.3.1. Structure of SLAM

SLAM receptors are self-ligands, meaning they can participate in either homotypic or heterotypic cell-cell interactions. The SLAM receptor consists of two extracellular immunoglobulin (Ig)-like domains namely variable (V) and constant (C2), a single transmembrane domain and a cytoplasmic tail with several tyrosine-based motifs (Fig 1.2). The SLAM-associated proteins (SAP) family of adaptors are recruited to the cytoplasmic domain in response to phosphorylation of the tyrosine motifs (Veillette et al., 2007).

The V domain of SLAM is important as a receptor for MeV entry because of the specificity of MeV H interaction with this region. The inability of MeV to infect mice has been attributed to the differences in the V domain of SLAM (Sidorenko and Clark, 2003).

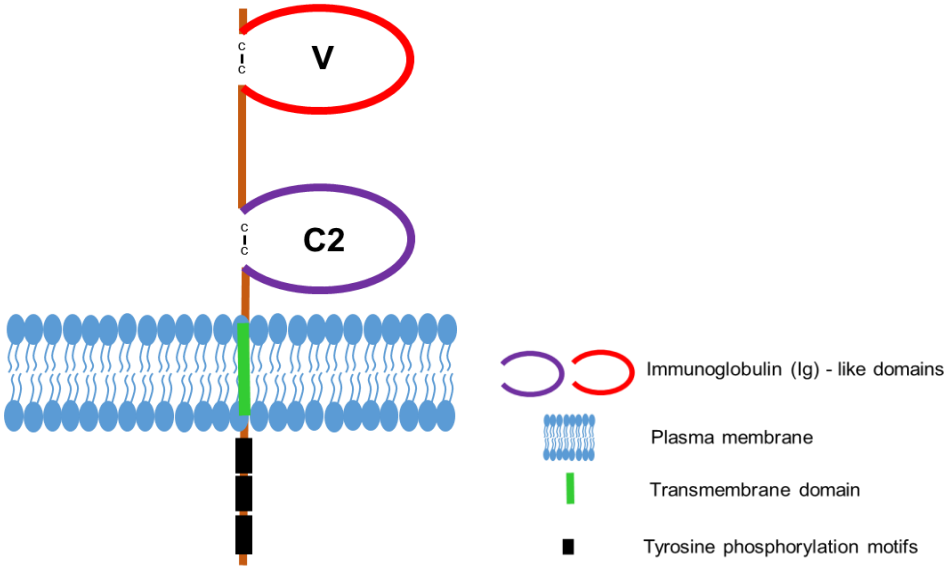

Fig 1.3 Structure of SLAM/CD150 receptor. MeV uses CD150/SLAM for cell entry. It is expressed on immune cells, including activated lymphocytes, dendritic cells and macrophages. The extracellular domain of SLAM is composed of variable (V) and constant (C2) Ig-like repeats. The intracellular

domain consists of a transmembrane domain with tyrosine phosphorylation motifs.

1.3.2. Role of SLAM in phagocytosis

It has been shown that SLAM acts as a microbial sensor in macrophages that help in the elimination of Gram-negative bacteria like *E-coli*. This role of SLAM has been attributed to its regulation in phagosome maturation and production of free radical species by the NADPH oxidase (nicotinamide adenine dinucleotide phosphate-oxidase) NOX2. It does so by first recruiting the Vps34-Vps15-beclin1 complex to the phagosomes which catalyzes the conversion of phosphatidylinositol (PtdIns) to phosphatidylinositol 3 phosphate (PtdIns3P). This in turn results in the recruitment of EEA-1 and the small GTPase Rab5 to the phagosomes and the subsequent production of reactive oxygen species (ROS), culminating in the elimination or phagocytosis of the engulfed bacteria (Berger et al., 2010a).

The SLAM mediated recruitment of Vps34-Vps15-beclin1 complex during phagocytosis overlap with another intracellular pathway called autophagy. Autophagy is a catabolic cellular process wherein superfluous intracellular components are enveloped in double membraned vesicles called autophagosomes and shuttled to the lysosomes for degradation. Autophagy mainly serves to alleviate cells from stressed conditions and is also shown to aid in cellular defense against invading microorganisms (Kudchodkar and Levine, 2009). Moreover, the toll like receptor (TLR) mediated triggering of phagocytosis has been shown to recruit autophagy proteins such as LC3 to phagosomes and the activation of ROS by NOX2 is required for the activation of antibacterial autophagy in human epithelial cells (Huang et al.,

2009). This might indicate a possible role of SLAM in canonical autophagy pathway and that requires further investigation.

1.3.3. Role of SLAM in MeV entry

MeV enters SLAM positive immune cells by promoting the direct fusion of viral and cell membranes. This membrane fusion reaction occurs at neutral pH and is initiated by the MeV hemagglutinin (H) and fusion (F) proteins. The merging of membranes is carried out by the F protein which exists as a metastable homo-trimer and needs to be proteolytically activated by stable interactions between the measles H protein and SLAM receptor on the cell membrane (Navaratnarajah et al., 2011). Receptor binding results in major conformational changes in the pre-fusion F protein that triggers the insertion of the fusion peptide into the plasma membrane, causing membrane fusion via the formation of a fusion pore. The fusion pore gradually expands, eventually resulting in virus-cell membrane fusion and virus entry (Plemper et al., 2011b).

1.3.4. Role of SLAM in MeV induced immunosuppression

MeV infections are commonly associated with severe prolonged immunosuppression that render the infected population highly susceptible to infection by opportunistic pathogens. This is also the main reason behind the high mortality rates among young children and elderly. Much of these effects can be attributed to the MeV - SLAM interaction. During measles infection, the activation of cell-mediated immunity results in the clonal proliferation of T lymphocytes. T_H1 cells (T helper cells -1) express higher amounts of SLAM than T_H2 cells and hence might be more susceptible to

measles infection. The resulting T_H1 to T_H2 shift results in an antibody mediated immune response rather than cell-mediated response (Sidorenko and Clark, 2003). This shift may also be mediated by the decrease in IL12 and IFN-gamma production occurring during measles infection (Griffin, 2010).

1.4. Measles endocytosis

The recent publication by Carneiro *et al* discusses an alternate role of SLAM in mediating MeV entry via a complex pathway involving macropinocytosis (Goncalves-Carneiro et al., 2017). Electron microscopy studies revealed extensive filopodia formation and cell contraction in MeV infected A549-SLAM cells (a human lung epithelia cell line stably expressing the human SLAM receptor) within 20 min post infection. Although the cells returned to their normal state at 60 min post infection, the authors hypothesized that this alteration in cell morphology might have a role in aiding MeV entry. MeV entry was not affected by the knockdown of proteins regulating endocytosis such as caveolin-1, clathrin and dynamin-mediated pathways of endocytosis, which indicated that these pathways were not utilized by the virus for entry. Colocalization of Dextran labelled endosomal structures called macropinosomes and MeV-N (MeV nucleoprotein) labelled MeV particles indicated that the virus was taken up by macropinocytosis. The activation of F protein at the cell surface may initiate virus entry by either membrane fusion or macropinocytosis and this might depend on whether the interaction with the SLAM receptor is mediated by the whole virus particle or MeV H-F complexes. Moreover, this pathway may be

beneficial for MeV entry into SLAM positive cells at the respiratory mucosa, which is an important phase in MeV pathogenesis.

Another recent study also reported similar findings linking MeV entry to macropinocytosis. Here they demonstrate that MeV interaction with cells during early time points post administration of the virus, results in increased uptake of fluorophore-conjugated dextran, via a macropinocytosis-like pathway. Virus entry was inhibited in the presence of the macropinocytosis inhibitor 5-(N-ethyl-N-propyl)amiloride (EIPA) and inhibitors of actin polymerization like cytochalasin-D and the authors speculate that MeV entry could occur via macropinocytosis, in addition to the well characterized membrane fusion mediated entry pathway for MeV. (Delpeut et al., 2017). Actin dynamics is also important during different stages of MeV life cycle involving virus particle trafficking and release, as shown by the effects of drugs that stabilize or disrupt actin filaments (Dietzel et al., 2013).

The interaction of MeV-Ed with its CD46 receptor is known to cause receptor crosslinking which in turn causes the internalization of CD46 by macropinocytosis via similar extensions of pseudopodia as seen with SLAM and MeV interaction discussed above (Crimeen-Irwin et al., 2003).

1.5. The need for effective antivirals against MeV

Despite the existence of an effective vaccine, measles continues to be a global health issue. There are several reasons for this, most important being the elective exemption from vaccination owing of personal, parenteral or religious beliefs. This was the consequence of a report published by Wakefield *et al* that associated the administration of measles mumps rubella (MMR) vaccine to autism and intestinal disease in children (Plemper and

Snyder, 2009, Wakefield et al., 1998). Although this claim was refuted by subsequent epidemiological case studies (Taylor et al., 1999, Dudley et al., 2018, Hviid et al., 2019), the direct consequence of low vaccination coverage was a lack of herd immunity which is crucial for the prevention of measles outbreaks. A herd immunity of greater than 95% is crucial for the prevention of periodic measles outbreaks (Orenstein and Gay, 2004). Thus, to effectively prevent measles outbreaks, maximum vaccination coverage with the population would need to be ensured. The availability of an effective antiviral could be used for post-exposure prophylaxis when-in, the patients and their immediate contacts can be administered the drug to prevent spread of the disease (Plemper and Snyder, 2009).

Currently, there are no specific and effective antivirals available for the treatment of measles. Ribavirin and IFNα, administered alone or in combination, have been used for the treatment measles. However, in most cases, this has been shown only to ameliorate the symptoms (Macaya-Ruiz et al., 2006). High dose Vitamin A has shown some promise in the treatment of measles (Plemper and Snyder, 2009).

1.6. ddBCNAs

Antiviral nucleoside analogues are the modified synthetic variants of naturally occurring nucleosides that are designed to specifically inhibit an integral part of virus cycle, mostly by affecting DNA/RNA replication or by inhibition of virus-encoded enzymes involved in nucleoside metabolism (Jordheim et al., 2013). Ever since its development in the 1960's, a range of nucleoside analogues have been developed to inhibit a wide range of

viruses including HIV, hepatitis b virus and herpes virus infections (De Clercq and Li, 2016).

1.6.1. Background

The use of 5-substituted pyrimidine nucleoside analogues as antiviral drugs began initially with the synthesis of 5-iodo-2′-deoxyuridine (IDU) by Prussof et al (Prusoff, 1959). This was followed by the synthesis of several variants of this compound differing in their 5-substituents, notably the drug brivudine ((E)-5-(2-bromovinyl)-20-deoxyuridine (BVDU)) which is a potent inhibitor of HSV -1(Andrei et al., 1992) and VZV(Andrei et al., 1995). The MoA of BVDU was attributed to the specific phosphorylation by virus encoded thymidine kinase, which converts BVDU to its 5′-monophosphate and diphosphate forms. Its subsequent phosphorylation to BVDU-TP by cellular nucleoside kinases, allows the incorporation of BVDU-TP into the growing viral DNA chain, thereby inhibiting viral replication and transcription (De Clercq, 2004) (Fig 1.3)

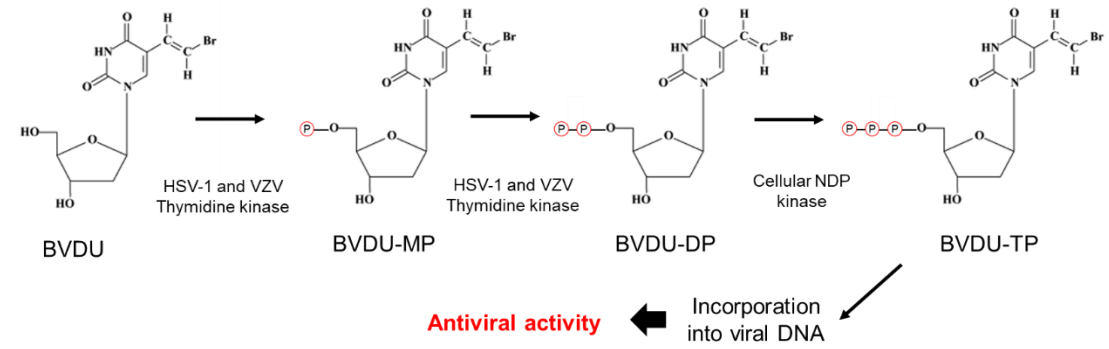

Fig 1.4. Antiviral activity of BVDU. HSV-1 and VZV thymidine kinases phosphorylate BVDU to BVDU monophosphate (BVDU-MP) and BVDU triphosphate (BVDU-DP) which is then converted to BVDU triphosphate (BVDU-TP) by the cellular kinase nucleoside 5'-diphosphate (NDP), leading to its incorporation in viral DNA. (Incorporated from (De Clercq, 2004))

Subsequently, the activity of 5-ethynyl substituted deoxyuridines was also investigated and found to possess antiviral activity against HSV 1, HSV 2 and VACV. However, the IC_{50} of these drugs was found to be close their cytotoxic concentration (De Clercq et al., 1981) and it was also noted that the antiviral activity of 5-alkynyl deoxyuridines decreased with increasing length of the side chains, the optimum length being <5 C atoms (McGuigan et al., 2001).

1.6.2. Alkyl furano pyrimidines

Furano pyrimidines were produced as by products during the synthesis of 5-alykynyl-2'-deoxyuridines and it was found that certain long chain alkyl homologues of these parent compounds possessed antiviral activity against VZV *in vitro* at nano molar concentrations(McGuigan et al., 1999). A series of compounds were synthesized with varying alkyl side chain lengths and SAR studies revealed the absolute requirement of long alkyl side chains of length C8-C10 for antiviral activity. The activity of the lead compound was 300-fold higher over the control drug Acyclovir and did not show any cytotoxicity *in vitro*. Mode of action (MoA) studies revealed that antiviral activity of the lead compound was specific only for VZV and not for other DNA viruses like HSV 1 and 2, VACVand cytomegalovirus (CMV). Hence the MoA was most likely to be dependent on the VZV thymidine kinase mediated phosphorylation of the drug to its 5'-triphosphate forms (McGuigan et al., 1999).

Following this lead, the McGuigan group then synthesized 2',3'-dideoxy variants of these alkyl furano pyrimidines, producing a series of lipophilic

alkyl furano pyrimidine dideoxy nucleoside analogues with varying side chain lengths. The lead compound (Figure 1.3 and hereby referred as cf2095) now lost its antiviral activity against VZV, but was found to be active against human cytomegalovirus with an IC_{50} of 0.5µM (McGuigan et al., 2004). The loss of activity versus VZV was attributed the lack of 3'-OH group which could have been important for the VZV thymidine kinase specificity of the drug. Moreover, the SAR profile and time of addition experiments suggested a non-nucleoside based MoA (McGuigan et al., 2004).

1.6.3. $_{L}$-ddBCNAs

To improve the antiviral activity of cf2095, a series of $_{L}$-chiral versions of this compound with varying ether side chains lengths were synthesized. A SAR study revealed that there was an actual correlation between the lengths of the ether side chains and the activity of these compounds (Figure 1.4 B). The lead compound with structure n-C9H18−O−n-C5H11 (Figure 1.4 A and hereby referred as cf2642) with a 5 -Carbon ether side chain lost its activity against HCMV but now showed antiviral activity against both measles wild type virus (IC_{50}-7.5µM) and VACV(IC_{50}-0.2µM) across three different biological assays. This in turn indicated a possible cellular target that might be affected (McGuigan et al., 2013) (see section 1.1. for more information). All the experiments performed as part of this PhD research work are done investigating the nature of the putative cellular target or process affected by cf2642.

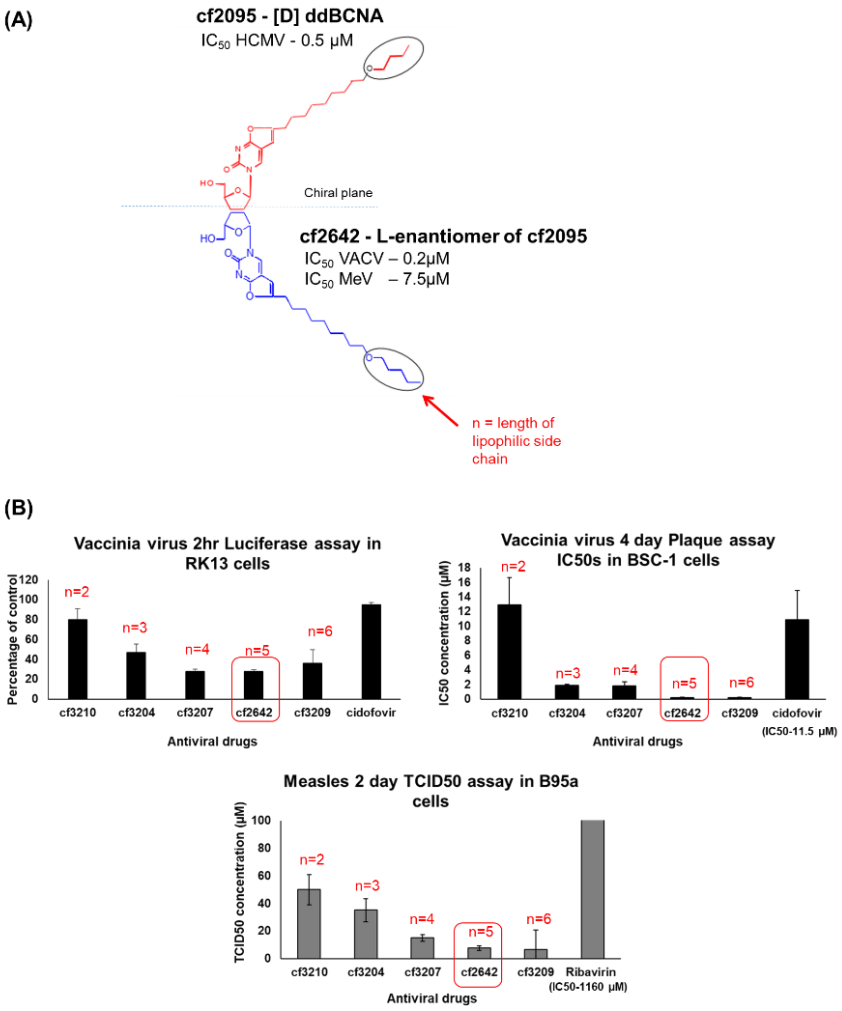

Fig 1.5 SAR of ddBCNA versus Orthopox and Paramyxoviruses:(A) Structure of the D-ddBCNA parent compound cf2095 and its enantiomer, the lead L-ddBCNA compound cf2642 **(B)** Graph shows the SAR profile of cf2642 for three different biological assays namely 4 day-Plaque assay and 2hr-luciferase reporter assay for VACVand 3 day-$TCID_{50}$ assay for MeV. The comparative activity of 5 different L- ddBCNAs with increasing ether side chain length (n= 2 to 6) and cidofovir / ribavirin controls is shown. The effect of Ribavirin versus MeV (IC_{50} 1160uM) is beyond the scale of this graph and hence is not indicated. The graph represents the results of three independent experiments. Source: (McGuigan et al., 2013, Farleigh, 2014)

In summary, the development of different variants of alkyl furano pyrimidines

is shown in Fig 1.5.

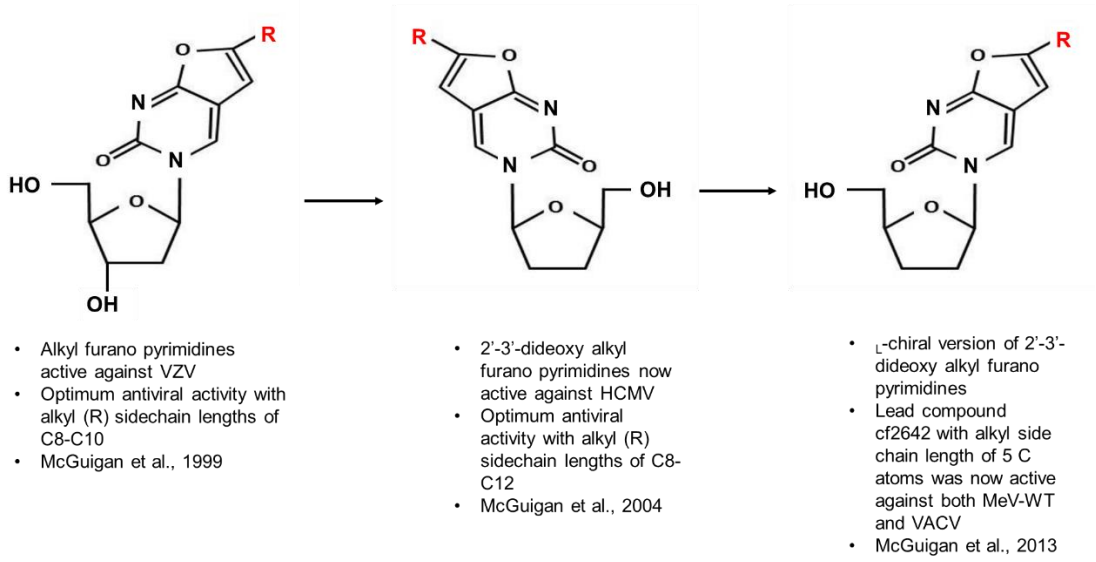

Fig 1.6. Development of lead L-ddBCNA cf2642. A summary of the development of ddBCNAs beginning from the synthesis of 2'-alkyl furano pyrimidinesis shown.

1.7. Cell-targeting antivirals

Pathogen-directed antivirals, although effective in some cases, can give rise to drug-resistant mutants. This is especially the case with RNA viruses that are more prone to mutations. One way to tackle this is to develop cell/host directed antivirals that target a specific component that is hijacked by the virus during its lifecycle (Schwegmann and Brombacher, 2008). An added advantage is that such antivirals often tend of have a broad spectrum of activity against viruses using a common cellular pathway(Yan et al., 2013).

1.8. Endocytosis

The plasma membrane of a cell restricts the free entry of substances into the cytoplasm. While transmembrane proteins allow the transport of amino acids, sugars etc. into cells, the transport of larger substances, macromolecules, metabolites, lipids and proteins into cells are facilitated by

endocytosis. The term endocytosis refers to the process by which cells internalize fluids, macromolecules, nutrients, membrane proteins, lipids, solutes etc. from the extracellular milieu by the *de novo* formation of vesicles formed by plasma membrane invaginations (Hoeller et al., 2005). Material has been shown to enter the cells via a number of different endocytic pathways regulated by distinct proteins such as clathrin and caveolin and emanating from distinct sites of the plasma membrane such as lipid rafts. Primary functions of endocytosis are to recycle and degrade for a number of physiological reasons including membrane turnover, providing cells with nutrients following traffic to lysosomes and degradation, antigen presentation in specialized immune cells and downregulation of receptors such as signaling growth factors (Doherty and McMahon, 2009).

1.8.1. Clathrin Mediated Endocytosis (CME)

Clathrin-mediated endocytosis engulfs components from the extracellular milieu by the formation of plasma membrane invaginations that are coated with characteristic triskelion shaped proteins called clathrin that surround other cytosolic proteins that are recruited to the plasma membrane. These include adaptor proteins that are known to recognize specific sections of the cytosolic domains of receptors to often form receptor clusters for subsequent invagination. CME by a long margin is the best characterised endocytic pathway so far identified. The 100-120 nm clathrin coated pits then pinch off from the plasma membrane and loose the clathrin coat before entering the cytoplasm and rapidly fusing with early/sorting endosomes that then direct traffic to other cellular locations such as the lysosomes or for recycling. CME helps in the intake of metabolites, hormones, low-density

lipoprotein, transferrin, growth factors and even certain viruses (Kaksonen and Roux, 2018)(Marsh and McMahon, 1999).

1.8.2. Caveolae Mediated Endocytosis

Endocytosis mediated by caveolae does not involve clathrin coats and is associated with approximately 60-80nM wide flask-shaped invaginations that are formed on regions of plasma membrane that are enriched in cholesterol and termed lipid rafts. These cholesterol- and sphingolipid-rich invaginations are commonly found in fibroblasts, smooth muscles, type I pneumocytes, adipocytes and endothelial cells (Rothberg et al., 1992). The caveolar pathway aids in the endocytosis of albumin, autocrine motility factor, tetanus and cholera toxins and even viruses like polyoma and simian 40 (Kumari et al., 2010).

1.8.3. Macropinocytosis

Macropinocytosis (cell drinking) is associated with the engulfment of relatively large amounts of extracellular fluid. These 0.2-10μM macropinosomes basically originate from plasma membrane ruffles and is a highly coordinated triggered process which has been best described to occur in cells activated with growth factors such as EGF and PDGF that through binding to their cognate receptors cause cell signalling, actin rearrangement and membrane ruffling. These ruffles fold in and back to the plasma membrane and at the same time engulfs the extracellular fluid to give rise to an increase in fluid phase endocytosis. There is evidence to suggest the process is constitutive in some cells and commonly occurs in immature dendritic cells with a role in immune surveillance. Intracellular pathogens including shigella, salmonella influenza, VACVand HIV-1 have

all been shown to exploit macropinocytosis as a means of entry into cells (Kumari et al., 2010). Actin is critical for macropinocytosis to occur and several actin regulating roteins have thus been shown to be involved in this process including Pak-1 and cdc42.

1.8.4. Phagocytosis

Phagocytosis is the preferred route by which cells like macrophages internalize large particulate matter like cell debris, microorganisms and apoptotic cells. The engulfed materials then find its way to internal membrane compartments called phagosomes which then fuse with lysosomes to form phagolysosome wherein the contents are degraded. Both macropinocytosis and phagocytosis have common features like the large size of internalized cargo, similar membrane modelling pathways during internalization and pathways initiated by phosphoinositide 3 kinase (PI3K) dependent processes (Kumari et al., 2010) .

1.9. Autophagy

Autophagy is an evolutionarily conserved catabolic pathway wherein damaged organelles or protein aggregates targeted for elimination are sequestered within double membraned vesicles called autophagosomes, which are then shuttled towards lysosomes for degradation. It helps in the maintenance of cellular homeostasis and in the combat of cellular stress induced during nutrient limiting conditions. Autophagy often serves as a cellular defence against invading pathogens like viruses, by either targeting them for degradation in lysosomes or by facilitating the induction of humoral immune responses through antigen presentation. However, many viruses

are known to promote or subvert the autophagy machinery to their advantage (Kudchodkar and Levine, 2009)(Dong and Levine, 2013).

1.9.1. Mechanism of Autophagy

There are mainly three types of autophagy namely microautophagy, chaperone-mediated autophagy and macroautophagy. In microautophagy, cytoplasmic components are directly engulfed by protrusions from the lysosomal membrane, while chaperone-mediated autophagy involves the selective degradation of cytoplasmic components which are marked by KFERQ-like sequences. This further involves specific interactions with the lysosomal LAMP 2a protein that spans the lysosomal membrane. This protein is often used via immunofluorescence to label components of autophagy and the late endocytic pathway

Macroautophagy (hereby referred as autophagy) is the most widely studied form of autophagy and involves the *de novo* formation of a phagophore that eventually develops into a double membraned vesicle called autophagosome (Fig 1.6). The autophagosome may then fuse with endosomes to form Amphisomes or fuse with the lysosome to form the autolysosome wherein the components are degraded by lysosomal hydrolases (Klionsky, 2007). Much of the information about the mechanisms of autophagy in mammalian cells came from work using yeast. Ohsumi's group initially studied autophagy in *Saccharomyces cerevisiae* and thereafter, he and many others like Klionsky and Thumm conducted pioneering research in the field and characterized more than 30 autophagy-related (Atg) genes in yeasts. Many of these Atg genes have known homologues in mammalian cells (Xie and Klionsky, 2007). There are mainly

three steps involved in the autophagy pathway: Initiation, elongation and fusion. A brief outline of the steps is shown in (Fig 1.6).

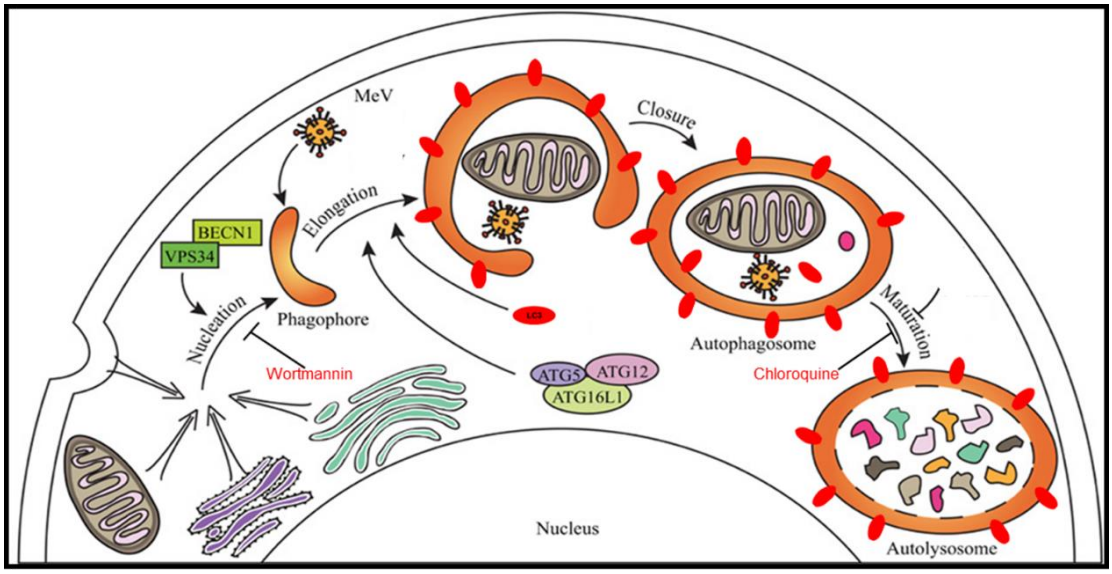

Fig 1.7Autophagy pathway. Autophagy is a cellular process by which cells eliminate unwanted cellular components by encapsulating them in double membrane vesicles called autophagosomes that then fuse with lysosomes and are degraded. Several steps are involved in this process. Nucleation involves the formation of an isolation membrane from various membrane sources (endoplasmic reticulum, Golgi, plasma membrane or mitochondria). This matures to form a phagophore which then elongates to form a double membrane vesicle called autophagosome that sequesters cellular components (senescent organelles like mitochondria, intracellular pathogens like viruses) targeted for degradation. The autophagosome then matures and fuses with lysosomes to form an autolysosome that degrade the components within. Wortmannin is a PI3Kinhibitor that inhibits formation of autophagosomes, while chloroquine increases the pH of lysosomes and prevents autolysosome formation. The key proteins involved in autophagy are indicated. - Adapted from (Petkova et al., 2013)

1.9.1.1. Initiation

Autophagy is initiated when cells are under stress, for example during starvation of essential nutrients and amino acids. Although a variety of signaling cascades can trigger autophagy in response to different stresses, the classic example is that of mTOR (mechanistic target of Rapamycin)

inhibition. The serine/threonine kinase mTOR, is a critical regulator of autophagy and also responds to changes in the extracellular environment and controls autophagy and various cellular pathways like initiation of mRNA translation, cell growth and proliferation, and cytoskeletal reorganization (Ravikumar et al., 2010).The mTOR is associated with the Unc-51 like kinase 1/2 complex (ULK1/2-ATG13-FIP200-ATG101) that is composed of ULK 1/2, ATG13, the focal adhesion kinase family interacting protein of 200 kDa (FIP200) and ATG101. Under nutrient rich conditions, mTOR phosphorylates the ULK1/2-FIP200-Atg13 complex and this inhibits autophagy by keeping the ULK1/2 kinase activity in check. However, when mTOR is inhibited either by Rapamycin or by the activity of AMPK (5' AMP-activated protein kinase) during starvation (Kim et al., 2011), mTOR hypo-phosphorylates ULK1/2 and this leads to the induction of autophagy. This is followed by the translocation of the activated ULK1/2 complex to specific endoplasmic reticulum (ER) domains in the cytoplasm that are thought to be associated with the formation of the pre-autophagosomal structure (PAS). The ULK1/2 complex then recruits the Class III PI3K complex to produce phosphatidylinositol 3-phosphate (PI3P), this first step towards the *de novo* synthesis of the phagophore or isolation membrane. The process is also aided by function of two effector proteins of PI3P namely DFCP1 (double-FYVE-containing protein 1) and WIPI (WD-repeat protein interacting with phosphoinositides) (Axe et al., 2008). The Class III PI3K complex consists of the mammalian autophagy protein Beclin-1, p150, Atg14L and ultraviolet irradiation resistance-associated gene (UVRAG) and is the major effector of autophagosome synthesis.

1.9.1.2. Elongation

Elongation of the phagophore to form the autophagosome involves Atg12–Atg5 -Atg16 complex that is catalysed by the function of several ubiquitin like conjugation systems. Initially the Atg7 (E1 like enzyme) and Atg10 (E2 like enzyme) form the Atg12–Atg5 complex and then Atg16 becomes non covalently attached to Atg5, resulting in the Atg12–Atg5-Atg16 complex (Klionsky, 2012) This complex is known to attach to the growing phagophore and possibly contributes to the curvature of the growing autophagosome. In the next step, Atg4 protease cleaves the microtubule associated protein, light chain 3 (LC3) at its C-terminus to form LC3-I and the Atg3 (E2 like enzyme) adds the lipid Phosphatidylethanolamine (PE), forming LC3-II / LC3-PE (Fig 1.7) Once lipidated with PE, the LC3-II becomes associated with both the inner and outer membranes of the mature form of the autophagosome and hence is used as a marker for monitoring autophagy flux (Ni et al., 2011).

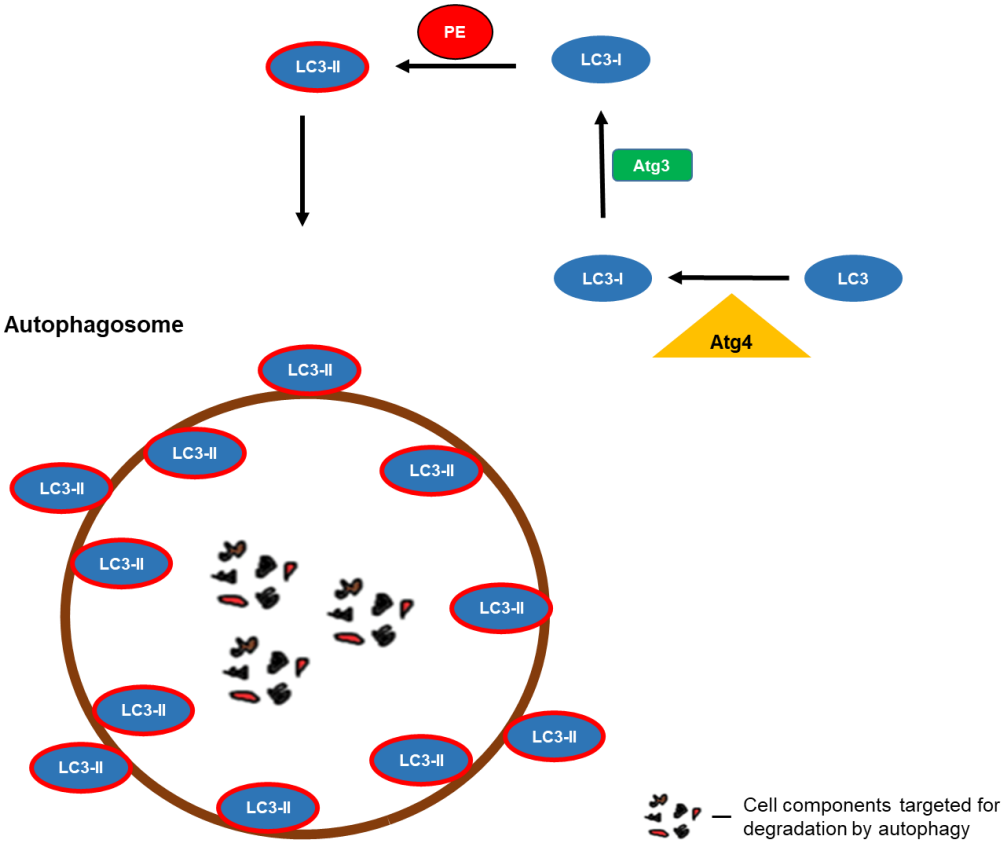

Fig 1.8 Conversion of LC3-I to LC3-II. During the induction of autophagy, LC3 is first cleaved by the protease enzyme Atg4 to form LC3-I. The enzyme Atg3 then lipidates LC3-I by adding PE to form LC3-II. The LC3-II then binds to the inner and outer membranes of the growing autophagosome before fusing with lysosome.

1.9.1.3. Fusion

The final step in autophagy involves the fusion of the autophagosome with the lysosome to form the autolysosome, wherein the contents are degraded by the cocktail of hydrolytic enzymes present in lysosomes. This is followed by the recycling of the building contents to the cytosol for the synthesis of new macromolecules (Ravikumar et al., 2010).

1.10. MeV induced autophagy

Both MeV-Ed and MeV have been shown to induce successive phases of autophagy in infected cells to promote virus spread and to escape from the host apoptosis machinery(Meiffren et al., 2010, Richetta and Faure, 2013). The virus by itself is not destroyed by autophagy, but it helps in delaying the antiviral host immune defence**.** MeV-Edinduces two successive phases of autophagy, the first mediated by the CD46-GOPC scaffold protein mediated pathway and the second by the MeV C protein-IRGM pathway. However, in the case of MeV, since the virus does not use the CD46 receptor, the first wave of autophagy does not occur during its life cycle. Instead, the MeV IRGM pathway coupled with the autophagy induced by the syncytia formation helps the virus to escape from host mediated immune responses (Richetta et al., 2013).

IRGM (immunity regulated GTPase M) form a part of Immunity Related Guanosine Triphosphatases or IRGs that mainly serve as an innate immune mechanism for the clearance of pathogens (Li et al., 2009). They have been implicated in the induction of autophagy in response to many viral infections by interacting with autophagy-associated proteins ATG5, ATG10, MAP1CL3C and SH3GLB1. Moreover, the siRNA knockdown of IRGM has been shown to inhibit autophagy induced by MeV, Hepatitis C virus (HCV) and HIV-1 (Gregoire et al., 2011).

1.11. Hypothesis

Initial studies on cf2642 had shown that the drug inhibits both vaccinia and measles viruses and that antiviral activity against the former was shown to occur at early (2 hr) time points post treatment(Farleigh, 2014).

Given that both these viruses are enveloped, and that cf2642 possesses a lipophilic side chain, leads to the attractive hypothesis that the antiviral effects of this compound may be a direct result on virus/cell membranes, thereby affecting virus entry or early events occurring therein.The goal of this PhD project is to evaluate this hypothesis and, more importantly, to identify the precise host target of cf2642 which results in the inhibition of viruses predominantly replicating in the cytoplasm.An antiviral compound that targets a key component of the host cell machinery, which results in its antiviral activity and at the same time does not induce cytotoxicity, is an important stride towards the development of antiviral compounds that restrict the development of drug resistant viruses.

1.12. Aims and Objectives

a) To elucidate the effects of cf2642 on intracellular membrane trafficking.
b) To perform endocytic characterization in HeLa and VeroSLAM cells.
c) To perform mode of action studies based on both live and non-virusbased receptor-clustering assays

Chapter 2 - Materials and Methods

2.1. Materials

2.1.1. Cell lines

1. **HeLa**: (ATCC, CCL-2) - Human epithelial cells: established from the cervical adenocarcinoma of a black 31-year old female. This cell line contains Human Papilloma Virus 18 oncogenes (E6 and E7)
2. **VeroSLAM**: (ECACC) African Green Monkey Kidney cells stably expressing the human signalling lymphocytic activation molecule receptor (ECACC Catalogue number - 04091501).

2.1.2. Virus

1. **MeV**: Measles virus wild-type strain isolated from a patient with acute measles (Erlangen, Germany, 1990) -Kind gift from Jurgen Schneider-Schaulies, Universitat Wurzburg, Germany.(Erlenhoefer et al., 2001)
2. **MeV-GFP**: Wild-type IC (Ichinose)-B strain of measles virusexpressing Green Florescent Protein (GFP) - Kind gift from Prof. Yusuke Yanagi, Kyushu University, Japan.(Hashimoto et al., 2002)

2.1.3. Equipment

2.1.3.1. Plastics and glassware

All general use tissue culture plasticware, laboratory disposables and organic solvents were purchasedfrom Fisher Scientific - Loughborough, UK. Supplier details and catalogue numbers of other materials are listed in Appendix C. General usage chemicals and reagents were supplied by Sigma-Aldrich (Poole, UK) unless otherwise indicated in Appendix C.

2.2. Methods

2.2.1. Cell Culture

2.2.1.1. Cell culture medium

All cells were maintained in 1x Dulbecco's Modified Eagles Medium (DMEM) containing 4.5g/L (25mM) glucose and L-glutamine without sodium pyruvate supplemented with 10% (v/v) fetal bovine serum (FBS) in the absence of antibiotics (complete media). Cells were incubated in humidified incubators under tissue culture (TC) conditions (37ºC with 5% CO2). For maintenance of VeroSLAM cells, the medium was supplemented with 0.4 mg/mL geneticin to maintain the stable expression of SLAM.

2.2.1.2. Routine cell maintenance

All cell lines were maintained as per the requirement for each experiment and to not allow them to be over-confluent. Cells were split once they reached 70-80% confluence. The medium in the flask was first aspirated and cells were washed once with 2 mL sterile PBS (phosphate buffered saline) to remove traces of FBS. For trypsinization, PBS was aspirated, replaced with 2 mL 0.05% trypsin EDTA (Ethylenediaminetetraacetic acid) and the flask was placed in the incubator for 5 min to allow cells to detach. Cells were then collected in 8 mL complete media and centrifuged at 300 x *g* for 4 min. As per the split-ratio for each cell line (see Table 2.1), the appropriate volume of medium was used to re-suspend the cells before being transferred to new T-75 tissue culture flasks. All cell lines were maintained up to a passage number of 25, after which the cells were discarded and a fresh batch was revived for use (see section 2.3.4 -

Thawing cells). Passage number refers to the number of times a cell line was split previously.

Table 2.1 - Split ratios for cell lines used for this project. The ratios are for subculture after 3-5 days

Cell line	Split ratio
HeLa	1:6
A431	1:4
VeroSLAM	1:6
B95a	1:4

2.2.1.3. Freezing cells

All low-passage number cell lines received from their respective source (see section 2.1.1) were first grown to 70-80% confluence and stocks made for future use. For preparing cell stocks, the cells were trypsinized, centrifuged at 300 x *g* for 4 min and re-suspended in cell freezing medium (45% DMEM, 45% FBS and 10% DMSO) at a density of 2 x 10^6 cells/mL. The cells were then transferred to cryogenic vials, placed in a Mr. Frosty Freezing container and stored at -80°C for up to 24 hours, after which the vials were transferred to a liquid nitrogen cylinder for long-term storage.

2.2.1.4. Thawing cells

The revival of cells stored in liquid nitrogen was done by placing cryogenic vials in a 37°C water bath to allow for rapid thawing. Once completely thawed, cells were transferred into a sterile 15 mL tube containing 10 mL complete medium and centrifuged at 300 x *g* for 4 minutes to remove all traces of DMSO. The supernatant was then discarded, cell pellet re-

suspended in 15 mL complete media and transferred to a sterile T-75 tissue culture flask. After overnight incubation to allow the cells to adhere, the medium in the flask was replaced with fresh complete media to get rid of floating dead cells.

2.2.1.5. Mycoplasma testing

Note: *During the second year of my PhD research work at the School of Pharmacy, it was found that the cells that were used during the first-year work at the School of Medicine were contaminated with mycoplasma. Following this, it was decided that all the work done during that period had to be repeated using mycoplasma free cells. This aspect of the work was done in collaboration with Dr. Joachim Bugert's laboratory at the Bundeswehr Institute for Microbiology in Munich, Germany. All the subsequent work at the School of Pharmacy were done with mycoplasma free cells, confirmed by routine mycoplasma screening checks done in the laboratory.*

Mycoplasma contaminations were ruled out with routine testing by mycoplasma PCR (LookOut mycoplasma detection kit, Sigma). The procedure was followed as per the manufacturer's instructions. Cells were grown to 90-100% confluence and 1 mL of medium was transferred to a sterile 1.5ml Eppendorf tubes. The contents were centrifuged at 500 x *g* for 5 minto remove any cell debris that might be present. The tubes were then placed on a heating block and heated to 95°C for 5 min to prepare stable templates for PCR analysis. These served as the test samples. Two sets of ready-made PCR reaction tubes were provided with the detection kit. The Test Reaction tubes which contained only the primers were used for testing

the samples and negative control. The Positive Control Reaction tubes contained the primers along with positive control DNA.

For mycoplasma detection, 2 µL of each test sample was added to the Test Reaction tubes. 2 µL of deionized water served as the negative control. No samples were added to the positive control reaction tubes. 23µL of DNA polymerase rehydration buffer (dNTPS) was added to the Test Reaction tubes and 25µL of the buffer to the Positive Control Reaction tubes, so that all tubes had equal volumes. JumpStart™ Taq DNA Polymerase (0.5 µL) was then added to all tubes, the contents were mixed by gently tapping and the tubes were transferred to a thermocycler. The temperature cycle was set as per the conditions below:

1 cycle	*94 °C for 2 minutes (Initial denaturation)*
x40 cycles	*94 °C for 30 seconds (Denaturation)* *55 °C for 30 seconds (Annealing)* *72 °C for 40 seconds (Elongation)*
Cool down	*to 4–8 °C*

The results were analyzed by agarose gel electrophoresis.

2.2.2. Agarose gel electrophoresis

A 1.5 % agarose gel was used for electrophoresis. Briefly, 3 g agarose was added to 200 mL TAE buffer (40 mM Tris, 20 mM acetic acid, 1 mM EDTA)

and heated in a microwave on full power until the contents were fully dissolved. The mixture was then allowed to cool for few minutes and 25 µL of ethidium bromide (10mg/mL) was added. The agarose mixture was then poured in to a gel box and a 10-well comb was placed, supported by a groove provided in the gel box. After 60 min, once the gel was solidified, the comb was carefully removed and the gel was submerged in 1X TAE buffer. The wells were loaded with 8 µL each of the samples and controls, alongside 4 µL of a 100bp DNA ladder (50 µg/mL) and run at 80V for 2 hr until the bands were well separated. The gel was then imaged using a Bio-Rad ChemiDoc Imaging system.

2.2.3. Immunofluorescence microscopy (IF)

2.2.3.1. Seeding of cells

Cells maintained in complete media were seeded onto 12 well tissue culture plates containing sterile round glass coverslips. The plate was incubated for 24 hr under TC conditionsto allow for 70-80% confluence before fixation. The following seeding densities were used:

HeLa - 120,000 cells/well
VeroSLAM - 80,000 cells/well

The below sections detail the basic protocols that were followed for the corresponding experiments. The treatment of cells and incubation times prior to this varies depending on each experimental condition.

2.2.3.2. Fixation

2.2.3.2.1.Paraformaldehyde fixation and permeabilization

Cells were first washed 3 times (3x) with warm PBS and 500µL of 3% paraformaldehyde (PFA) solution was added per well. After 15 min

incubation, the cells were washed 3x with PBS and permeabilized with PBS containing 0.1% Triton X-100 and 50mM ammonium chloride (NH_4Cl) for 5 min. The cells were again washed 3x with PBS. In some cases, permeabilization of PFA fixed cells was done by 5 min incubation with PBS containing 0.01% saponin and 50mM NH_4Cl.

2.2.3.2.2. Methanol fixation

Cells were washed 3x with ice-cold PBS and 500 µL of ice-cold methanol (stored at -20ºC) was added per well. Immediately after this, the plate was kept in a -20°C freezer for 3 min The plate was then brought to room temperature (RT) and the cells were quickly washed 3x with PBS to remove all traces of methanol. No permeabilization step was done here.

2.2.3.2.3. Immunolabeling

2.2.3.2.3.1. Antibodies

The information about all primary and secondary antibodies used for immunolabeling are provided in Table 2.2. The table also includes information on the antibodies that were used for SLAM-receptor clustering experiments (section 2.2.16).

The antibody dilutions used for immunolabeling are mentioned in the table and were based on information provided in the product-data sheets. In some cases, in-house standardizations were done to determine the appropriate dilutions to be used.

Table 2.2 - Primary and secondary antibodies, dilutions and fixation methods used for Immunolabeling

Target protein and organelles	**Primary Antibody and Dilutions used**	**Secondary Antibody (1:500 Dilution)**	**Fixation method**
Early Endosome Antigen - 1 *Early endosomes*	Goat polyclonal anti-EEA1: N-19, Santa Cruz sc-6415 *1:200 Dilution*	Donkey anti-Goat Alexa Fluor - 488: A-11055, Invitrogen	PFA
LAMP-1 *Late endosomes and lysosomes*	Mouse monoclonal anti LAMP1 - FITC: H4A3, Santa Cruz sc-20011 *1:250 Dilution*	Nil (Directly labelled primary antibody)	Methanol
LAMP-1	Rabbit polyclonal anti LAMP1: L1418, Santa Cruz	Chicken anti Rabbit Alexa Fluor-647	
LC3B (Microtubule associated protein Light Chain 3B) *Autophagosomes*	Rabbit polyclonal anti-LC3B: #2775, Cell Signalling *1:500 Dilution*	Chicken anti-Rabbit Alexa Fluor-488: A-21441, Invitrogen	Methanol
Rab5 *Early endosomes*	Rabbit Monoclonal anti-Rab5: #3547 Cell signalling *1:500 Dilution*	Chicken anti-Rabbit Alexa Fluor-488: A-21441, Invitrogen	Methanol
Rab7 *Late endosomes and lysosomes*	Rabbit Monoclonal anti-Rab7: #9367, Cell signalling	Chicken anti-Rabbit Alexa Fluor-488: A-21441, Invitrogen	Methanol
SLAM (Signalling Lymphocyte Activation Molecule) *SLAM receptors*	*Mouse monoclonal anti SLAM/CD150 [IPO-3]: Abcam ab2604 *1:250 Dilution*	*Chicken anti-mouse Alexa Fluor-647: 21463, Invitrogen	PFA
Tubulin *Microtubules*	Mouse monoclonal anti-α-tubulin: T9026, Sigma Aldrich) *1:2000 Dilution*	Chicken anti-mouse Alexa Fluor-647: 21463, Invitrogen	Methanol

**These antibodies were also used for live imaging in SLAM-receptor clustering experiments (see section 2.2.16)*

2.2.3.2.3.2. Direct Immunolabeling

Cells grown on glass cover slips were fixed with 3% PFA for 15 min, washed 3x and permeabilized for 5 min with PBS containing 0.01% saponin and 50mM NH_4Cl. After washing the cells again, the cover slips were incubated for 30 min with blocking buffer (2% FBS, 2% BSA in PBS). This was done by first pipetting small drops (approximately 100 µL) of the blocking buffer on a parafilm placed on the flat surface of a workbench. The parafim is placed on a moist surface so that it remains fixed and the number of drops of blocking buffer varied depending on the number of conditions. Incubation of cells with blocking buffer was done by placing the cover slips cell-side down over these drops. This was followed by 60 min incubation with 100 µL of LAMP1-FITC antibody (1:250 dilution)diluted in blocking buffer containing 1 µg/mL Hoechst 33342. While incubating the cells with primary antibody, the coverslips were placed in dark. The cells on coverslips were then washed 3x 5 min with PBS by first aspirating the medium present in the wells and washing once with 500 µL PBS per well. The contents were again aspirated, fresh PBS added, and incubated for 5 min. This was again repeated twice. Finally, the coverslips were placed on to glass slides using 10 µL Dako fluorescence mounting medium and allowed to dry at RT for 2 hr. The glass slides with the coverslips were then either used directly for imaging by confocal microscopy (see section 2.2.7.1) or stored in a refrigerator at 4ºC until used.

2.2.3.2.3.3. Indirect Immunolabeling - Single antibody

The cells that were fixed on cover slips were first incubated with 150 µL blocking buffer (2% FBS, 2% BSA in PBS) for 30 min. This was followed by

60 min incubation with 100 µL of the primary antibody diluted in blocking buffer (Table 2.2). Cells were then washed 3x 5 min with PBS and incubated for 30 min with blocking buffer containing the appropriate anti species Alexa Fluor secondary antibody (Table 2.2) and Hoechst (1 µg/mL). Again, the cells were washed 3x5 min with PBS, mounted on to glass slides using 10 µL Dako fluorescence mounting medium and allowed to dry at RT for 2 hr. The glass slides containing the coverslips were then either used directly for imaging (see section 2.2.7.1) or stored in a refrigerator at 4ºC until used.

2.2.3.2.3.4. Indirect Immunolabeling - Double antibody

As mentioned above, the cells that were fixed on cover slips were first incubated with 150 µL blocking buffer (2% FBS, 2% BSA in PBS) for 30 min. This was followed by 60 min incubation with 100 µL of the primary antibody diluted in blocking buffer. Cells were then washed 3x5 min with PBS and incubated for another 60 min with 100 µL blocking buffer containing an appropriate dilution of the second primary antibody. This antibody was of a different species from that of the first primary antibody used. The cells were then washed 3x5 min with PBS and incubated with blocking buffer containing 1 µg/mL Hoechst 33342 and two appropriate anti-species Alexa Fluor secondary antibodies (1:500) corresponding to the primary antibodies used. After a final 3x5 min washing step, the cells were mounted on to glass slides using 10 µL Dako fluorescence mounting medium and allowed to dry at room temperature for 2 hr. The glass slides containing the coverslips were then either used directly for imaging (see section 2.2.7.1) or stored in a refrigerator at 4ºC.

2.2.4. Direct Fluorescence methods

2.2.4.1. Rhodamine phalloidin

Rhodamine Phalloidin was used for the staining of actin filaments. Cells on cover slips were fixed with 3% PFA and permeabilized with PBS containing either 0.1% Triton X-100 or 0.05% saponin, and 50mM NH_4Cl. The cells were then incubated with staining solution containing 0.5 µg/mL Rhodamine phalloidin and 1 µg/mL Hoechst33342 diluted in PBS. After an incubation period of 15 min in dark, the cells were washed 3x 5 min with PBS and mounted on glass slides using 10µL Dako fluorescence mounting medium. The glass slides with the coverslips were then either used directly for imaging (see section 2.2.7.1) or stored in a refrigerator at 4ºC.

2.2.5. Live cell Microscopy

2.2.5.1. Mitotracker staining

HeLa cells were seeded in 35mm MatTek imaging dishes at a seeding density of 270,000 cells/mL and incubated for 24 hr to reach confluence. After appropriate treatment conditions, the medium was aspirated and replaced with 50nM MitoTracker Red CMXRos solution prepared in serum free DMEM. After 5 min incubation, the medium was removed, cells washed 2x with warm PBS, and replaced with fresh imaging media (DMEM without Phenol red, supplemented with 10% FBS) before live imaging (see section 2.2.7.1).

2.2.6. Lysosome labelling with Dextran-fluorophore conjugates

Cells were seeded in 35mm MatTek live cell imaging dishes, the following seeding densities were used: HeLa - 150,000 cells/well and VeroSLAM -

120,000 cells/well, and incubated for 24 hr to reach confluence. The cells were then pulsed for 3 hr with 0.2 mg/mL 10kDa Dextran Alexa Fluor 488 (diluted in complete media) by incubating the cells with 200µL of the preparation at TC conditions. The dishes were then washed 2x with sterile warm PBS and 1 mL complete medium was added. After an 8hr chase at TC conditions, the cells were treated/not with 10µM cf2642 for 12 hr at TC conditions and then pulsed with 0.2 mg/mL 10kDa Dextran-Alexa 647 for 3 hr in the presence/absence of 10µM cf2642 at TC conditions. The cells were then chased for a further 3 hr w/o of 10µM cf2642 and live images were acquired by confocal microscopy (see section 2.2.7.1). The dispersal of lysosomes was calculated by drawing concentric ROIs at 1µM distance from each other around the nucleus. The intensity of fluorescence was then calculated at 0, 1, 2 and 3µM from the nucleus using ImageJ-Fiji. For this purpose, a macro was created as shown in Appendix B. The java program first splits the red and green channels and creates a nucleus mask to exclude the background and select only the area occupied by the nucleus. This is then used to draw concentric ROIs at 1µM distance apart, up to 3 µm around the nucleus.The red and green intensities are measured and the output is displayed in a table. A sample image is shown below, which shows the composite image to be analyzed, the split red and green channels, the nucleus mask and finally the 3 µm ROI around the nuclei.

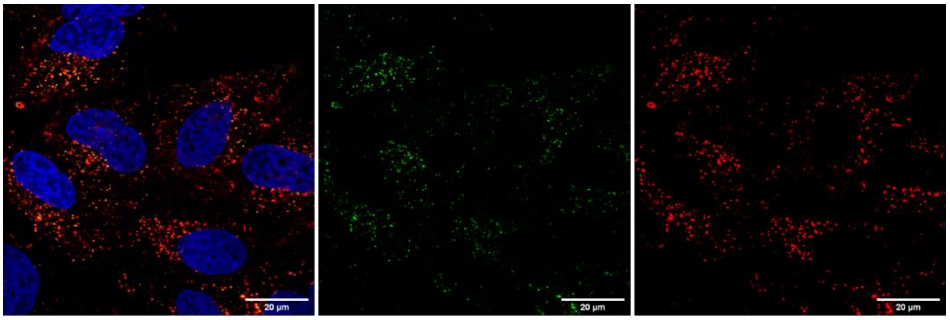

Merge Dextran 488 - Green Dextran 647 - Red

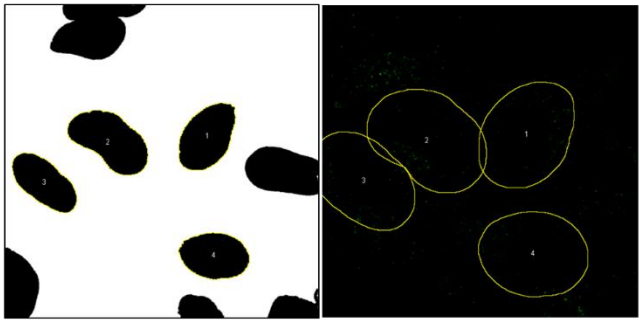

Merge Dextran 488 - Green

2.2.7. Microscopy

2.2.7.1. Confocal microscopy

Confocal fluorescence microscopy images were acquired on a Leica SP5 inverted confocal laser scanning microscope. A 63x HCX PL APO 63x 1.4 NA oil-immersion objective (Leica Type F immersion oil) was used for all confocal experiments in this thesis. Lasers 405, 488, 543 and 633 nm were used interchangeably and the “Gain” and “Off-set” settings were optimized for each experiment to obtain image acquisition without saturation. The Leica Application Suite X (LAS X) software was used for capturing images. The sequential scanning mode was used to prevent bleed-through resulting due to spectral overlap of excitation/emission spectra of the different fluorophores used. Images were scanned at 400 Hz with a line average of three, to reduce noise. For live imaging experiments, the laser scanning speed was increased to either 700Hz or 1000Hz for fast imaging. The TC conditions required for live imaging was facilitated using an Ibidi gas incubation system which includes a temperature stage that maintains the temperature at 37ºC and provides a humidified atmosphere supplied with 5% CO_2 within a closed environment.

2.2.8. Western Blotting

The below sections detail the basic protocols that were followed for the corresponding experiments. The treatment of cells and incubation times prior to this varies depending on each experimental condition.

2.2.8.1. Seeding of cells

Cells were seeded in 6-well tissue culture plates in complete media and allowed to incubate for 24 hr under TC conditions before treatment. The

cells were subjected to different treatment conditions before collecting lysates. The following seeding densities were used.

HeLa - 240,000 cells per well
VeroSLAM - 160,000 cells per well

2.2.8.2. Lysate collection and preparation

2.2.8.2.1. Lysate collection

The medium was first aspirated from all wells, cells washed twice with ice-cold PBS and 150µL of NP-40 lysis buffer (150 mM NaCl, 50 mM Tris base pH 8 and 1% Nonidet P-40 with protease inhibitors) was added to each well. The plate was then placed on ice and moved to a belly dancer shaker for 15 min to allow proper contact of the lysis buffer to all parts of the well. The contents were then scraped using a cell scraper, transferred to ice-cold 1.5 mL centrifuge tubes and centrifuged at 13,800 x *g* for 10 min. The supernatants were then pipetted into fresh 1.5mL centrifuge tubes placed on ice.

2.2.8.2.2. Quantification of total protein content by BCA assay

The protein concentration of the cell lysates was determined by bicinchoninic acid (BCA) assay. Bovine serum albumin (BSA) protein standards were prepared in lysis buffer at concentrations ranging from 0 to 1 mg/mL. Cell lysates were diluted 1:5 in lysis buffer so that they fit within the working range of the BSA protein standards. 200µL of working BCA solution (49 parts bicinchoninic acid with 1part copper sulphate pentahydrate) was then pipetted into a 96 well plate.Triplicatemeasurements for both BSA standards and samples were made. 10 µL of the standards/samples were

added to the wells, the plate was incubated at 37ºC for 30 min and absorbance was measured at 562 nm using a plate reader. The concentration of total protein of cell lysates were measured using a calibration curve created by plotting the absorbance measurements against standard protein concentrations prepared with bovine serum albumin (BSA)

2.2.8.3. Preparation of cell lysates

Sample concentrations were adjusted to make 100µL of 1µg/µL protein per sample and a suitable volume of 4x loading buffer (2% sodium dodecyl sulphate [SDS], 10% glycerol, 0.02% bromophenol blue, 62.5 mM Tris-HCL) were added to each of the samples. The samples were then denatured by heating at 95°C for 5mins and centrifuged at 13,800 x *g* for 30 s.

2.2.8.4. Western Blotting protocol

2.2.8.4.1. Preparation of SDS-PAGE gels

The SDS-PAGE gels were cast and run on a Bio-Rad Mini-Protean II SDS-PAGE kit. Both the front and back plates were properly cleaned and wiped with ethanol and assembled in the clamp frame so that they were secured within the casting stand. Both the Resolving and stacking gels were prepared as per the list of ingredients in Tables 2.3 and 2.4 below. In both cases, Tetramethylethylenediamine (TEMED) was added only at last. Western blotting protocol used here was as per Laemmli's protocol (Laemmli, 1970).

Table 2.3 - List of ingredients for preparation of Resolving gel

% of Gel	12%
Total Volume	10 mL
40% acrylamide/Bis	3 mL
3 M Tris pH 8.8	1.25
10% SDS	100 µL
10% APS (freshly made)	75 µL
TEMED	7.5 µL

Table 2.4 - List of ingredients for preparation of Stacking gel

% of Gel	10%
Total Volume	10 mL
40% acrylamide/Bis	1.1 mL
1 M Tris pH 6.8	1.3 mL
Distilled water	7.22
0.1% Bromophenol blue	300 µL
10% SDS	100 µL
10% APS (freshly made)	75 mL
TEMED	100 µL

The stacking gel was first poured between the glass plates and allowed to reach up to 3/4th of the height, giving enough space for the stacking gel. Isopropanol (500µL) was added over the top in order to get an even surface. Once the resolving gel was set, the isopropanol was removed by

washing 2x with distilled water. Any excess water between the plates was removed and the stacking gel was poured up to the top. A 10 well plastic comb was carefully placed, avoiding the formation of air bubbles. The gel was then allowed to dry and the comb was carefully removed. The gel - glass plate apparatus was then carefully transferred to the SDS-PAGE tank, immersed in running buffer (385 mM glycine, 250 mM Tris base, 0.5% SDS) and the samples were loaded.

2.2.8.4.2. Sample loading and SDS-PAGE

15 µg protein from each sample was loaded onto a 4% acrylamide stacking gel alongside 10 µL of the protein standard molecular weight marker. Protein separation was done at 100 V on a 12% acrylamide resolving gel for 90 min.

2.2.8.4.3. Protein transfer and Ponceau staining

A Bio-Rad Mini Trans-Blot Electrophoretic Transfer Cell apparatus was used to transfer proteins onto a Polyvinylidene fluoride (PVDF) membrane, as per the manufacturer's instructions. Protein transfer was done at 100V for 1 hr at 4°C. The membrane was then washed gently in distilled water.

The PVDF membrane was immersed in Ponceau S solution for 5 min. The membrane was rinsed once in distilled water and checked for proper protein transfer. The membrane was then gently rinsed in distilled water until all traces of the stain was removed.

2.2.8.4.4. Protein detection by immunoblotting

The PVDF membrane was first blocked with 5% milk prepared in PBST (0.025% Tween20 in PBS) solution. The membrane was then incubated overnight in a cold room 4°C on a belly dancer shaker with primary antibodies (see Table 2.5) diluted in 2% milk. The primary antibodies used were as follows:

The membrane was washed again for 3x 5 min in PBST and incubated for 1 hr at RT (on a shaker) with the secondary antibody diluted in 2% milk in PBST.

Table 2.5 - Primary and secondary antibodies for Western blot

Primary Antibody	Secondary Antibody
Rabbit Anti-LC3B antibody - 1:1000 dilution (Abcam ab51520)	Goat anti rabbit IgG, HRP - 1:2000 dilution (Fisher 31460)
Mouse GAPDH antibody - 1:1000 dilution (Abcam ab8245)	Goat anti-mouse IgG, HRP - 1:2000 dilution (Fisher 31430)

The membrane was washed a further 3 x 5 min in PBST before development. The detection of proteins was done using SuperSignal West Femto chemiluminescence reagent. 1 mL each of the reagents were mixed and together and applied to the PVDF membrane and incubated at RT for 5 min. The excess solution was removed and the membrane was directly imaged using a Bio-Rad ChemiDoc system.

2.2.8.4.5. Quantification of bands

The quantification of band intensities from digital images was done using Fiji/ImageJ software. Initially, the “Rectangle” selection tool was used to draw a narrow box enclosing the bands corresponding to the protein of interest.

The Analyze>Gels>Select First Lane command was used to select the box and identify it as lane “1”.

Profile plots were then drawn with the Analyze>Gels>Plot Lanes command and the resulting plot showed the relative density of all the bands within the selected box. The plots provided information about the size (width of peak) and darkness (height of peak) of the bands.

The width of the peaks represented the size/area of the bands and the peak height represented the shade/darkness of the bands. The “Straight” line tool was then used to draw a line across the base of all the peaks and the “Wand” tool was used to select all the peaks. Now the measurements corresponding to the band intensities appeared as a pop up window, which were then exported to excel for analysis. The values for band intensities we normalized to the loading control for the final analysis.

2.2.9. Cell viability

Cell viabilities were determined using the CellTiter-Blue® cell viability assay as per the manufacturer’s instructions. Cells were seeded in black 96-well plates and incubated for 24 hr under C conditions to reach 70-80% confluence. After treatment of the cells, 20µL of CellTiter-Blue reagent was added to each of the wells and the plates were incubated for 4hr.

Staurosporine (1 µM) was used as positive control for cytotoxicity and DMSO was used a vehicle control. At the end of the incubation period, fluorescence (544Ext/590Ems) measurements were acquired using a Fluostar Optima fluorescent plate reader.

2.2.10. LDH cytotoxicity Assay

Cell viability was measured using LDH cytotoxicity Assay Kit as per the manufacturer's instructions. Briefly, VeroSLAM cells were seeded in 96 well tissue culture plates and incubated at TC conditions for 24 hr prior to treatment of cells. Cells were treated or not with 10µM cf2642 for 24 hr, followed by which 50 µL of the contents from each well were transferred to a flat bottom 96 well tissue culture plate and 50 µL of the Reaction Mixture was added to all wells. The plates were incubated for 30 min in dark and 50 µL of Stop solution was added to all wells. After gentle tapping to remove bubbles, absorbance was measured at 490nm using a plate reader. The cells were incubated with the following controls were used for the calculation for LDH release and cytotoxicity.

- Spontaneous LDH Activity Controls (sterile ultrapure water)
- Maximum LDH Activity Controls (10X lysis buffer)
- Positive control (prepared by diluting 1 µL LDH positive control in 10 mL 1% BSA in PBS)
- Blank (complete medium only)

The LDH release was calculated by subtracting the absorbance at 650 nm (background) from that of 450 nm. This value was used to calculate the percentage of cytotoxicity as per the formula:

% Cytotoxicity = (Compound-treated LDH activity – Spontaneous LDH activity) / Maximum LDH activity – Spontaneous LDH activity × 100

2.2.11. Production of MeV stocks and titration

2.2.11.1. Production of MeV stock

VeroSLAM cells were maintained in five T-150 tissue culture flasks containing DMEM supplemented with 2.5% FBS, 10mM HEPES (4-(2-hydroxyethyl)-1-piperazineethanesulfonic acid) and 25mM Magnesium sulphate ($MgSO_{4)}$ in the absence of geneticin. The HEPES served to maintain the pH of the extracellular medium and $MgSO_4$ stabilized the virus particles released from infected cells (Weiss et al., 2012). For virus inoculation, media from the flasks was aspirated and 2 mL of MeV stock ($TCID_{50}$ titre - 10^4 virions/mL) was added gently to come in contact with the cell monolayer. The flasks were tilted sideways to allow even contact with all cells and then incubated for 1 hr under TC conditions for virus adsorption. Then 15mL of fresh complete medium was added to the flasks and further incubated for up to 72 hr. The cells were observed under the microscope to check for cytopathic effects (CPE) - appearance of multinucleated giant cells confirmed the presence of CPE. The cells were then scraped from the walls of flasks, mixed with the medium and passed through 25-gauge hypodermic syringe needles to release intracellular virus particles. The resulting virus stock was centrifuged at 800 x *g* for 15 min to remove cell debris. The stock was then supplemented with 20% FBS and stored as 2 mL aliquots at -80ºC until needed.

2.2.12. Titration of MeV stocks by TCID50 assay

50% tissue culture infective dose (TCID50) method, also known as end point dilution assay, was used to titrate the MeV virus stocks. B95a cells were seeded in a 96 well plates and grown to ~80% confluence. A series of eight 10-fold dilutions of the virus was prepared in complete media and added to the corresponding wells. Both virus and non-infected (mock) controls were also made. The plate was incubated for 3 days and observed for CPE. Virus titer was calculated based on the method previously described by Reed and Muench (Reed and Muench, 1938). An estimation of the number of virus particles in the stock was made based on the average lowest dilution at which CPE was observed.

2.2.13. MeV syncytia assay

VeroSLAM cells were seeded 6 well tissue culture plates at a density of 160,000 cells per well and incubated for 24 hr at TC conditions. Cells were then infected with MeV at MOI 0.5 in the presence or absence of 10µM cf2642 and incubated for 12 hr at TC conditions. Bright field images were captures using a Leica DMIRB inverted microscope equipped with a 10x objective.

2.2.14. MeV plaque assay

2.2.14.1. Crystal violet solution

A 1 L crystal violet solution was prepared by diluting 2.5 g crystal violet in 50 mL 37% formalin, 100 mL of ethanol and 850 mL distilled water.

2.2.14.2. Plaque assay

VeroSLAM cells were seeded in a 6 well tissue culture plate at a density of 200,000 cells per well and incubated for 12 hr at TC conditions. Cells were then infected with MeV at MOI 0.5 in the presence or absence of 1, 5 and 10µM cf2642 and incubated at TC conditions for 12 hr. At the time of infection/treatment, a 24 well plate was seeded with VeroSLAM cells so that they are confluent after 12 hr when the above mentioned incubation period is completed. After the 12 infection/treatment period, the supernatants from all wells were carefully transferred to a sterile 24 well plate and three 5-fold dilutions were made using complete medium. The diluted supernatants were then used to infect the previously prepared 24 well plate with VeroSLAM cells. Infection was done by incubating cells with the supernatants (all dilutions) for 60 min to allow virus adsorption. The contents were then aspirated and cells washed gently with warm PBS. An overlay (500 µL) containing 1.5 % agarose dissolved in DMEM containing 2 % FBS was gently added to all wells and the plate was incubated for 3 days at TC conditions. A crystal violet staining solution (see above) was then added to all wells and the plate was left at RT for 4 hr. The contents of the wells were then aspirated and cells washed 4x with PBS until all residues of the staining solution were removed. The plate was then left to dry at RT before counting the plaques. The virus titres were calculated by counting the number of plaques in each well and multiplying it by ten to the power of the dilution factor.

2.2.15. MeVautophagy

VeroSLAM cells were seeded in 6 well tissue culture plates at 160,000 cells per well and incubated for 24 hr at TC conditions to reach confluence. Cells were then infected with MeV at MOI0 0.5 in the presence or absence of 10µM cf2642 and 50 µM chloroquine for 12 hr. Protein expression levels of LC3B and GAPDH were then analyzed by western blotting as in section 2.2.8.4.

2.2.16. SLAM-receptor clustering

2.2.16.1. Antibody-mediated clustering of SLAM receptors

The clustering of SLAM receptors in VeroSLAM involved the use of Alexa Fluor 647 conjugated secondary antibodies commercially available from Fisher. Since they contain 5 mM sodium azide which is toxic to cells, the preservative was first removed from the antibody.

2.2.16.1.1. Purification of antibody using centrifugal filters

Chicken anti-mouse Alexa Fluor - 647 antibody (300 µL see Table 2.2) was first diluted in 1 mL sterile PBS. Amicon Ultra 50K centrifugal filters contain two parts: a small tube with the 50 kDa filters at its bottom, which is inserted into a larger 0.5 mL collection tube. The antibody-PBS solution was transferred equally to two 0.5mL filter tubes. These were inserted into their respective collection tubes and centrifuged at 13,800 x *g* for 10 min. The filter tube was then carefully removed, placed inside the collection tube in an inverted position, and centrifuged at 1000 x *g* for 2 min to transfer the eluate to the bottom of the tube. To collect any residual antibodies attached to the filter, this step was again repeated by adding 20 µL PBS to the filter device.

2.2.16.1.2. Calculation of dye-protein ratio

In order to use the new purified antibody solution for experiments, it was important to determine whether there was any loss in the protein:dye conjugation (dye:protein or F/P molar ratio). The F/P ratio provides information about the number of fluorophore dye molecules that are conjugated to the antibody (protein) binding sites. The ratio obtained was then compared to the value for the original antibody solution. Measurement of the F/P ratio was done using a UV spectrophotometer.

2.2.16.1.3. Measurement of absorbance

The absorbance measurement was done using a UV spectrophotometer. A blank value was first set using a cuvette filled with 200µL PBS. The absorbance at two different wavelengths A_{MAX} (absorbance at 650nm) and A_{280} (Absorbance at 280 nm)were measured using a Cary 60 UV spectrophotometer. Similarly, absorbance was measured for the control chicken anti-mouse Alexa Fluor-647 antibody taken directly from the vial (without filtration) and the filtered antibody. The antibody solutions were diluted 1:50 in PBS for absorbance readings.

Calculation of the protein concentration and dye-protein mole ratio was done as per the formula:

Protein concentration (M) = $[A_{280} - (A_{MAX} \times CF) / \varepsilon] \times$ *Dilution factor*

Moles dye per molecule protein = [A_{MAX} of labelled protein/ (ε´ x protein concentration (M))] x Dilution factor

- *Extinction molar coefficient (ε) of IgG = 210,000M-1 cm-1*
- *Extinction coefficient of the dye/fluorophore molecule (ε´) of Alexa Fluor 647 = 270,000*
- *Correction factor (CF)* = A_{280}/A_{MAX} of the fluorophore = 0.3

- *Dilution factor = 50 (1:50 dilution)*

2.2.16.1.4. Clustering of SLAM receptors

2.2.16.1.4.1. Seeding of cells

VeroSLAM cells were seeded in 35 mm glass bottom MatTek dishes at a cell density of 160,000 cells per dish and incubated for 24 hr at TC conditions to reach 70-80% confluence.

2.2.16.1.4.2. Fixed cell imaging

2.2.16.1.4.2.1. Dose response of Alexa Fluor-647 conjugated secondary antibodies

Live VeroSLAM cells were first incubated with 2 µg/mL mouse anti SLAM antibody (see Table 2.2) diluted in complete DMEM for 30 min w/o 10µM cf2642 at TC conditions. The cells were then washed 3x with warm PBS and incubated with 2, 6 and 10µg/mL chicken anti mouse Alexa Fluor-647 secondary antibody for 60 min in the presence or absence of 10µM cf2642 at TC conditions. This was followed by a further 3x wash with PBS and cells were further incubated (chase) w/o 10µM cf2642 for 60 min at TC conditions. Finally, the cells were washed 2x with warm PBS and fixed with 3% PFA for 15 min and permeabilized for 5 min with PBS containing 0.05% saponin and 50 mM NH_4Cl. Immunolabelling with LAMP1-FITC antibody was done to label the lysosomes (see section 2.2.3 for IF protocol).

For the quantification of internalized SLAM positive vesicles, the images were first split in to red (SLAM), green (LAMP1) and blue (nuclei) channels. Region of interests (ROIs) were then drawn around cells to include only the internal region of the cells. This was done by using the SLAM labelling of the

plasma membrane and Hoechst stain of the nucleus as a guide. A macro (see Appendix 1) was used to measure the following parameters: total number, area and integrated density of the internalized SLAM-positive vesicles. The measurements were taken for 30 cells per condition.

2.2.16.1.4.2.2. Indirect SLAM-receptor clustering – 2 and 6 hr

Live VeroSLAM cells were incubated with 2 µg/mL mouse anti SLAM antibody diluted in complete DMEM for 30 min w/o 10µM cf2642 at TC conditions. The cells were then washed 3x with warm PBS and incubated with 6 µg/mL chicken anti mouse Alexa Fluor-647 secondary antibody for 60 min in the presence or absence of 10µM cf2642 at TC conditions. This was followed by a further 3x wash with PBS and cells were further incubated (chase) w/o 10µM cf2642 for either 1 or 5 hr at TC conditions. Finally, the cells were washed 2x with warm PBS and fixed with 3% PFA for 15 min and permeabilized for 5 min with PBS containing 0.05% saponin and 50 mM NH_4Cl. Immunolabelling with LAMP1-FITC antibody was done to label the lysosomes (see section 2.2.3 for IF protocol).

Cells without SLAM-clustering served as the no-clustering controls wherein the cells were incubated with the primary mouse anti-SLAM antibody w/o cf2642 as mentioned above, washed 3x with warm PBS and incubated with complete media w/o cf2642 for either 1.5 or 5.5 hr before fixing the cells. In this case, immunolabelling was done to label both SLAM (mouse anti-SLAM antibodies) and the lysosomes (LAMP1-FITC antibodies).

2.2.16.1.4.2.3. Indirect SLAM-receptor clustering using unconjugated secondary antibodies.

Live VeroSLAM cells were incubated with 2 µg/mL mouse anti SLAM antibody diluted in complete DMEM for 30 min on ice. The cells were then washed 3x with warm PBS and incubated with 6 µg/mL goat anti mouse Alexa Fluor-647 secondary antibody for 60 min in the presence or absence of 10µM cf2642 at TC conditions. This was followed by a further 3x wash with warm PBS and cells were further incubated (chase) w/o 10µM cf2642 for either 1 or 5 hr at TC conditions. Finally, the cells were washed 2x with warm PBS and fixed with 3% PFA for 15 min and permeabilized for 5 min with PBS containing 0.05% saponin and 50 mM NH_4Cl. Immunolabelling was done with Rabbit anti-LAMP1 antibodies to label the lysosomes and donkey anti-goat Alexa Fluor-488 secondary antibodies to label the SLAM receptors. (see section 2.2.3 for IF protocol and Table 2.2 for details on primary and secondary antibodies used).

Cells without SLAM-clustering served as the no-clustering controls wherein the cells were incubated with the primary mouse anti-SLAM antibody w/o cf2642 as mentioned above, washed 3x with warm PBS and incubated with complete media w/o cf2642 for either 1.5 or 5.5 hr before fixing the cells. In this case, immunolabelling was done to label both SLAM (mouse anti-SLAM antibodies) and the lysosomes (Rabbit anti-LAMP1 antibodies).

2.2.16.1.4.2.4. Indirect SLAM-receptor clustering in live cells

VeroSLAM cells were seeded in 35 mm glass bottom MatTek dishes at a cell density of 100,000 cells per dish and incubated for 24 hr at TC conditions to reach 70-80% confluence. Cells were then pulsed for 2 hr with

0.2 mg/mL 10 kDa Dextran Alex Fluor-488 and chased for 18 hr to label the lysosomes. Cells were then incubated with 2 µg/mL mouse anti SLAM antibody diluted in complete DMEM for 30 min w/o 10µM cf2642 at TC conditions. The cells were then washed 3x with warm PBS and incubated with 6 µg/mL chicken anti-mouse Alexa Fluor-647 secondary antibody for 60 min in the presence or absence of 10µM cf2642 at TC conditions. This was followed by a further 3x wash with warm PBS and cells were further incubated (chase) w/o 10µM cf2642 for either 1 or 5 hr at TC conditions. Live images were then captured by confocal microscopy (see section 2.2.7.1).

Cells without SLAM-clustering served as the no-clustering controls wherein the Detran-488 labelled cells were incubated with the primary mouse anti-SLAM antibody w/o cf2642 as mentioned above, washed 3x with warm PBS and incubated with complete media w/o cf2642 for either 1.5 or 5.5 hr before imaging. Cells were incubated with either vehicle (DMSO) or cf2642 to serve as controls without incubation with any antibodies. For the secondary antibody controls, cells were initially incubated for 30 min w/o cf2642, washed and incubated with 6 µg/mL chicken anti-mouse Alexa Fluor-647 secondary antibody for 60 min w/o cf2642, washed and incubated for either 1 or 5 hr w/o cf2642 at TC conditions.

2.2.16.1.4.3. Actin labelling

VeroSLAM cells were seeded in 35 mm glass bottom MatTek dishes at a cell density of 100,000 cells per dish and incubated for 24 hr at TC conditions to reach 70-80% confluence. Cells were incubated with 2 µg/mL mouse anti-SLAM antibodies w/o 10µM cf2642 for 30 min at TC conditions

and clustered with 6 µg/mL chicken anti mouse Alexa Fluor - 647 antibodies in the presence of absence of cf2642 for 60 min. Cells were then chased for either 30 or 60 min w/o 10µM cf2642 at TC conditions. This was followed by fixation of cells with 3% PFA and permeabilization for 5 min with PBS containing 0.05% saponin and 50 mM NH_4Cl. The actin filaments and nuclei were labelled by incubating cells for 30 min with PBS containing rhodamine phalloidin and 1 µg/mL Hoechst. Cells were then washed 2x with PBS and the MatTek dishes containing cells (with PBS) were used for imaging.

2.2.17. Transferrin uptake assay

Live VeroSLAM cells were initially incubated with serum free DMEM for 30 min at TC conditions, followed by which cells were incubated with serum free medium containing 1X cell mask deep red plasma membrane stain and 5 µg/mL transferrin conjugated with Alexa Fluor-488 (Tf-488) for 30 min on ice. Cells were then chased at 37ºC for up to 30 min in the presence or absence of 10µM cf2642 and live images were captured at 10 min intervals.

2.3. Dextran uptake assays

2.3.1.1.1. Dextran uptake assay by MeV

VeroSLAM cells were seeded in 24-well tissue culture plates at a seeding density of 40,000 cells/well and incubated for 24 hr at TC conditionsto reach ~80% confluence. The cells were then washed with ice-cold PBS and gently scraped from the surface using the rubber end of a 1 mL syringe plunger.

Cells were then transferred to 1.5 mL Eppendorf tubes and centrifuged at 300 x *g* for 4 min. The tubes cells were then placed on ice, infected or not with MeV (MOI 0-100) in ice-cold complete medium and incubated for 60 min. Subsequently, the cells were moved to a 37°C water bath and 0.1 mg/mL of 10kDa Dextran Alexa Fluor 488 (Dextran-488) with or without 10µM cf2642 was added during the last 5 min of the 5, 15 and 30 min time points as shown in Fig 2.1. At the end of each time point, the tubes were placed on ice for 10 min, washed 2x with ice-cold FACS medium (PBS containing 10% FBS) and centrifuged at 300 x *g* for 5 min. Finally, the cells were fixed for 15 min with 3% paraformaldehyde (PFA), washed 2x with ice-cold FACS medium and used for flow cytometry analysis (see section 2.2.13.3.9).

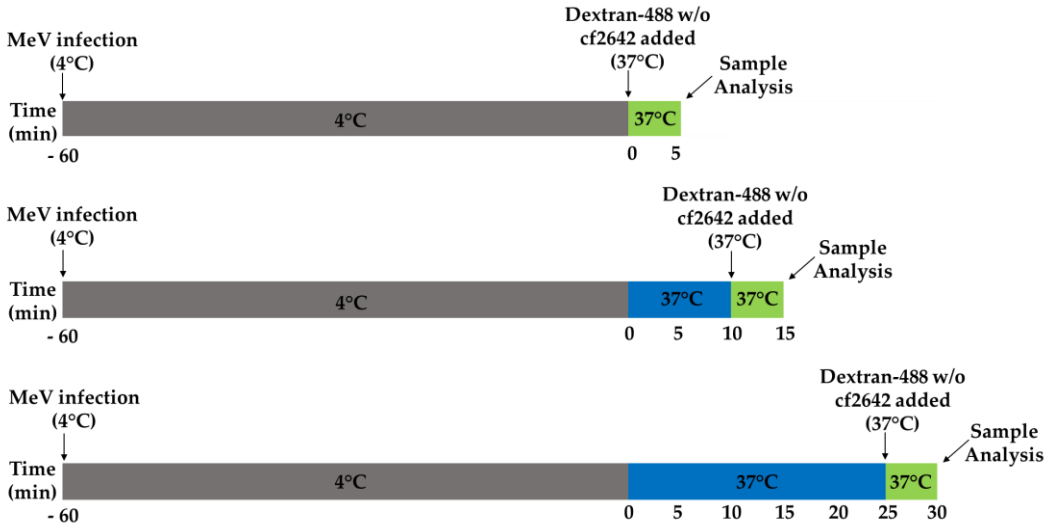

Fig 2.1 Methodology for Dextran-488 uptake assay using MeV. VeroSLAM cells were infected with virus at 4ºC for 60 min, moved to 37 ºC and Dextran - 488 w/o 10µM cf2642 was added at different time points as indicated. Initially, the cells were exposed to Dextran-488, only during the initial 5 min (marked in green), after which the cells are processed for analysis. For the 15 and 30 min time points, cells were first incubated at 37°C for 10 and 25 min respectively, followed by the addition of Dextran-488 during the last 5 min.

2.3.1.1.2. Dextran uptake assay by direct SLAM-receptor clustering

The methodology followed here was similar to section 2.2.15.1 above, but without the use of live virus. VeroSLAM cells were seeded in 24-well tissue culture plates at a seeding density of 40,000 cells per well and 24 hr post seeding, the cells were washed with ice-cold PBS, scraped from the surface, transferred to 1.5 mL Eppendorf tubes and centrifuged at 300 x *g* for 4 min. The tubes were placed on ice and the cells incubated for 60 min with 6µg/mL of rabbit anti-SLAM polyclonal antibodies diluted in ice-cold complete medium. Subsequently, the cells were moved to a 37°C water bath and 0.1 mg/mL of 10kDa Dextran Alexa Fluor 488 (Dextran-488) with or without 10µM cf2642 was added during the last 5 min of the 5, 15 and 30 min time points as shown in Fig 2.1. At the end of each time point, the tubes were placed on ice for 10 min, washed 2x with ice-cold FACS medium and centrifuged at 300 x *g* for 5 min. Finally, the cells were fixed for 15 min with 3% paraformaldehyde (PFA), washed 2x with ice-cold FACS medium and used for flow cytometry analysis (see section 2.2.13.3.9).

2.3.1.1.3. Dextran uptake assay by indirect SLAM-receptor clustering

The methodology followed here was similar to section 2.2.17.1.3 above, but using a combination of primary and secondary antibodies to cluster SLAM receptors. VeroSLAM cells were seeded in 24-well tissue culture plates at a seeding density of 40,000 cells per well and 24 hr post seeding, cells were incubated for 30 min with 2 µg/mL mouse anti-SLAM antibody at TC conditions. (see Table 2.2 for details about the antibody). Cells were then washed 2x in warm PBS and incubated with 6 µg/mL Alexa Fluor-647

conjugated polyclonal chicken anti-mouse antibodies for 60 min on ice. The cells were then gently scraped from the wells, transferred to 1.5 mL Eppendorf tubes and moved to a 37ºC water bath. Then 0.1 mg/mL of 10kDa Dextran Alexa Fluor 488 (Dextran-488) with or without 10µM cf2642 was added during the last 5 min of the 5, 15 and 30 min time points as shown in Fig 2.1. At the end of each time point, the tubes were placed on ice for 10 min, washed 2x with ice-cold FACS medium and centrifuged at 300 x g for 5 min. Finally, the cells were washed 2x with ice-cold FACS medium and used for flow cytometry analysis (see section 2.2.13.3.9).

2.3.2. Actin labelling in MeV infect cells

VeroSLAM cells were grown over glass cover slips in 12 well plates and 24 hr post seeding, the cells were infected or not with MeV (MOI-10) for 30 min in the presence or absence of 10µM cf2642. Cells were then washed with warm PBS and fixed with 3% PFA for 15 min. Cells were permeabilized with 0.01% Trixon X 100 in PBS for 10 min, washed and further incubated for 30 min with PBS containing 0.2 µM Alexa Fluor 647 Phalloidin and 5 µg/mL DAPI to stain Actin filaments and nucleus respectively. The cover slips were mounted on glass slides using Dako mounting fluid and allowed to dry at room temperature before imaging. (see section 2.2.7.1 for details on microscopy)

2.3.3. cf2642 MoA studies

In order to study the MoA of cf2642 against MeV, a series of experiments were performed to test the effect of the drug on different stages of virus life cycle.

2.3.3.1.1. Time of addition (ToA) assay

VeroSLAM cells were seeded at a density of 40,000 cells per well in a 24 well plate and incubated for 24 hr at TC conditionsso that cell confluence was at about 70-80% at the time of infection. Cells were then infected or not with MeV-GFP (MOI - 0.5) and treated with 10µM cf2642 at different time points pre and post-infection. At the end of the T0 + 12 hr time point, cells were further incubated for 12hr at TC conditions. Cells were then scraped from the wells using the rubber end of a 1 mL syringe plunger, re-suspended in ice-cold FACS medium and centrifuged at 300 x *g* for 5 min. Finally, the cells were fixed for 15 min with 3% PFA and washed 2x with ice-cold FACS medium. Flow cytometry analysis (see section 2.2.20.1.3) was performed to analyze the number of GFP positive cells.

2.3.3.1.2. Measles entry and spread assay

VeroSLAM cells were seeded in a 12 well tissue culture plate at 60,000 cells/well and incubated at TC conditionsfor 24 hr to reach ~80% confluence. Cells were infected or not with MeV-GFP (MOI - 0.5) for 2 hr in the presence or absence of 10µM cf2642. Then the cells were washed 2x with sterile warm PBS and further incubated in the presence or absence of 10µM cf2642 for further 24 hr at TC conditions. To study the effects of cf2642 on virus spread, cf2642 was either added either only during the initial

2 hr incubation step or only during the subsequent 24 hr incubation. The cells were then scraped from the wells, fixed with 3% PFA for 15 min and the percentage of EGFP positive cells was analyzed by flow cytometry (see section 2.2.13.3.9 below).

2.3.3.1.3. Flow cytometry analysis

The flow cytometry analysis involved in the cf2642 MoA studies varied with the type of instrument used, cell type, detection parameters and the gating of cells. Hence, the information pertaining to all these experiments are summarized in this section.

Section 2.2.18.1.1 - The Dextran-488 fluorescence in MeV infected cells was analyzed on a BD FACSCanto II flow cytometer using a 488 nm laser and 530/30 filter. Cells were first gated using FSC-A/SSC-A to remove dead cells and debris, followed by FITC-A/FSC-A, to separate Dextran-488 positive cells.

Section 2.2.18.1.3- Dextran-488 fluorescence in SLAM-clustered cells was analyzed on a BD FACSVerse flow cytometer using a 488 nm laser and 527/32 filter. Cells were first gated using FSC-A/SSC-A to remove dead cells and debris, followed by Alexa 488-A/FSC-A, to separate Dextran-488 positive cells.

Sections 2.2.20.1.1 and 2.2.20.1.2 - The analysis of EGFP positive cells was done on a BD FACSCanto II flow cytometer using a 488 nm laser and 530/30 filter. Cells were first gated using FSC-A/SSC-A to remove clumped/aggregated cells formed as a result of virus induced CPE. Then the cells were gated by FITC-A/FSC-A, to separate the EGFP positive cells.

2.3.3.1.4. Impedance assay

Impedance assay measurements were acquired using an RTCA xCELLigence instrument (ACEA Biosciences). Initially, complete medium (100 µL) was added to all wells in a 16 well plate (E Plate-16) that is provided as part of the instrument. The plate was then placed inside the xCELLigence Instrument equipped with plate cradles, and the entire apparatus was placed inside an incubator at TC conditions. The xCELLigence software was then used to set the background values from the E plate-16 inside the incubator. The plate was then removed and VeroSLAM cells were seeded at 10,000 cells (in 100 µL complete medium) per well, followed by which the plate was replaced in the xCELLigence Instrument inside the incubator. The time intervals for acquiring the impedance measurements in real time was set using the xCELLigence software. During the initial 24 hr time period post seeding of cells, measurements were taken every 15 min. After 24 hr, the plate was removed from the incubator and infected or not with MeV at MOI 0.5 in the presence or absence of 1, 5 and 10µM cf2642 in sterile conditions. The plate was then replaced in the incubator and remaining impedance measurement cycle was initiated. Impedance measurements were acquired at 1 min intervals from 24 to 27 hr post infection and at then 15 min intervals during 27 to 100 hr incubation periods. After completion of the cycle, the plates were removed from the incubator and discarded appropriately. The measurements were then exported into an excel sheet for analysis.

2.3.3.1.5. Statistics

The statistics for all flow cytometry data represent Median Fluorescence Intensity (MFI) from three (or four) independent experiments. Statistical analysis was done using two-tailed unpaired Students t-test and a P value of < 0.05 was considered statistically significant.

Chapter 3 - Effect of cf2642 on cell viability, MeV autophagy and virus titres

3.1. Introduction

The MoA of cf2642 against MeV and VACVwas hypothesized to target a cellular pathway that in turn contributes to the antiviral activity against both these viruses. (McGuigan et al., 2013). On that note, initial studies were performed to test the effect of cf2642 on cell viability of two cell lines namely HeLa and VeroSLAM that were used in this study. Subsequent experiments were performed to test the anti MeV effects of cf2642 in VeroSLAM cells using both microscopy and estimation of virus titers.

Autophagy is a cellular process which involves the degradation of cellular components targeted for elimination(Dong and Levine, 2013). See section 1.8 for more details.MeV has been previously shown to induce autophagy in infected cells starting from 12 hr and up to 16 hr post infection. This, coupled with autophagy induced as a result of syncytia formation, serves as a feedback loop to maintain successive autophagy flux during infection. Since MeV induced autophagy facilitates in virus spread and escape from host mediated immune responses (Richetta et al., 2013), the effect of cf2642 on this cellular process was investigated.

In this chapter all MeV experiments were performed at the Bundeswehr Institute for Microbiology in Munich, Germany, while other experiments were performed in the School of Pharmacy, Cardiff University.

3.2. Results and Interpretation

3.2.1. Analysis of cf2642 toxicity

Viability assays were performed for both HeLa and VeroSLAM cells to assess the effect of cf2642 against a human (HeLa) as well as a non-human primate (VeroSLAM) cell lines. This was done to test whether any antiviral activity observed in the subsequent experiments were not just an artefact caused as a result of *in vitro* drug toxicity. Briefly, HeLa and VeroSLAM cells were treated with increasing concentrations of cf2642 and cell viability was analyzed at 12, 24, 48 and 72 hr post treatment using CellTiter-Blue assay.

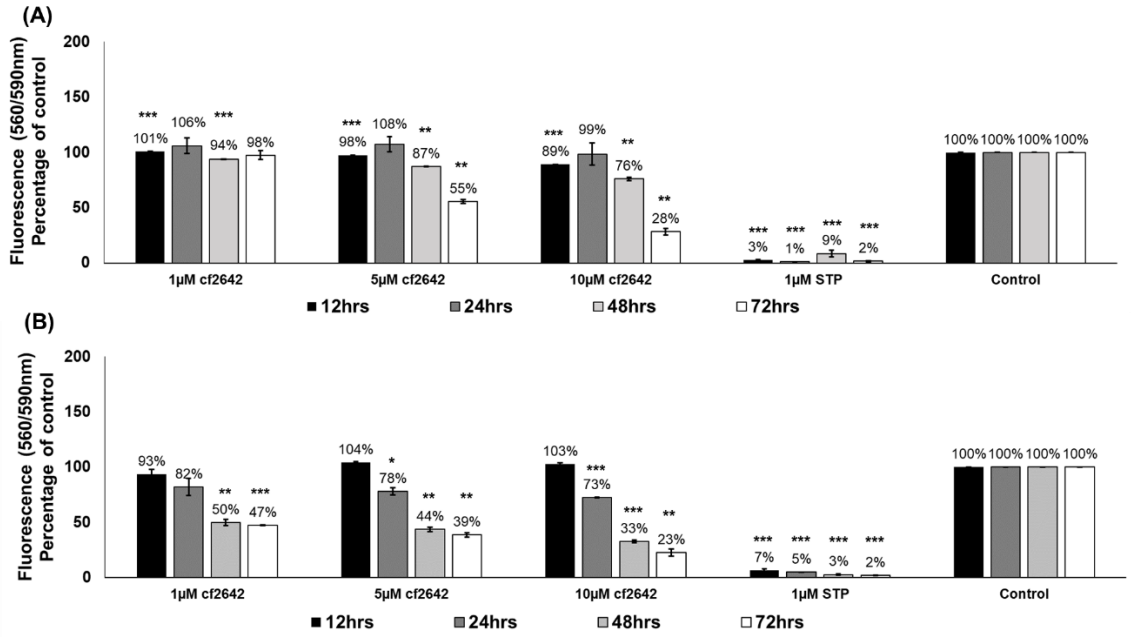

Fig 3.1 cf2642 causes a time and dose-dependent decrease in cell viability: HeLa and VeroSLAM cells were treated with 1, 5, 10μM cf2642 and 1μM Staurosporine (STP) as positive control. Cell viability up to 72 hr post treatment was measured using CellTiter-Blue assay. Cell viability results for (A) HeLa and (B) VeroSLAM cells are shown as percentage of untreated (diluent) control. The error bars show mean ± SD of three independent experiments. The results were quantified and shown as percentage increase of fluorescence intensity normalized to the control. Student's t-test was performed to assess the p values; **p < 0.01, ***p < 0.001.

Figure 3.1 (A) demonstrates no significant decrease of viability in HeLa cells in the presence of 1µM cf2642 even at 72 hr post treatment. A 13 and 24% decrease in viability was evident starting at 48 hr post treatment with 5µM and 10µM cf2642, respectively and more substantial cytotoxicity was observed for both drug concentrations at 72 hr post treatment.VeroSLAM cells showed different toxicity profiles (Fig 3.1 (B)) with significant toxicity in the presence of 1µM cf2642 noted only at the longer time points 48-72 hrs. Cell viability remained unaffected at 12hr post treatment with both 5 and 10µM cf2642, but longer treatment time points showed a steady increase in cytotoxicity. In the presence of 10µM cf2642, cells remained completely viable at 12hr post treatment, after which, a 27% decrease in viability was observed at the 24hr time point. The positive control for cytotoxicity (1µM Staurosporine) showed > 90% loss in cell viability for both HeLa and VeroSLAM cells. Taken together, the findings indicate that treatment with 10µM c2642 did not result in loss of viability up to 12hr post treatment in both cell lines tested. The steady decrease in cell viability of VeroSLAM cells after 12 hr indicates that this cell line is more sensitive to the effects of cf2642. In light of these data, a working concentration of 10µM c2642 or lower, was used for all subsequent experiments using HeLa and VeroSLAM cells.

This difference in cytotoxicity profiles of L-ddBCNAs/cf2642 across different cell lines was previously reported by Dr. Laura Farleigh and was speculated to be due to the cell-targeting effects of the drug(s) on cell lines derived from different origins (Farleigh, 2014). Although HeLa and VeroSLAM cells were

not tested as part of that study, the same could hold true for these cell lines as well.

While performing this experiment a change in colour of tissue culture medium from red to yellow in the cf2642 treated conditions, indicative of medium acidification. This phenomenon was first reported by Dr. Laura Farleigh who previously worked on cf2642 and it was shown that when the cell culture medium in cf2642 treated conditions were replaced after 16 hr post treatment, the cells were rescued from the toxic effects of the drug. Similar observations were noted in some subsequent experiments discussed in more detail in Chapter 4. Hence, the loss in cell viability over time may be an indirect effect of the drug.

3.2.2. Effect of cf2642 on MeV induced syncytia

MeV induced syncytia results in the formation of multinucleated giant cells and can be used to directly observe the effects of drugs against MeV, wherein the absence of syncytia formation would indicate antiviral activity (Mathieu et al., 2015). The effect of cf2642 on MeV induced syncytia was studied by infecting VeroSLAM cells with MeV in the presence or absence of the drug.

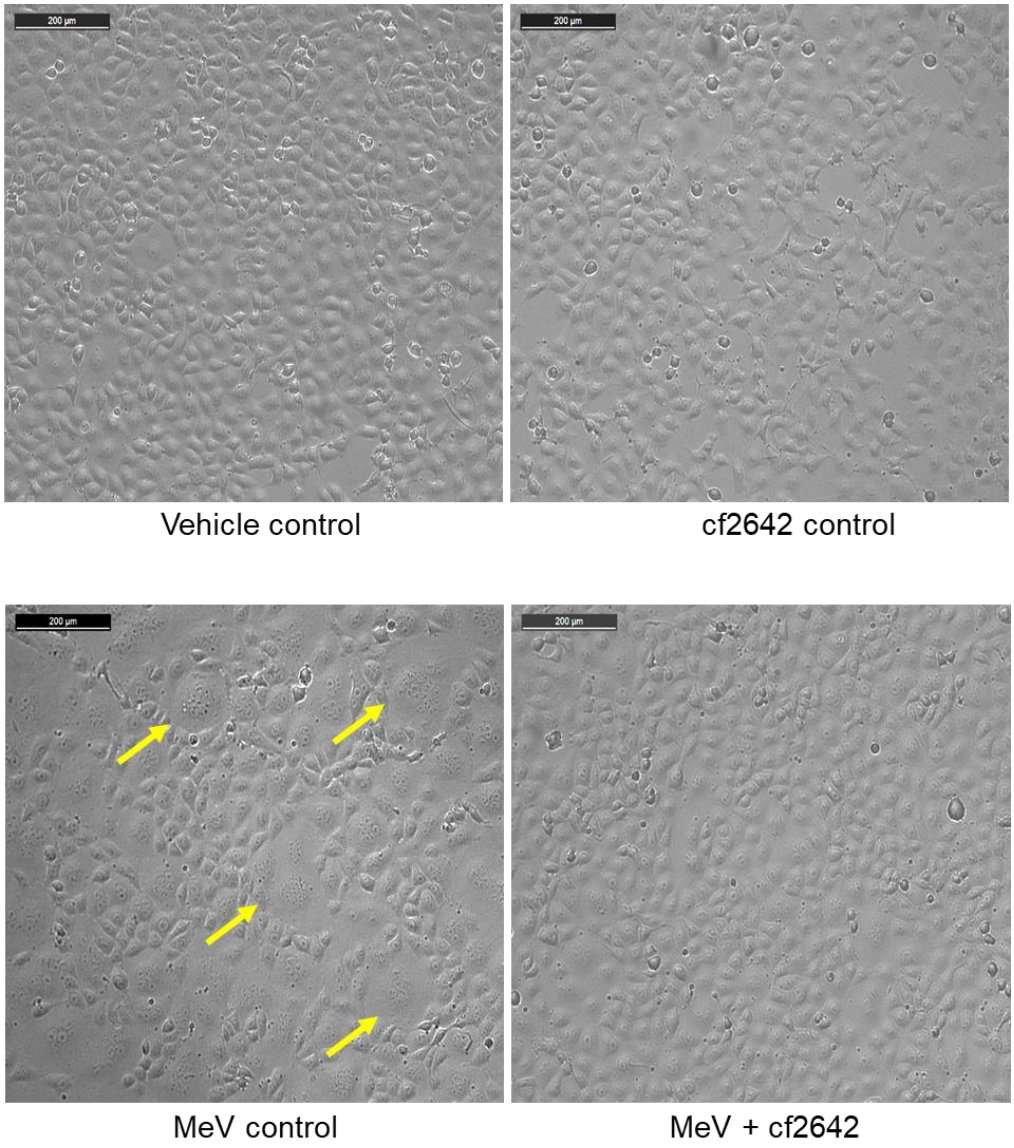

Fig 3.2. cf2642 inhibits MeV induced syncytia in VeroSLAM cells. Cells were infected with MeV at MOI 0.5 in the presence or absence of 10µM cf2642 and 12 hr post infection, images were captured using a wide field fluorescent microscope. Arrows indicate the presence of multinucleated giant cells. Images represents data from two independent experiments.

Fig 3.2 illustrates the effects of cf2642 on MeV induced syncytia in VeroSLAM cells. Incubation of cells with cf2642 did not result in any differences in cell morphology when compared to the vehicle control. MeV infected cells showed extensive formation of syncytia seen as large multinucleated giant cells and contained a large number of nuclei that were

clustered together. No evidence of syncytia formation was observed in virus infected cells treated with cf2642. Previous studies have shown that cf2642 inhibits MeV induced syncytia in B95a cells (Marmoset B lymphocytes immortalized with Epstein Barr virus) which naturally express the SLAM/CD150 receptor for MeV entry (Farleigh, 2014). The inhibition of syncytia formation in VeroSLAM cells treated with cf2642 provides direct evidence that antiviral activity of the drug against MeV is not limited to B95a cells alone.

3.2.3. Dose response effect of cf2642 on MeV titres

Previous work done using cf2642 demonstrated the antiviral activity of the drug against MeV in B95a cells (marmoset B-lymphocytes transformed by Epstein Barr virus) (McGuigan et al., 2013). Since a major part of this thesis is focussed on the use of VeroSLAM cells, it was important to determine whether the antiviral activity previously observed in B95a cells can be replicated in this cell line. The dose-dependent effect of cf2642 against MeV was therefore measured using virus plaque assays as described in 2.2.14.

Briefly, VeroSLAM cells were infected with MeV at MOI-0.05 and treated with the increasing concentrations of cf2642 from 1 to 10 µM. After a 12 hr incubation period, the supernatants were collected and used for plaque assays. Here, cells were fixed with paraformaldehyde 4 days' post infection and the plaques were counted manually. Virus titres were calculated by multiplying the average number of plaques in the wells with the virus dilution factor used for the assay.

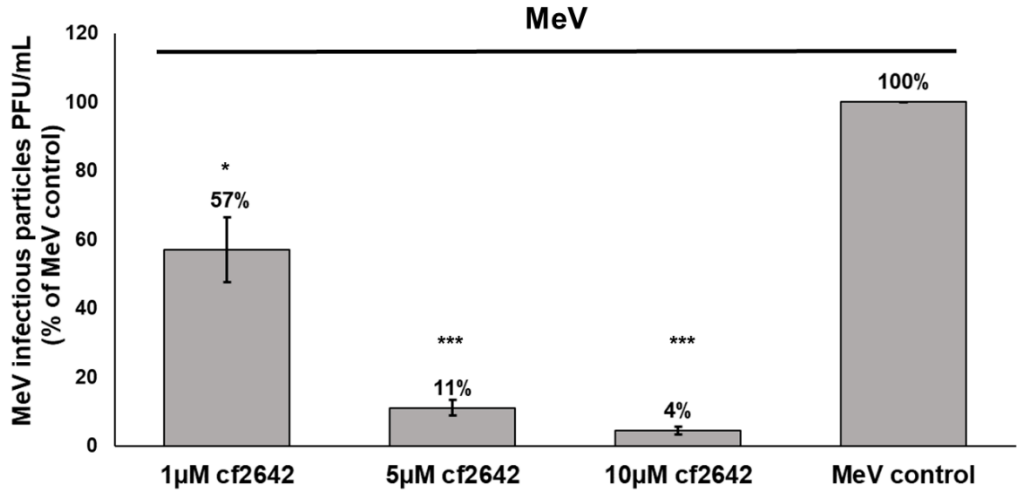

Fig 3.3. Dose dependent effect of cf2642 against MeV: VeroSLAM cells were infected with MeV at an MOI of 0.5 and treated or not with 1, 5 and 10µM cf2642 as indicated. Post treatment, (12 hr) the supernatant was collected and plaque assay was performed to titrate the virus. The results are represented as percentage increase of plaques compared to the MeV control. Student's t-test was performed to assess the p values; *$p < 0.05$, ***$p < 0.001$. Error bars represent mean ± SE of three independent experiments.

The results in Figure 3.3 demonstrate a significant 96% decrease in number of infectious MeV particles in the presence 10µM cf2642. A similar, but slightly reduced activity was observed in the presence of 5µM cf2642. The least activity was seen with 1µM cf2642, where only a 43% decrease in virus titre was observed. The data reveals a dose-dependent activity of cf2642 against MeV, with the maximum activity (IC90) seen at 10µM cf2642.However, previous data reported by McGuigan *et al*., showed the IC_{50} of cf2642 against MeV in B95a cells to be 7.5µM (McGuigan et al., 2013). The activity of a cell-targeting antiviral like cf2642 may vary across cell lines and this may be a contributing factor for these differences in antiviral activity. The variations in cytotoxicity of cf2642 against HeLa and VeroSLAM cells seen in Figure 3.1 serves as an ideal example. Also, two

different assays were used for analysis (plaque assay in this study versus TCID50 assay in McGuigan *et al*. paper)(McGuigan et al., 2013).

3.2.4. Effect of cf2642 on MeV induced autophagy - Immunofluorescence assay

This was done to test the effects of cf2642 on MeV induced autophagy by confocal microscopy. VeroSLAM cells were infected in the presence or absence of cf2642 and 12 hr post infection, labelled for LAMP1 and LC3 to label the late endosomes/lysosomes and autophagosomes respectively. Previous work done using cf2642 in HeLa cells, showed that the drug caused the scattering of lysosomes towards the cell periphery (Farleigh, 2014). The LAMP1 labelling was done to test whether the same results were also observed in VeroSLAM cells.

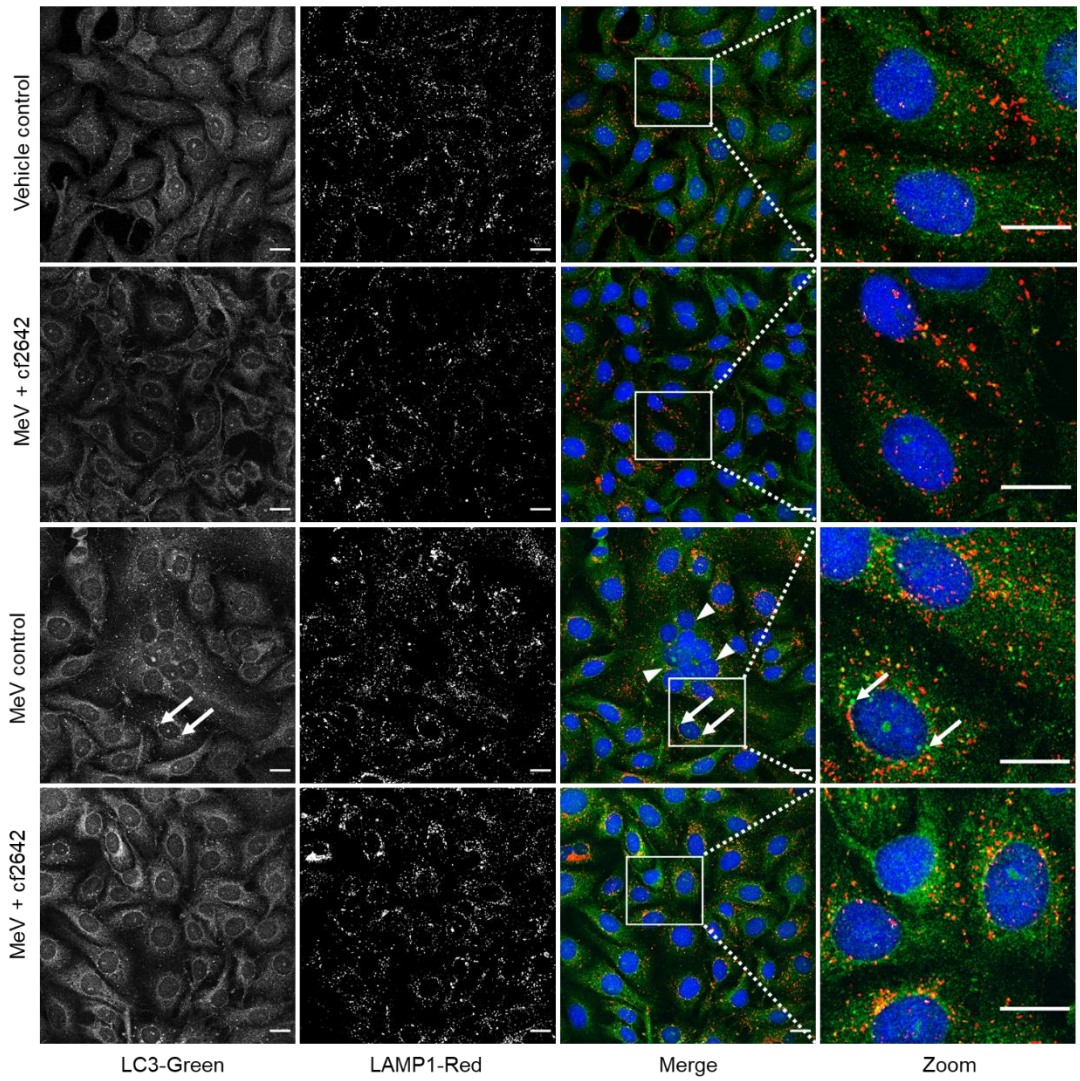

Fig 3.4 Microscopy analysis of the effect of cf2642 on MeV induced autophagy. VeroSLAM cells were infected with MeV at MOI 0.5 and incubated in the presence or absence of 10µM cf2642. Post infection/treatment (12 hr), cells were fixed with ice-cold methanol and immunolabelled with LC3B and LAMP1 antibodies to label the autophagosomes and late endosomes/lysosomes respectively. Single section images show LC3 (green) and LAMP1 (red) labelling both as grey scale and merged images. The nucleus was labelled with Hoechst 33342 and is shown in blue. Arrows show enlarged LC3B positive autophagosomes and arrow heads indicate syncytia formation by the fusion of cells. Images are representative of three independent experiments (scale bar = 20 µm).

Figure 3.4 demonstrates the presence of small LC3 positive structures in both the vehicle and cf2642 controls. No obvious differences in the number of these structures were found between the two conditions. Few cells

showed the presence of scattered LAMP1 positive vesicles in the cf2642 control, compared to the perinuclear arrangement observed in vehicle control.Multinucleated-giant cells (syncytia) indicated by the presence of fused nuclei, were observed in the MeV control. Slightly enlarged LC3B positive autophagosomes were also observed in virus infected cells. The increased number of LC3 positive vesicles (autophagosomes) in virus infected cells were mostly located around the vicinity of syncytia. The autophagosomes were in close proximity with LAMP1 positive late endosomes/lysosomes and indicate the formation of autolysosomes as part of an ongoing autophagy flux (Yoshii and Mizushima, 2017). No syncytia were seen in virus infected cells treated with cf2642, and the large autophagosomes seen in the MeV control were reduced. An inherent disadvantage of using IF assay for the study of autophagy is that it cannot be used to accurately measure an ongoing autophagy flux. In such cases, the results must be supported by western blot assays in the presence of lysosome inhibitors (see below). (Yoshii and Mizushima, 2017, Mizushima et al., 2010). This could be the reason why no significant increase of autophagosomes in MeV control was observed by confocal microscopy.

3.2.5. Effect of cf2642 on MeV induced autophagy – Western blot analysis

The effect of cf2642 on MeV induced autophagy was analyzed using western blot analysis to assess the expression levels of LC3 protein, a marker for autophagy (Yang et al., 2013). Three isoforms of LC3 namely LC3A, B and C exist in humans and they undergo various post translational modifications during autophagy. Soon after synthesis, this protein is first

cleaved at the carboxyl terminus to yield LC3-I and during the induction of autophagy, it is lipidated to form LC3-II (Mizushima et al., 2010) (see section 1.8 in chapter 1). The LC3B antibody used for western blotting and IF assays below, detects endogenous levels of total LC3B protein.

Cells were infected with MeV at an MOI of 0.5 either in the presence of absence of 10μM cf2642 and chloroquine controls. Following infection/treatment (12 hr), the cells were harvested and analyzed by western blotting. (see section 2.2.15 for methods).

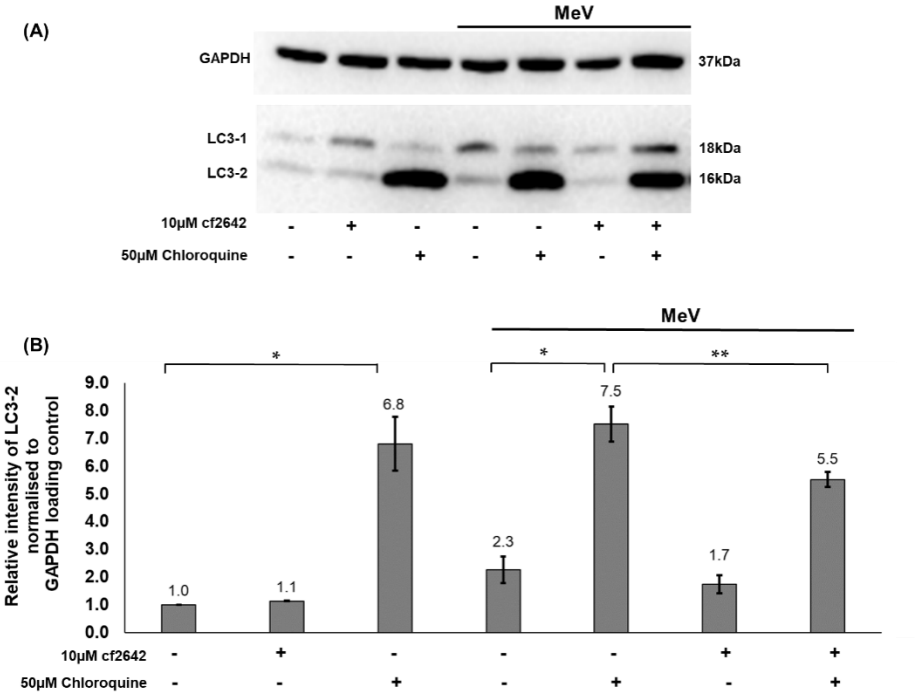

Fig 3.5. cf2642 inhibits MeV and induced autophagy: (A) VeroSLAM cells were infected with MeV at MOI 0.5 and treated in the presence or absence of 10 μM cf2642 and 50 μM Chloroquine as indicated. Post infection (12 hr), LC3-II expression was analyzed by western blot- one representative assay is shown. **(B)** Bar chart shows the relative intensity of LC3-II normalized to the GAPDH control. Student's t-test was performed to assess the p values; *p < 0.05, **p < 0.01. Error bars represent mean ± SE of three independent experiments.

Fig 3.5 A-B shows that minimal expression of LC3-II was observed in both vehicle control and cf2642 treated conditions (lanes 1 and 2 respectively), while LC3-II was significantly increased in the presence of chloroquine (lane 3). There was slightly increased LC3-II expression in the MeV control (lane 4), that was reduced in the presence of cf2642 (lane 6). MeV infection in the presence of chloroquine saw a significant increase in LC32 expression (lane 5) and this was reduced in the presence of cf2642 (lane 7). Overall, low expression of LC3-I was seen in all conditions except in virus infected cells treated with both cf2642 and chloroquine (lane 7) (Fig 3.5 A).

Autophagy is a degradative cellular process that occurs as part of the cells mechanism of getting rid of damaged organelles, dysfunctional proteins, or infectious microorganisms (Parzych and Klionsky, 2014, Rozières et al., 2017). Like many other viruses, MeV also induces autophagy as part of its life cycle and this helps in improving virus spread and escaping the host cell mediated immunity (Richetta et al., 2013). To test whether cf2642 inhibited MeV induced autophagy in VeroSLAM cells, a western blot analysis was performed to test the expression levels of the autophagy marker LC3-II in cells infected with MeV w/o 10µM cf2642. LC3-II is often used as a marker for autophagy flux changes because it is the only protein which stably associates with the autophagosome complex. Hence during an autophagy flux, the increase in the number of autophagosomes would lead to an increase in intracellular LC3-II levels. Autophagy is a dynamic process occurring in cells and while studying differences in autophagy flux using western blot analysis, it is important to confirm that the inhibition of

autophagy seen as a decrease in LC3-II protein levels is not because of an increased autophagy flux that results in rapid degradation of the protein (Loos et al., 2014). This can be solved using a lysosomotropic agent like chloroquine, which blocks the fusion of autophagosome-lysosome resulting in the accumulation of LC3-II positive autophagosomes in the cell (Mizushima et al., 2010). Hence, when cells are undergoing an autophagy flux, an increase in LC3-II expression in the presence of chloroquine, compared to that in the absence of the drug, will represent the overall number of autophagosomes that would have been degraded by autophagy (Yoshii and Mizushima, 2017). The western blot results show low levels of LC3-II expression in the vehicle control, indicating basal autophagy and this was unaffected in the presence of cf2642. The sharp increase in LC3-II expression seen in the presence of chloroquine indicates accumulation of autophagosomes due to the inhibition of autopahgosome-lysosome fusion. The MeV control caused only a slight increase in autophagy and this was partially reduced in the presence of cf2642, as seen by the slight decrease in LC3-II expression. No significant differences in LC3-II expression levels was seen between the chloroquine control and MeV + chloroquine condition, suggesting that the MeV-induced autophagy was minimal. However, when cf2642 was present along with MeV and chloroquine, this caused a significant decrease in autophagy compared to the MeV + chloroquine condition. This peak in LC3-II expression seen in both these conditions is the result of amplified LC3-II accumulation in the cell as a result of the inhibition of autophagosome-lysosome fusion by chloroquine. Since the virus induced increase in LC3-II expression was minimal, it is

difficult to interpret these results in terms of autophagy inhibition by cf2642 and further experiments using longer infection/treatment time points may be required for conclusive data.

3.3. Summary

Previous work performed using cf2642 has shown the antiviral activity of this drug against both MeV and VACV*in vitro* and that a common cellular target might be affected. A series of L-ddBCNAs with varying lipophilic side chain lengths were tested against these two viruses and a structure activity relationship showed that the antiviral activity was dependent on the length of the lipophilic side chain of these compounds(McGuigan et al., 2013). Prior to beginning MoA experiments using cf2642, the effect of cf2642 on cell viability was tested using two different cell lines namely HeLa and VeroSLAM. Although VeroSLAM cells were found to be more sensitive to the effects of cf2642, both cell lines remained viable at 12 hr post treatment. Viral plaque assay results showed a dose dependent decrease in MeV titer which demonstrated that the anti-MeV activity of cf2642 was not only limited to B95a cells, as shown in previous studies by Dr. Farleigh, but was effective also in VeroSLAM cells. This was also supported by the fact that treatment with cf2642 inhibited MeV induced syncytia in these cells. Based on the hypothesis that cf2642 inhibits a cellular target, subsequent work was focussed on testing the effects of this drug on a cellular process called autophagy that is crucial for the infectious cycle of MeV. Western blot analysis of autophagy did not reveal a significant increase in LC3-II expression in the presence of MeV and hence, a clear effect of cf2642 on this process was not observed. Confocal microscopy analysis revealed the

appearance of large LC3 positive structures in MeV control, that was mostly reduced in the presence of cf2642.

Note: Upon initiation of my period in the School of Pharmacy, it came to notice that the VeroSLAM cells used to perform some of the earlier experiments (sections 3.2.3 and 3.2.5) in this chapter may have been contaminated with mycoplasma. This was identified when the cells were moved from the Department of Medical Microbiology to the School of Pharmacy. The exact period of contamination is unknown. Figure 3.2.3 in this Chapter was obtained from the original cells. Attempts to repeat the analysis were unsuccessful and the period in Germany did not allow multiple attempts. However, it has already been shown that cf2642 at these concentrations was used her inhibit MeV replication and VACV plaque formation (Farleigh, 2014).All the other data in this chapter were repeated in mycoplasma free cells at the School of Pharmacy or the Bundeswehr institute and the original data is not shown in this thesis. This issue has also affected my ability to add other experimental data into this short chapter. All experiments presented in the longer Chapters 4 and 5 were performed in mycoplasma free cells.

Chapter 4 - Endocytic characterisation to elucidate the effects of cf2642 on cells

4.1. Introduction

The previous chapter explored the consequences of cf2642 treatment on MeV titers and its effects of virus induced cytopathic effects in VeroSLAM cells. The aim of the experiments in this chapter are to elucidate the pharmacological properties of cf2642 in an effort to understand the effects of the drug on cells, irrespective of MeV infection. On this account, endocytic characterisation studies were done in an effort to understand the effects of cf2642 on different subcellular structures.

Endocytic characterisation is a home laboratory term that involves studies on the spatial distribution of intracellular vesicles and organelles that are involved in endocytosis. This includes not only the different components of the endolysosomal pathway, but also organelles such as theGolgi network that are indirectly involved in endocytosis. This methodology is based exclusively on the use of fluorescence microscopy, where subcellular structures are labelled either using live or fixed cell microscopy. While live cell imaging allows the direct visualization of endocytic structures using fluorescent endocytic probes, fixed cell imaging involves halting cellular processes at specific points in time to label subcellular structures or organelles with specific antibodies or dyes. The spatial organization of the cell cytoskeleton is critical to all endocytic events (Smythe and Ayscough,

2006) and hence this also forms an integral component of endocytic characterisation.

The use of dextran conjugated fluorophores has been widely used as non-invasive optical imaging probes for the study of endocytosis by live cell microscopy (Varshosaz, 2012, He et al., 2018). Dextran are high molecular weight hydrophilic polysaccharides that are non-toxic to cells, relatively inert and contain α-1,6-polyglucose linkages resistant to cellular glycosidases, making them ideal for use as live cell probes (Hu et al., 2009). Dextran does not bind to a cellular receptor; thus it may enter cells through a number of endocytic pathways. It has been widely used as a marker for growth factor induced macropinocytosis(Jones, 2007). It has been shown that dextran accumulates in LAMP1 positive lysosomes after endosomal trafficking throughRab7 positive late endosomes(Humphries IV et al., 2011). When incubated with cells as a fluorescent probe, dextran can enter and label the entire endolysosomal system. The use of dextran in experiments performed in this chapter involves a pulse-chase process wherein, cells are first “pulsed” with dextran-conjugated fluorophores for a brief time period (1-3 hrs) to allow uptake. Following this, cells are washed to remove any conjugates that may be present on the cell surface and in the extracellular medium. Cells are then incubated with fresh cell culture medium to allow a much longer “chase”, to proceed; here the probe will be transported to lysosomes or potentially recycled. At the end of the chase period only lysosomes will be labelled with the probe and this then allows live cell imaging confocal microscopy the opportunity to assess whether any other molecule internalised to cells via endocytosis is also delivered to lysosomes.

Additionally, it allows for selective analysis of the effects of agents on the distribution of lysosomes.

4.2. Results and Interpretation

4.2.1. Effect of cf2642 on lysosomal scattering in HeLa cells

A previous study reported that lysosomes scatter towards the cell periphery when HeLa cells were incubated with cf2642(Farleigh, 2014). This phenomenon was detected by immunolabelling the lysosomes using CD63 (LAMP III) antibodies. Here the experiment was repeated in live HeLa and VeroSLAM cells which has the inherent advantage that the effects of cf2642 on lysosomal positioning can be visualized in real-time by labelling them with fluorophore conjugated dextran. Briefly, HeLa cells seeded in glass bottom MatTek dishes were pulse-chased with two different dextran Alexa Fluor conjugates (see methods section 2.2.6 in Chapter 2) in the presence of absence of cf2642. This allowed for analysis of the localisation of dextran by qualitative visualisation and also via labelling the nucleus, determining the position of the lysosomes as function of their distance away from the nucleus could also be analyzed.

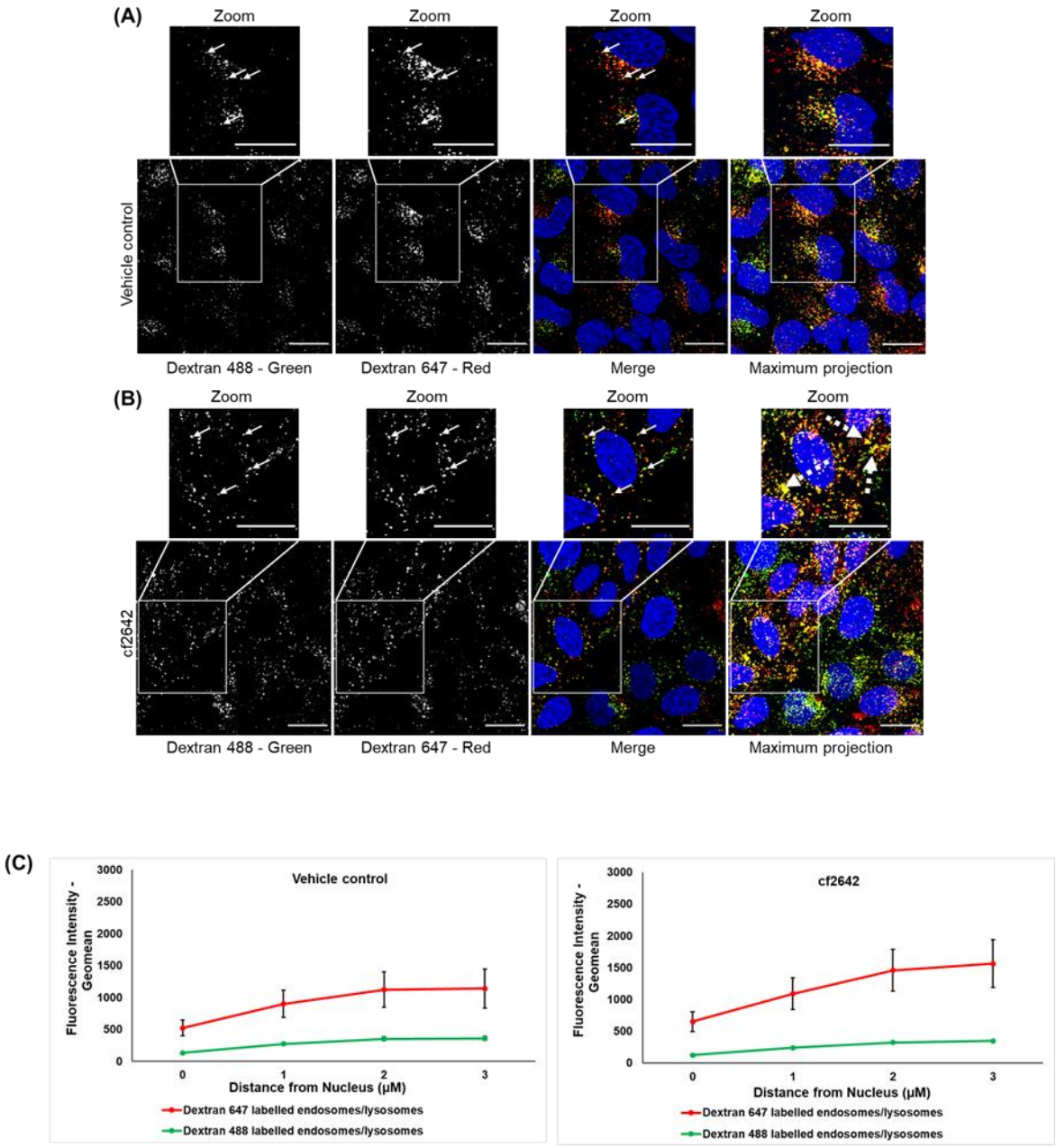

Fig 4.1. cf2642 causes the scattering of LE/lysosomes in HeLa cells. Cells were subjected to 3 hr pulse with 0.2 mg/mL Dextran-488 and 8 hr chase followed by a 12 hr incubation w/o 10µM c2642. Cells were then further pulsed for 3 hr with 0.2 mg/mL Dextran-Alexa 647 and chased for 3 hr w/o 10µM cf2642 before live imaging.**(A)** shows cells treated with vehicle (DMSO) and **(B)** shows cf2642 treated cells. Arrows indicate colocalization of Dextran-Alexa 488 and 647 labelled late endosomes/lysosomes and dotted arrows show aggregated lysosomal structures.**(C)** The dispersal of lysosomes up to 3 µM from the nucleus was calculated by drawing concentric ROIs up to 3 µM distance from nucleus. The intensity of fluorescence is plotted against distances from the nucleus. The error bars show mean ± SE of three independent experiments. (Scale bars = 20 µm)

Results show that Dextran-488/647 labelled LE/lysosomes in the vehicle control were mostly grouped together and localized in close proximity with the nucleus and that there was colocalization between the two fluorophores (Fig 4.1 A). In the presence of cf2642, the labelled endocytic vesicles appeared to be more scattered and positioned away from the nucleus. There was no evidence that the drug was impeding the delivery of Dextran 647 to Dextran 488 labelled structures (Fig 4.1 B). The maximum projection image also suggests that cf2642 is also affecting the morphology of the lysosomes manifest as aggregated structures in Figure 4.1 B zoom. The peripheral LE/lysosomes in cf2642 treated cells labelled with Dextran-647 were of higher intensity than that of the controls (Fig 4.1 C).

The initial 3 hr pulse with Dextran-488 and 8 hr chase allowed the internalization and transport of the fluorophore probe via the endolysosomal pathway to lysosomes. At this point in the experiment only lysosomes are fluorescent as the probe had been emptied from other endocytic organelles or recycled. The subsequent analysis in the absence or presence of cf2642 allowed for selective subcellular distribution of lysosomes (Dextran-488) and also Dextran-647 that had been pulsed to label the entire endolysosomal system. Shown was the expected colocalization of the two probes and no evidence that cf2642 was inhibiting traffic of dextran (647) to lysosomes. Noted however was a very pronounced effect of the drug on the subcellular localisation of lysosomes. At the end of the experiments the Dextran-488 fluorescence was low and this may be due to the fact that some of it was being recycled (Baravalle et al., 2005).

4.2.2. Effect of cf2642 on lysosomal scattering in VeroSLAM cells

Since VeroSLAM cells were used in most experiments of this thesis, the experiment in section 4.2.1 above was repeated to test the effect of cf2642 on lysosomal positioning in these cells. The protocol used here was the same as done for HeLa cells(see methods section 2.2.6 in Chapter 2).

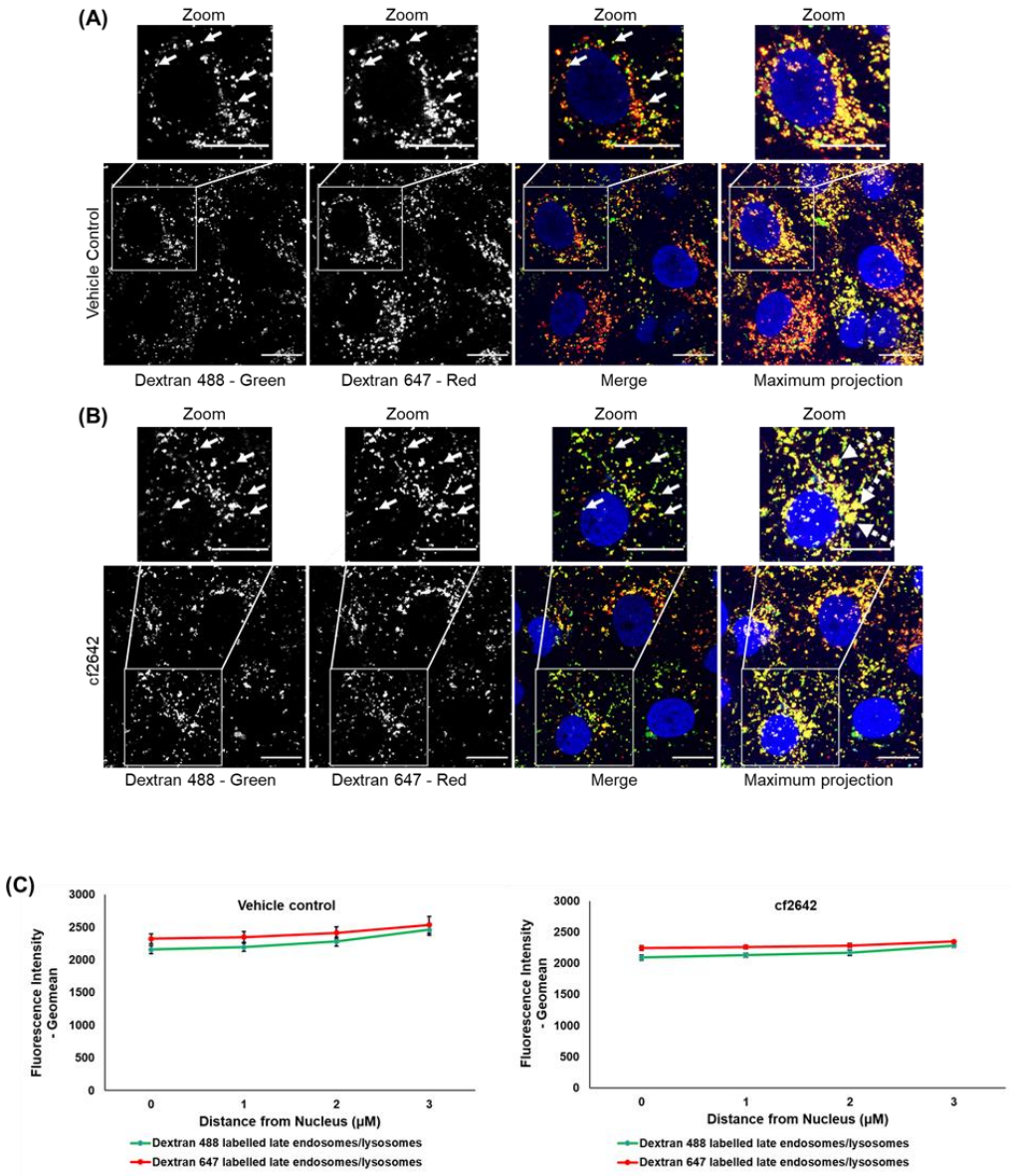

Fig 4.2. Late endosomes/lysosome dispersal in VeroSLAM cells: Cells were subjected to 3 hr pulse with 0.2 mg/mL Dextran-488 and 8 hr chase followed by a 12 hr incubation w/o 10μM c2642. Cells were then further pulsed for 3 hr with 0.2 mg/mL Dextran-Alexa 647 and chased for 3 hr w/o 10μM cf2642 before live imaging. **(A)** shows cells treated with vehicle (DMSO) and **(B)** shows cf2642 treated cells. Arrows indicate colocalization of Dextran-Alexa 488 and 647 labelled late endosomes/lysosomes and dotted arrows show aggregated lysosomal structures. **(C)** The dispersal of lysosomes up to 3 μM from the nucleus was calculated by drawing concentric ROIs up to 3 μM distance from nucleus. The intensity of fluorescence is plotted against distances from the nucleus. The error bars show mean ± SE of three independent experiments. (Scale bars = 20 μm)

In general, the lysosomes were more scattered in control VeroSLAM cells (Fig 4.2 A) compared with Hela and there was not an obvious effect on distribution of these organelles in cells treated with cf2642.The drug treated cells did however highlight large aggregates of fluorescence that was not noted in the HeLa cells (Fig 4.2 B Zoom). The overall fluorescence intensities of both Dextran-488 and 647 labelled vesicles were much higher compared to that of HeLa cells observed above. However, no significant differences in fluorescence intensities of these vesicles were observed between the control and cf2642 treated cells (Fig 4.2 C). As observed in the case of HeLa cells above, treatment of VeroSLAM cells did not have any effects in the endocytic uptake of dextran labelled fluorophores.

4.2.3. Endocytic Characterisation

As part of endocytic profiling studies, immunolabelling of various endosomal compartments were performed in both HeLa and VeroSLAM cells at various time points.

4.2.3.1. Effect of cf2642 on Rab5 labelled vesicles in HeLa and VeroSLAM cells

Rab5 is a GTPase of the Ras superfamily that are localized on the early endosomes and regulate their maturation to late endosomesand is a widely used marker for early endosomes (Pfeffer, 2017). Labelling of Rab5 positive vesicles were performed to test whether cf2642 had any effect on the localisation of early endosomes. Briefly, cells were treated or not with 10µM cf2642 at two different time points and fixed, before immunolabelling. (see section 2.2.3.2.3.3 in Chapter 2).

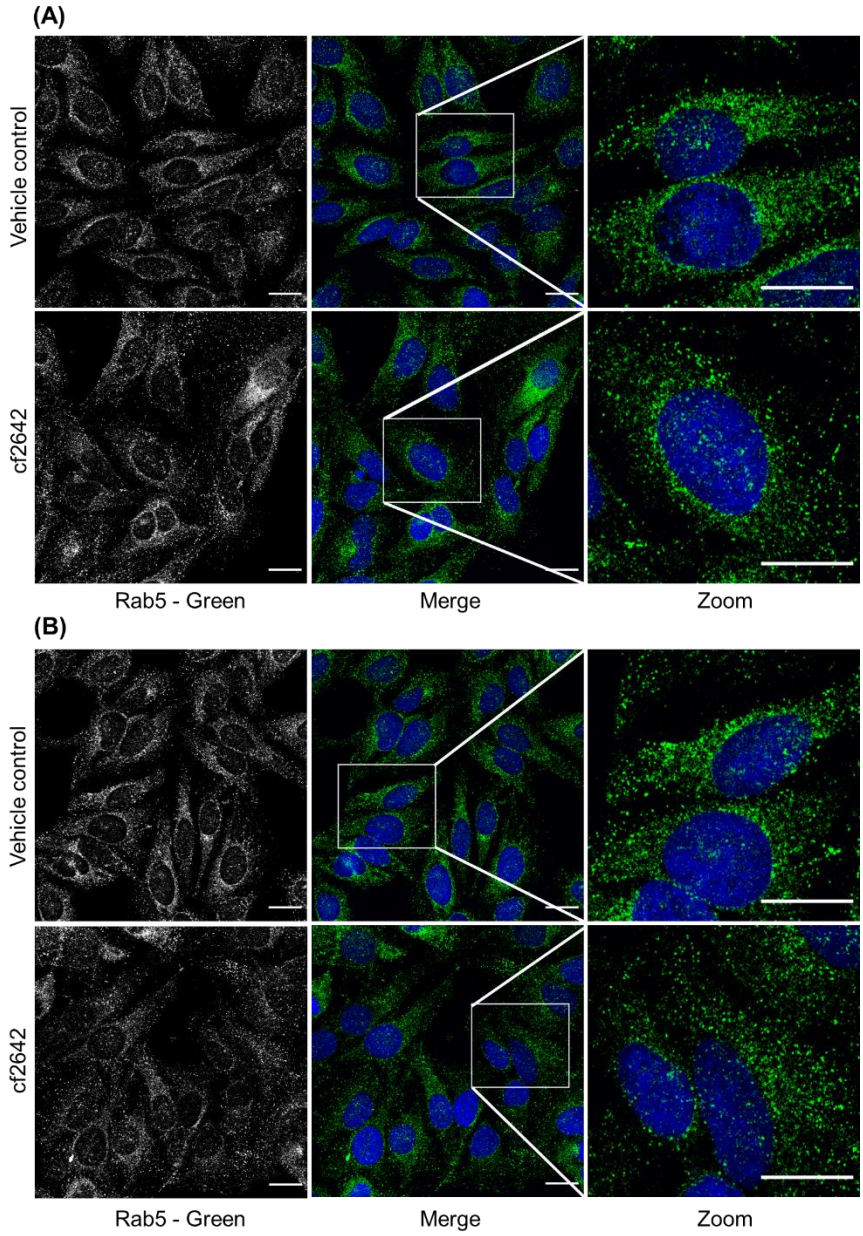

Fig 4.3 Effect of cf2642 on Rab5 in HeLa cells. Cells were treated or not with 10µM cf2642 for **(A)** 2 hr or **(B)** 12 hr and fixed with ice-cold methanol before immunolabelling with a Rab5 specific antibody. The data represent one representative image of three independent experiments. (Scale bars = 20 µm)

Figure 4.3 highlights scattered and perinuclear localization of Rab5 positive structures in the control cells of both 2 and 12 hr time points. Cell treated with cf2642 at the 2 hr time point were very similar to control cells but a

longer (12 hr) incubation with the drug resulted in a more scattered localisation compared to the shorter 2hr time point investigated here.

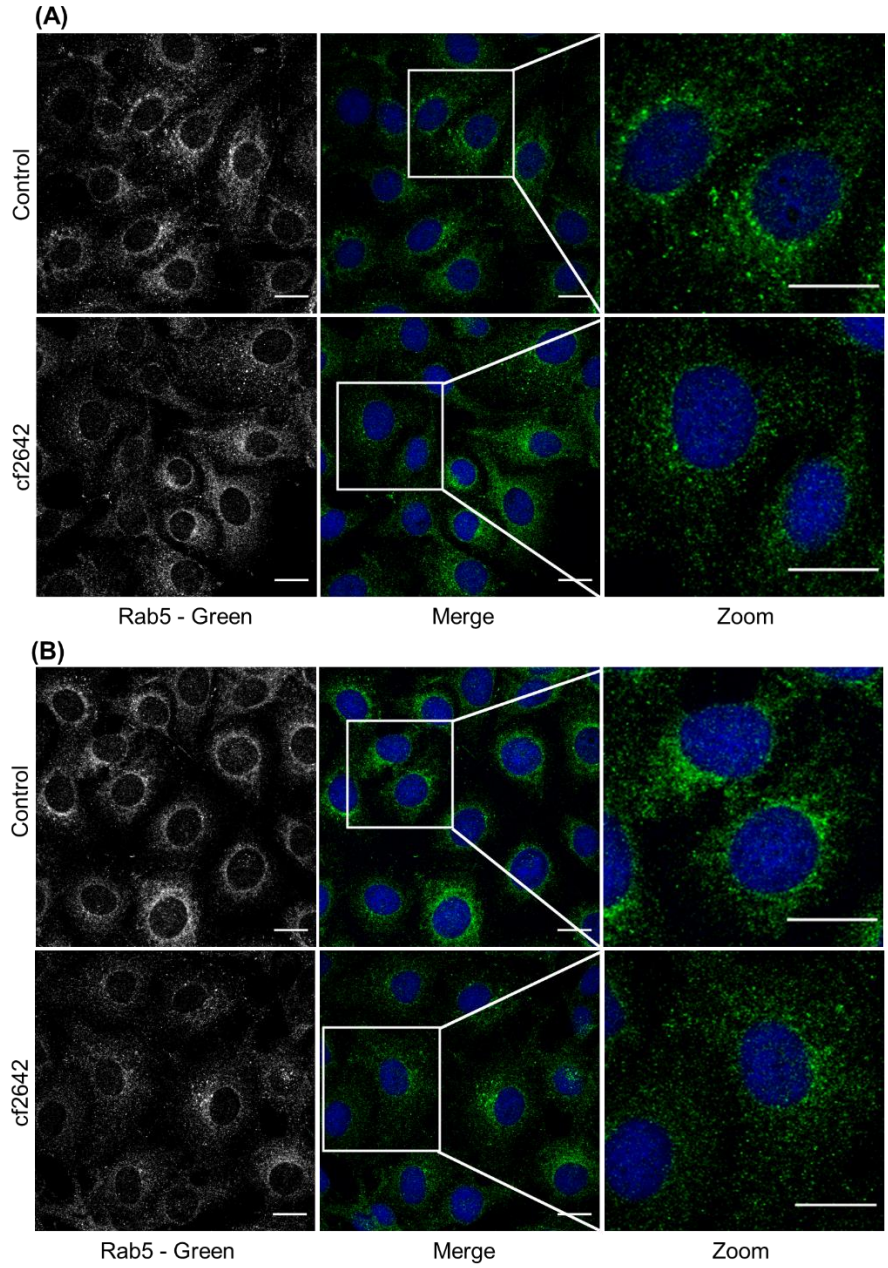

Fig 4.4 Effect of cf2642 on Rab5 in Vero SLAM cells. Cells were treated or not with 10µM cf2642 for **(A)** 2 hr or **(B)** 12 hr and fixed with ice-cold methanol before immunolabelling with a Rab5 specific antibody. The data represent one representative image of three independent experiments. (Scale bars = 20 µm)

Perinuclear localization of Rab5 positive structures in VeroSLAM cells were similar to that of HeLa cells above. cf2642 caused the scattering of Rab5 vesicles 12 hr post treatment, though the positioning of these vesicles remained unchanged when treated for 2 hr (Figure 4.4). The data also highlights that the antibody used here also recognizes monkey Rab5; the same is true for antibodies recognizing EEA1 and Lamp1 below.

The scattering of Rab5 positive vesicles were prominent only after prolonged (12hr) treatment of both HeLa and VeroSLAM cells, indicating the this is associated with the late, rather than early effects on the drug on cells. It also shows that this scattering of vesicles is not limited to lysosomes as seen earlier (section 4.3.1).

4.2.3.2. Effect of cf2642 on EEA1 labelled vesicles in HeLa and VeroSLAM cells

EEA1 mediates the homotypic fusion of early endosomes and is a major effector of Rab5 GTPases (Mills et al., 1999)(Stenmark et al., 1996). Given that cf2642 causes the scattering of Rab5 positive vesicles (section 4.4.1), the effect of this drug on EEA1 positive structures was tested in both cell lines.

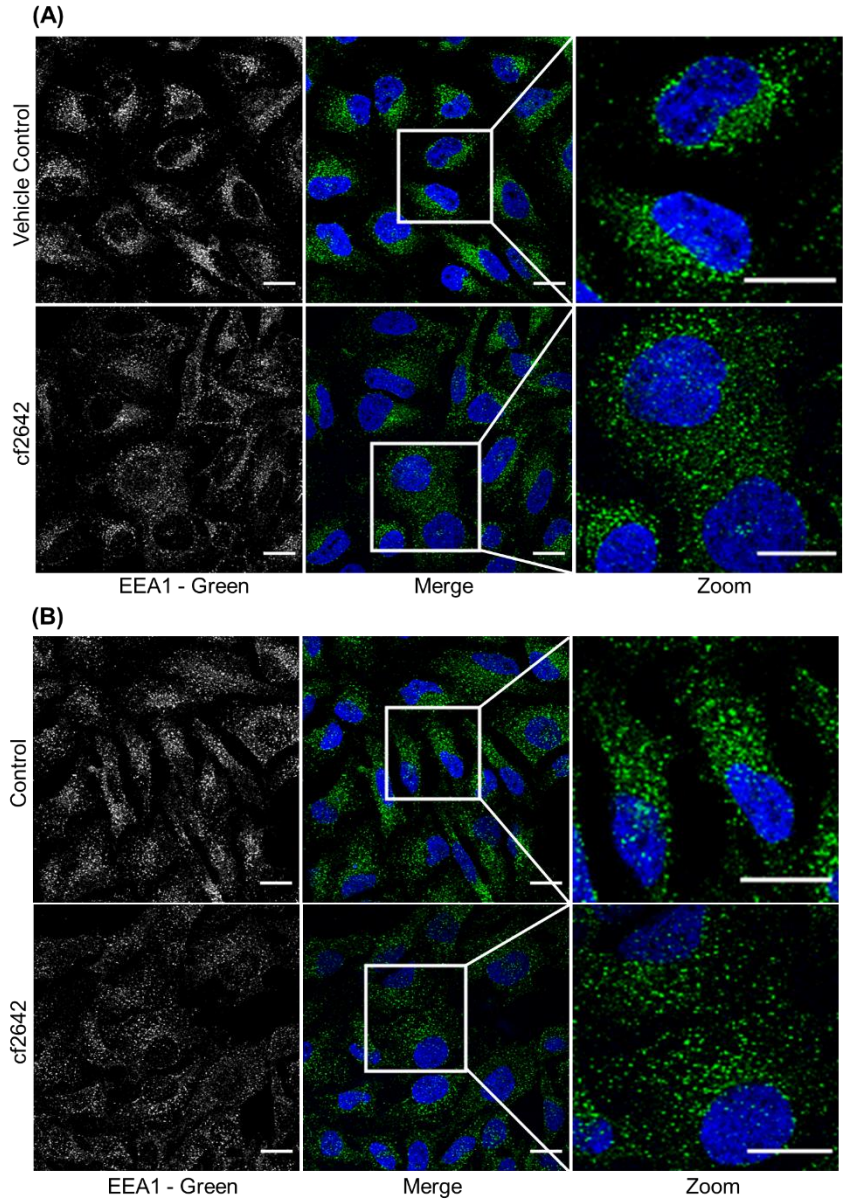

Fig 4.5 Effect of cf2642 on EEA1 in HeLa cells. Cells were treated or not with 10µM cf2642 for **(A)** 2 hr or **(B)** 12 hr and fixed with 3% paraformaldehyde, permeabilized and immunolabelled with a EEA1 specific antibody. The data represent one representative image of three independent experiments. (Scale bars = 20 µm)

The results show shows perinuclear EEA1 labelled structures particularly enriched in a juxtanuclear region in HeLa cells. As observed for Rab5, the drug caused a scattering of these structures that was particularly prominent at the 12 hr time point. Although the cells manipulation used here did result in EEA1 scattering in control cells, the perinuclear positioning of these

vesicles was clearly observed in cells 12 hr post treatment with cf2642 (Fig 4.5). Since the scattering of vesicles in the was seen only at 12 hr post treatment, which could mean that either this requires prolonged incubation with the drug or that it is associated with the late effects of cf2642.

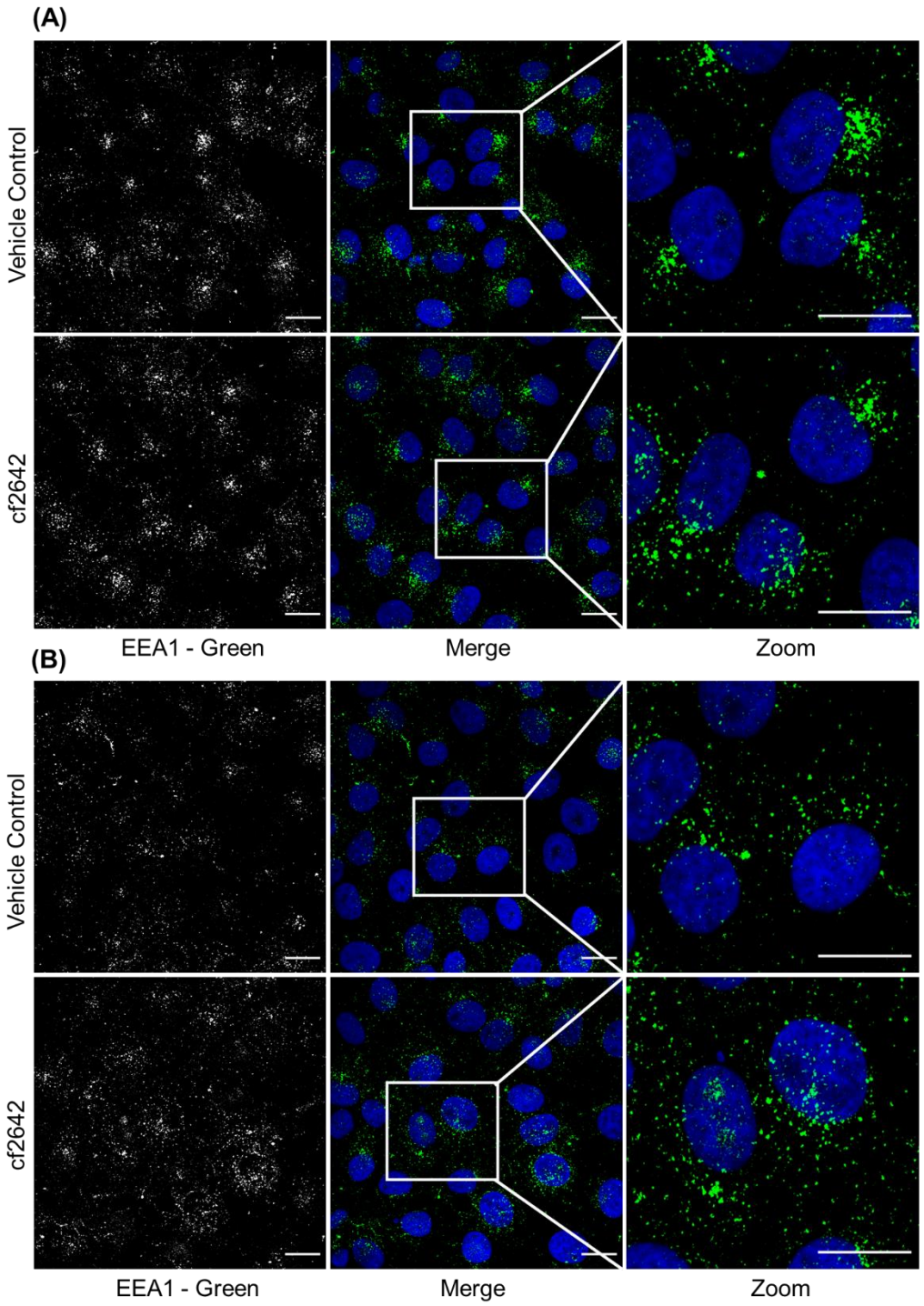

Fig 4.6 Effect of cf2642 on EEA1 in VeroSLAM cells. Cells were treated or not with 10µM cf2642 for **(A)** 2 hr or **(B)** 12 hr and fixed with 3% paraformaldehyde, permeabilized and immunolabelled with a EEA1 specific antibody. The data represent one representative image of three independent experiments. (Scale bars = 20 µm)

EEA1 labelling in VeroSLAM cells also revealed predominantly juxtanuclear localization of these vesicles and no differences were observed between control and cf2642 treated cells at 2 hr time point. These vesicles were much more scattered in control cells 12 hr post treatment, similar to the cf2642 treated cells (Fig 4.6). It is unclear why the EEA1 labelled vesicles in 12 hr treated vehicle controls were scattered, but may be associated with the manipulation of cells during the experiment. Since there were no differences between the control and cf2642 treated cells at this time point, it is not possible to interpret the data as being a true effect of cf2642.

4.2.3.3. LAMP1 labelling in HeLa and VeroSLAM cells

LAMP1 is a very widely used lysosomal marker and has been shown to mediate fusion of lysosomes and autophagosomes; there is also evidence that the protein is located on late endosomes (Eskelinen, 2006). Given that cf2642 inhibited measles induced autophagy, its effect on LAMP1 labelled structures was tested. Cells were incubated in the presence or absence for 10µM cf2642 for 12 hr and fixed before immunolabelling for this protein.

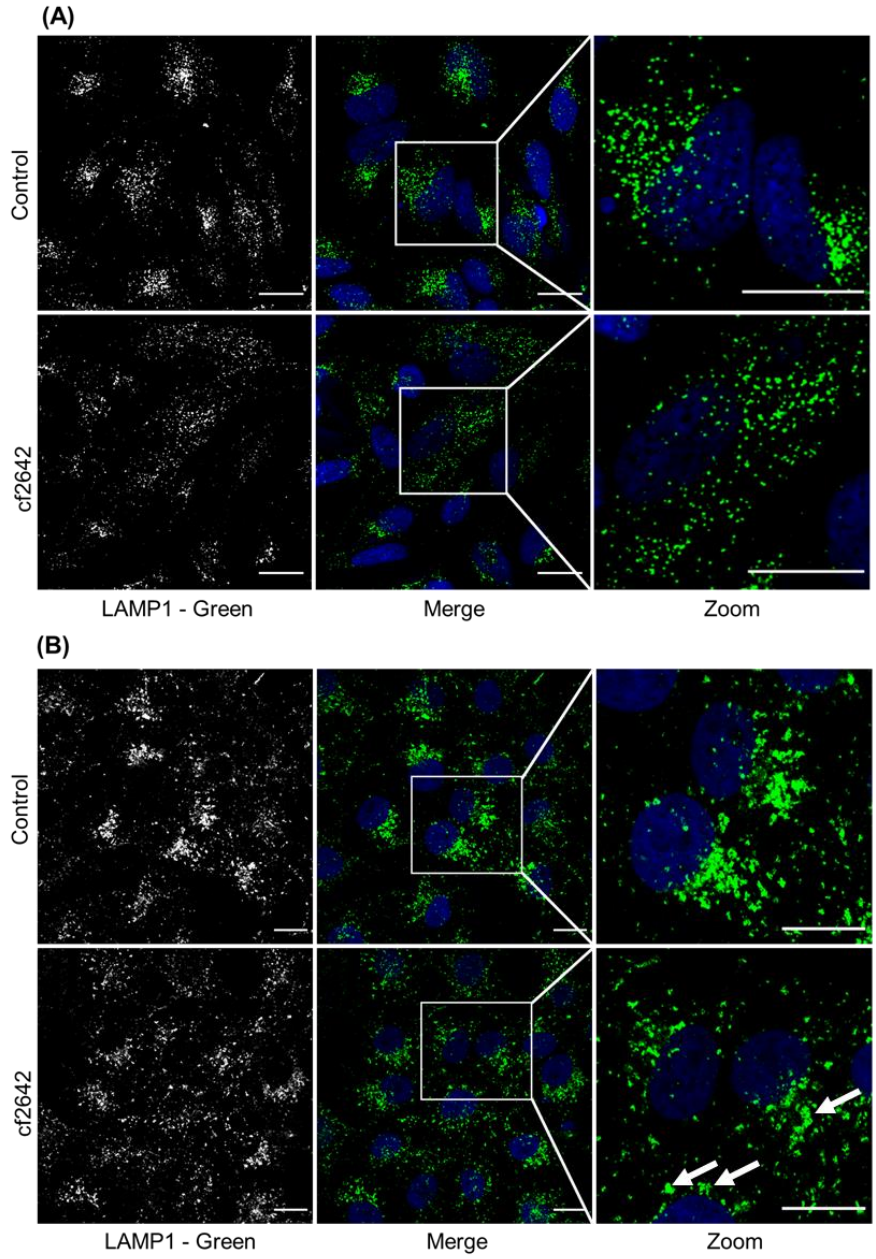

Fig 4.7 Effect of cf2642 on LAMP1 positive structures. (A) HeLa and **(B)** VeroSLAM cells were treated or not with 10µM cf2642 for 12 hr and fixed with 3% paraformaldehyde, permeabilized and immunolabelled with a LAMP1 specific antibody. Arrows show the presence of amorphous LAMP1 positive structures. The data represent one representative image of two independent experiments. (Scale bars = 20 µm)

The results in Figure 4.7 highlight that LAMP1 positive structures in both HeLa and Vero SLAM cells are highly enriched in a juxtanuclear cluster. Most notably in HeLa cells the LAMP1 phenotype in cf2642 treated cells

was very different with the vesicles scattered all over the cytoplasm. A similar but less pronounced difference was observed in VeroSLAM cells that were noted for having large amorphous LAMP1 labelled structures.Lysosomes are known to be positioned at the cell periphery in responses to decreased intracellular pH (Heuser, 1989). The cf2642 scattering phenomenon observed in this study may therefore be a consequence of this effect and this merits further investigation. Commercial probes such as 5-(and-6)-carboxyl seminaphthorhodafluor (SNARF-1) are available for measuring intracellular pH (Ramshesh and Lemasters, 2012). The laboratory has experience of performing experiments with this probe and given more time these would be interesting experiments to perform

Overall, the results from experiments 4.3.1 to 4.3.3 has shown that the scattering of vesicles was common to Rab5, EEA1 and LAMP1 positive structures, indicating that the effects of cf2642 is not limited to any single population of endocytic vesicles. As MeV has been recently shown to enter cells by endocytosis, (Delpeut et al., 2017, Goncalves-Carneiro et al., 2017) these effects could conceivably affect the ability of the virus to effectively use this process for entry and replication. This study did not however show that endocytosis was required for viral replication. Previous unpublished studies in our group have strongly suggested that the drug does not affect MeV entry (Farleigh, 2014)) but it remains to be seen whether subsequent downstream traffic is affected by the drug.

4.2.3.4. Effect of cf2642 on actin network

Actin filaments provide structural integrity to cells and the actin cytoskeleton is heavily implicated in endocytosis, especially at locations of the initiation of endocytic processes at the plasma membrane (Carlsson, 2018, Mooren et al., 2012). Actin has particular relevance in driving the formation of plasma membrane ruffles that are extremely prominent in macropinocytosis (Falcone et al., 2006). Actin depolymerising drugs such as cytochalasin D are well characterised inhibitors of this process (Dutta and Donaldson, 2012)

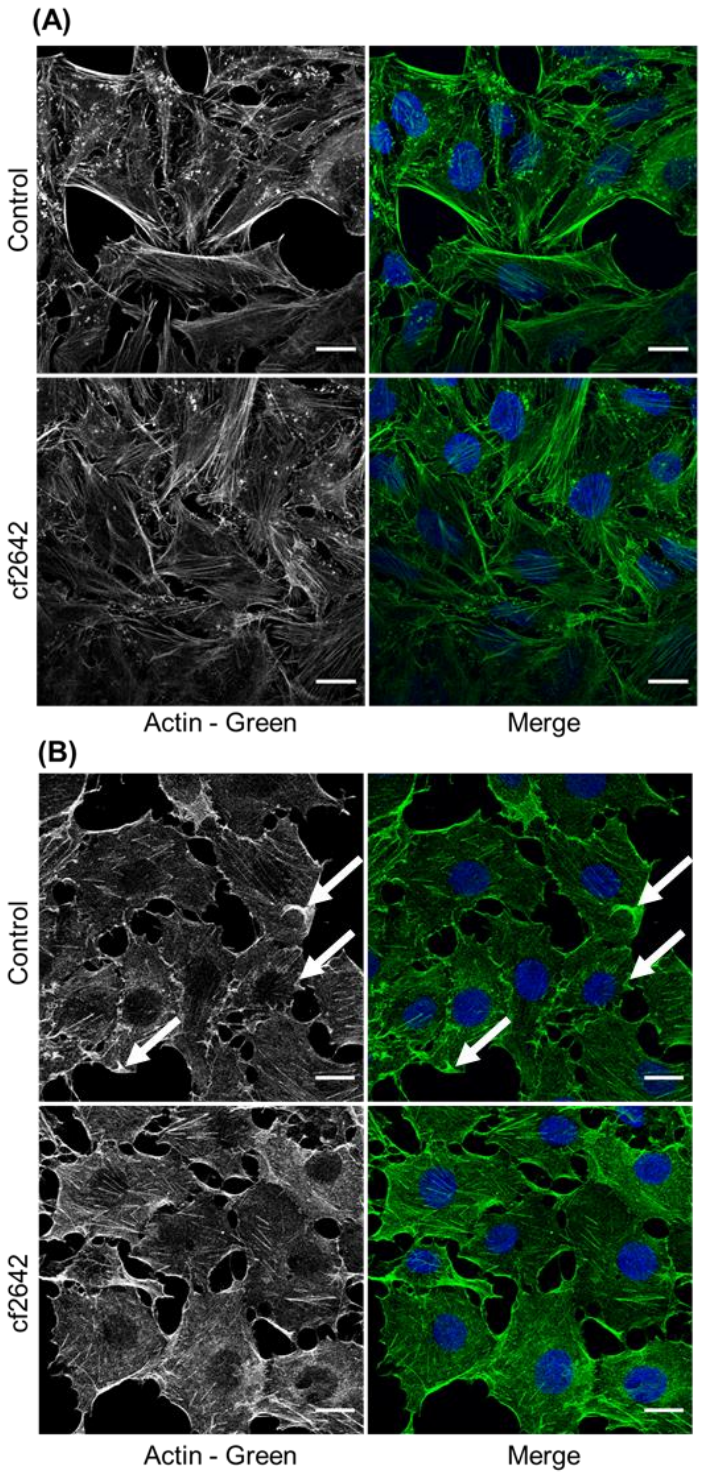

Fig 4.8 Effect of cf2642 on actin network. (A) HeLa and **(B)** VeroSLAM cells were treated or not with 10µM cf2642 for 12 hr and fixed with 3% paraformaldehyde and labelled with rhodamine phalloidin to visualize the actin network. Arrows indicate actin ruffles. The data shows one representative image of three independent experiments. (Scale bars = 20 µm)

Cells were incubated for 12 hrs with diluent control or cf2642 prior to fixing and labelling with the actin probe Rhodamine-Phalloidin, followed by confocal microscopy. Results in Figure 4.8 show clear labelling of actin microfilaments in both cell types. VeroSLAM cells in the absence of cf2642 showed evidence of actin ruffles, but these were mostly absent in the drug treated cells. No differences were observed between control and cf2642 treated HeLa cells. The absence of any observable effects on the actin cytoskeleton in the presence of cf2642 provides more evidence to the fact that the drug is non-toxic at this time point. For example, cytotoxicity resulting in apoptosis of cells would cause extensive changes to the actin network including cell rounding and membrane blebbing (Desouza et al., 2012).

4.2.3.5. Effect of cf2642 on the Golgi network

The goal of this study was to explore the possible effects of cf2642 on the Golgi apparatus that is heavily involved in both secretory and endocytic pathways. Membrane traffic between the endoplasmic reticulum (ER) and the Golgi complex is also critical for the assembly of enveloped viruses like MeV and VACV(Vale-Costa and Amorim, 2016, Brimacombe et al., 2011). In such cases, defects on ER to Golgi traffic can have significant inhibitory effects on virus egress from cells. To label the Golgi control of cf2642 treated cells were treated with BODIPY FL C5- ceramide (Chazotte, 2008) an established fluorescent probe to tag this organelle for fluorescence microscopy.

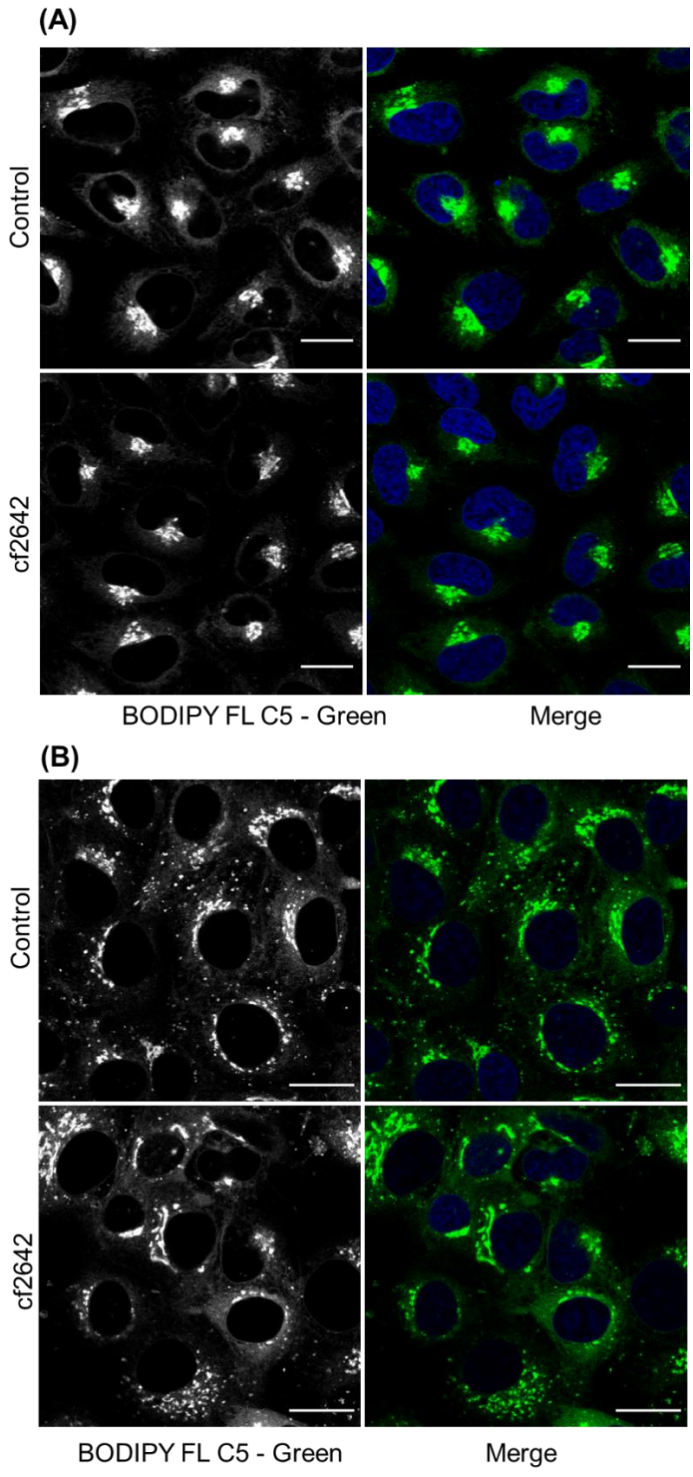

Fig 4.9 Effect of cf2642 on Golgi network. (A) HeLa and **(B)** VeroSLAM cells were treated or not with 10µM cf2642 for 12 hr and incubated on ice with 5µM BODIPY FL C_5 - ceramide for 30 min, washed and incubated for 30 min with fresh medium at TC conditions. Nuclei were labelled with Hoechst before imaging. The data shows one representative image of three independent experiments. (Scale bars = 20 µm)

Typical perinuclear localisation of the BODIPY-ceramide labelled Golgi apparatus was seen in HeLa cells but a quite different localisation was seen in VeroSLAM cells where this probe showed high heterogeneity within the cell population with many cells showing more scattered labelling that is not typically observed with this probe. In some cells, the probe labelled distinct structures, almost completely surrounding the nucleus. No obvious differences were observed in this localisation, in both cell types, after incubation with cf2642 (Fig4.9). Enveloped viruses like measles use the cellular secretory pathway for membrane biogenesis and any disruption of this process could invariable hamper the virus lifecycle. The BODIPY FL C5-ceramide marker used here is a well-documented fluorescent structural marker for labelling the Golgi apparatus (Chazotte, 2008). The absence of any observable changes between control and cf26642 treated cells shows that the secretory pathway is not affected.

4.2.4. LDH cytotoxicity assay for the study of plasma membrane damage

Lactate dehydrogenase (LDH) is a cellular enzyme that is released into the extracellular environment upon plasma membrane damage (Chan et al., 2013b) Here it can be measured as the added lactate is converted to pyruvate via the reduction of NAD+ to NADH in the presence of LDH. The enzyme diaphorase then uses NADH to reduce the tetrazolium salt (INT) present in the assay reagent into a red formazan product, that is directly

proportional to the amount of LDH released. The level of formazan formation can be calculated by measuring absorbance at 490 nm. (see section 2.2.10 in Chapter 2 for methodology). This assay was done to test whether the cf2642 effects observed above were caused by plasma membrane damage; an unidentified agent obtained with the assay kit was used as a positive control for membrane permeabilization.

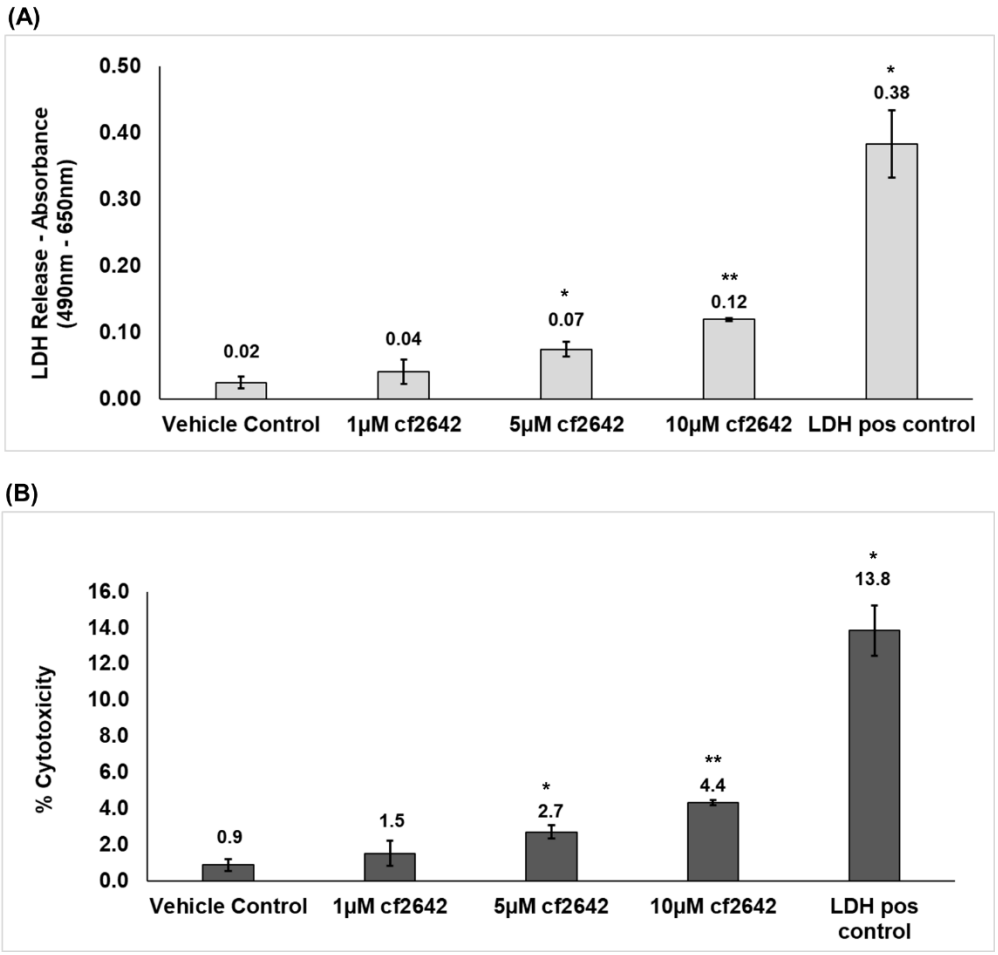

Fig 4.10 cf2642 causes the release of LDH in VeroSLAM cells. VeroSLAM cells were treated with increasing concentrations of cf2642 as indicated and 24 hr post treatment, the amount of LDH released into the extracellular medium was measured using the LDH cytotoxicity assay. **(A)** shows the amount of LDH released and **(B)** indicates the corresponding cytotoxicity. Student's t-test was performed to assess the p values; *p <

0.05, **p < 0.01. Error bars represent mean ± SE of three independent experiments.

Data in Figure 4.10 A and B show the amount of LDH released as a product of enzyme activity and the cytotoxicity calculated as per manufacturer's instructions. The results indicate a dose dependentincrease of LDH release from cells in the presence of cf2642 that is significant at 5µM or higher. However, this release caused <5 % toxicity compared to 12% observed with the LDH positive control. Though a significant amount of LDH was released form cells with cf2642 at 5µM or higher, this only resulted in a 4.4 % increase in cytotoxicity. This suggest that the noted 27% decrease in viability by cf2642 (Chapter 3) was most likely the result of apoptosis induction and not cell necrosis (Chan et al., 2013a, Wang et al., 2014). It does however remain to be determined if cf2642 effects on plasma membrane permeability occur at early time points and that the cells can overcome this by repair and that released LDH is degraded (Kendig and Tarloff, 2007). This could be tested by performing the same LDH release assays at much earlier time points after cf2642 addition.

4.3. Summary

The findings from live imaging experiments using dextran fluorophores demonstrated that treatment of HeLa and VeroSLAM cells with 10µM cf2642 did not have any effects on the constitutive uptake of extracellular cargo via endocytosis and their subsequent transport along the endocytic pathway. Although the labelled LE/lysosomes were scattered in the presence of cf6242, this was also evidence of mislocalisation of early edosomes

highlighted by Rab5 and EEA1positive structures. It remains to be seen whether this scattering phenomenon induced by cf2642 can have effects in MeV entry. Recent publications have shown the MeV uses an alternate mode of cell entry, to fusion with the plasma membrane, utilising a clathrin-independent endocytic uptake mechanism called macropinocytosis. MeV particles that enter via this pathway are localized in large vesicles called macropinosomes (Goncalves-Carneiro et al., 2017, Delpeut et al., 2017). It is not known how the virus escapes these vesicles to underdo replication, but any effects of cf2642 on these structures and subsequent maturation may have direct effects on MeV entry occurring via macropinocytosis. No apparent differences were observed in the Golgi network labelled with BODIPY FLC5 ceramide markers. Some of the effects observed in this chapter may have been caused by cf2642 cell injury and plasma membrane permeability. The results from actin labelling suggested this was not the case as no effects were observed but an LDH assay was performed to investigate this. Thisshowed no plasma membrane permeabilization strongly suggesting that cf2642 induced toxicity is most likely due to the induction of apoptosis and this occurs only after 12-14 hr post treatment with the drug.

Chapter 5: Investigation into the mechanism by which cf2642 inhibits MeV infection

5.1. Introduction

Previous work has shown that the antiviral effect of cf2642 against VACV occurred within two hours post infection. A range of possible targets were tested which indicated that the drug did not affect virus entry but targeted a cellular component that is required throughout the virus life cycle (Farleigh, 2014). Since the antiviral activity of cf2642 was seen against both VACVand MeV, it was speculated that the drug possibly affected a commonly used membrane microdomain. (McGuigan et al., 2013). Similar MoA studies when performed with MeV (rather than VACV) in a different cell line could provide more insights into the cellular targets of cf2642. An added advantage of such an approach is that these findings can then be correlated with the previous MoA data to narrow down the precise cellular target of cf2642 that hinders the life cycle of both viruses. The experiments described in this chapter were performed to elucidate the early effects of cf2642 on VeroSLAM cells that in turn contributes to its anti-measles activity.

MeV entry is initiated by specific interaction between the virus H protein and its receptor SLAM/CD150 (Laksono et al., 2016). This is in turn followed by a cascade of events involving conformational changes of the virus H and fusion (F) proteins, culminating in virus entry via the fusion of virus and host cell plasma membrane at neutral pH (Plemper et al., 2011a) (see section

1.1.3 in Chapter 1). As described in 1.7.3 macropinocytosis is an endocytic pathway that manifests as actin-dependent plasma membrane protrusions or ruffles driving large volumes of the extracellular milieu into cells. These membrane ruffles fold back upon the cells, thereby enclosing the extracellular components within large intracellular structures called macropinosomes (Kerr and Teasdale, 2009). Macropinocytosis has also been exploited by enveloped viruses including Ebolavirus, influenza A, VACVand Nipah virus (Mercer and Helenius, 2009).

The entry of MeV Ed via interaction with CD46 receptors has been shown to result in the internalization and subsequent downregulation of these receptors from the plasma membrane. The initial MeV Ed - receptor interaction on the plasma membrane of susceptible cells results in clustering of CD46 receptors and their internalization via a macropinocytosis-like pathway involving the formation of pseudopodia and membrane protrusions(Crimeen-Irwin et al., 2003). A similar phenomenon was also shown to occur when the CD46 receptors are clustered using antibodies in the absence of live virus . This is different from the constitutively occurring pathway wherein CD46 receptors are internalized via clathrin mediated endocytosis and recycled back to the cell surface via the recycling pathway (Crimeen-Irwin et al., 2003). Recent studies using SLAM positive cells have intriguingly shown a similar macropinocytosis-like entry mechanism for MeV(Delpeut et al., 2017, Goncalves-Carneiro et al., 2017). However, to date there has not been any study involving the antibody-mediated clustering of SLAM to study MeV entry.

This chapter was primarily focused on MoA studies pertaining to the hypothesis that the effects of cf2642 on MeV induced macropinocytosis as an alternative uptake mechanism to that of direct fusion with the plasma membrane. The experiments and data are presented below.

5.2. Results and Interpretation

5.2.1. MeV induced uptake of Dextran-488 in VeroSLAM cells

The administration of MeV to SLAM positive cells in vitro has been shown to result in extensive membrane protrusions and blebs, similar to macropinocytosis. These changes occur very early during the virus-cell interaction and are thought to occur as a result of the clustering of SLAM receptors on the membrane surface (Goncalves-Carneiro et al., 2017). Another study reported the use of fluorescent dextran during the early periods of MeV interaction with VeroSLAM cells, to show that MeV entry can also occurs via a macropinocytosis-like pathway. In this study, an increased uptake of Dextran conjugates was shown to occur at 15 min post administration of MeV with cells, and was speculated to be a direct result of virus induced SLAM receptor clustering (Delpeut et al., 2017). As part of the MoA studies in this chapter, initial experiments were performed to test whether this finding can be replicated in our laboratory setting.

VeroSLAM cells were exposed to MeV as previously described (Delpeut et al., 2017), but with minor modifications. Firstly, the optimum MOI of MeV which can induce high uptake to Dextran-488 at 15 min post administration of virus was determined. VeroSLAM cells were washed with ice-cold PBS

and infected with MeV (MOI 0-100) for 60 min. This was followed by the addition of Dextran-488 on ice at different time points and the uptake was measured by FACS after bringing the cells to 37ºC and fixing with 3% PFA. (see methods section 2.2.18.1.1 for details and section 2.2.20.2.3 for details on flow cytometry analysis)

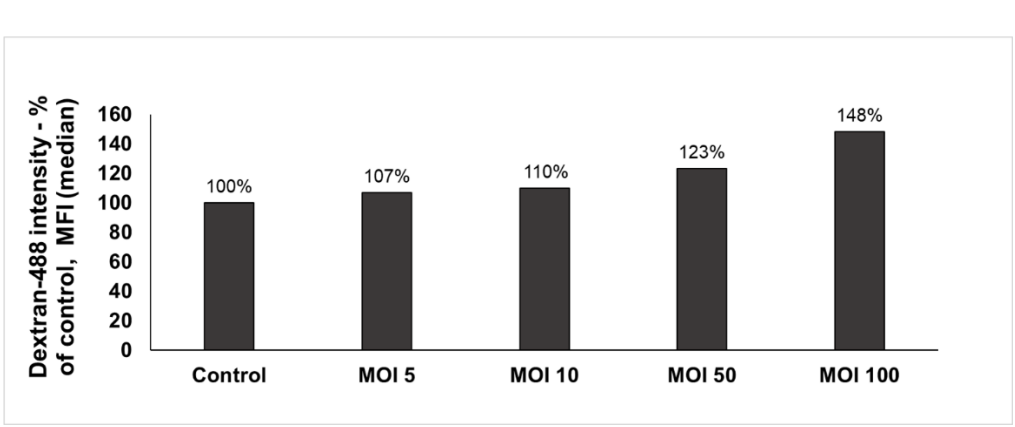

Fig. 5.1. **Dextran-488 uptake induced by MeV is dependent on the MOI.** VeroSLAM cells were infected or not with MeV of increasing MOI's 5, 10, 50 and 100 on ice for 1 hr and moved to 37°C for 15 min. 0.1 mg/ml, Dextran-488 was added during the last 5 min and the fluorescence intensity was analyzed by flow cytometry. The results were quantified and shown as percentage increase of Dextran-488 intensity normalized to the non-infected controls. The results represent data from 1 experiment.

The data in Fig 5.1 depicts the effect of increasing MOIs on the uptake of Dextran-488 in VeroSLAM cells. Results as n=1 suggest that there is a relationship between virus numbers and dextran endocytosis with 100 MOI giving a clear increase in this process. This MOI was then used in the subsequent experiment that also allowed the investigation of whether cf2642 could influence this increase in dextran uptake. The effect of time, following viral infection, on dextran uptake was also analyzed.

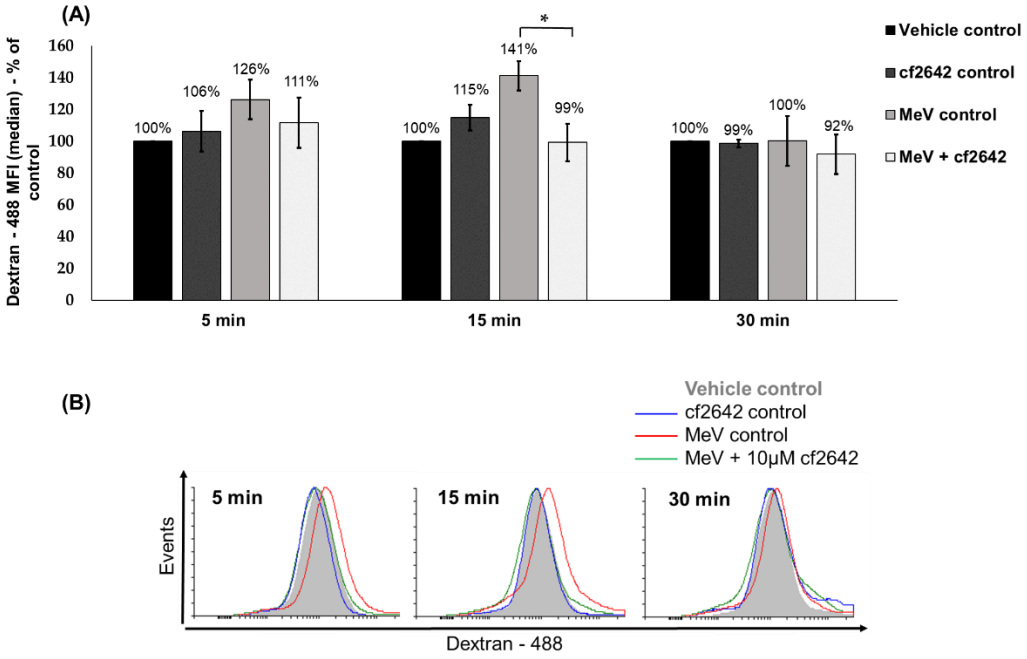

Fig 5.2. MeV stimulates Dextran-488 uptake in VeroSLAM cells, and is inhibited by cf2642. Cells were infected or not with MeV (MOI-100) on ice for 60 min and moved to 37°C for the indicated time periods. 0.1mg/mL Dextran-488 in the presence of 10µM cf2642 or vehicle (DMSO) was added during the last 5 min and the fluorescence intensity was analyzed by flow cytometry. The vehicle control served as a measure of steady state uptake of Dextran-488. **(A)** The results were quantified and shown as percentage increase of Dextran-488 intensity normalized to the vehicle control. Student's t-test was performed to assess the p values; *p < 0.05. Error bars represent mean ± SE of four independent experiments. **(B)** Histogram overlays illustrating the effect of cf2642 on Dextran-488 intensity. Data from one representative experiment is shown.

Results in Fig 5.2 shows a 41% increase in Dextran-488 uptake over the vehicle control occurring at 15 min post administration of MeV in VeroSLAM cells and this was reduced to control levels in the presence of 10µM cf2642. Surprisingly dextran uptake was reversed to control levels after 30 mins. This is

also clearly evident by the shift in fluorescence intensity as seen in the histogram overlay in Fig 5.2B. Uninfected controls when treated with cf2642 resulted in minor, non-significant increases in Dextran-488 uptake at both 5 and 15 min time points. At all three time points, MeV infected cells when treated with cf2642, caused the reduced uptake of Dextran-488. In agreement with previous reports (Delpeut et al., 2017), Dextran-488 uptake experiments demonstrated that MeV induces a transient increase in fluid-phase uptake in VeroSLAM cells at 15 min post-administration of virus. In the presence of 10µM cf2642, this effect was significantly reversed after only very short incubations. Here, the clear effects of virus induced macropinocytosis required MOI of 100 that is higher than previously used to show these effects (Delpeut et al., 2017). However, these published studies were performed in serum starved cells that are much more responsive to plasma membrane activation of receptors. The induction of macropinocytosis and associated changes in cell membrane morphology occurring during MeV entry into SLAM positive cells has been speculated to be a direct result of SLAM receptor clustering mediated by the virus particles (Goncalves-Carneiro et al., 2017).

5.2.2. Dextran-488 uptake induced by SLAM-receptor clustering with polyclonal antibodies

SLAM receptor clustering using antibodies was done to mimic MeV induced effects on cells in a virus-free setting. By replicating virus-induced effects on cells using this technique, it is possible to better characterize the cell targeting effects of cf2642. The addition of polyclonal antibodies against plasma membrane receptors is a well characterized method for inducing

clustering (Crimeen-Irwin et al., 2003). SLAM was initially performed to test whether the virus induced Dextran-488 uptake shown in Fig 5.2 can be replicated in the absence of live MeV. This was done by using polyclonal antibodies against the SLAM to cluster these receptors. The methodology followed was similar to that described in section 5.1, except that polyclonal anti-SLAM antibodies were used instead of live virus (see section 2.2.18.1.2 in methods and section 2.2.20.2.3 for details on flow cytometry analysis)

.

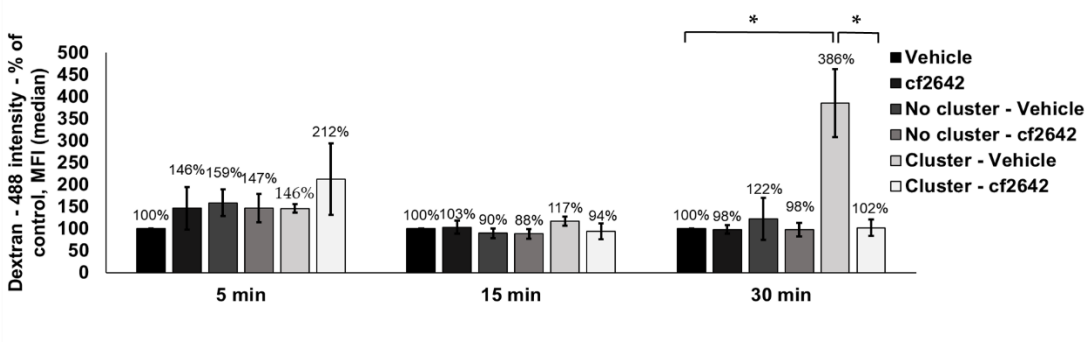

Fig 5.3.Clustering of SLAM receptors stimulates Dextran-488 uptake in VeroSLAM cells, and is inhibited by cf2642. Cells were incubated with 6µg/mL polyclonal rabbit anti SLAM antibody for 60 min on ice, moved to 37°C for the indicated time periods and 0.1mg/mL Dextran-488 in the presence of 10µM cf2642 or vehicle (DMSO) was added during the last 5 min. Cells were then fixed with 3% PFA, washed with PBS and the fluorescence intensity was analyzed by flow cytometry. The results were quantified and shown as percentage increase of Dextran-488 intensity normalized to the vehicle control. The vehicle control served as a measure of steady state Dextran-488 uptake. Student's t-test was performed to assess the P values; *$p < 0.05$. Error bars represent mean ± SE of four independent experiments

Results shown in Fig 5.3 depicts a significant increase in Dextran-488 uptake occurring at 30 min post addition of polyclonal anti-SLAM antibodies. This is also significantly reduced close to control levels in the presence of 10µM cf2642. Comparatively low levels of uptake of Dextran-488 was

observed in the no antibody control - vehicle and cf2642 controls at all three time points, but none were statistically different from the controls. A similar increase was also observed with the cf2642 control at 5 min time point. Slightly higher uptake of Dextran-488 was seen in clustered cells at 5 min in the presence of cf2642, but this was also not statistically significant. Polyclonal anti-SLAM antibodies caused a significant increase in fluid-phase uptake of Dextran-488, but in this case at a later (30 min) time point compared to live virus (15 min). No significant increase in Dextran-488 uptake was observed at this time point in the no cluster controls using monoclonal anti-SLAM antibodies. This confirms that the observed increase in fluid-phase endocytosis at 30 min is a direct result of SLAM-receptor clustering. This early induction of fluid-phase endocytosis with MeV suggests that the virus promotes earlier activation of macropinocytosis via SLAM interaction and/or interaction with another plasma membrane component. Moreover, the interactions of MeV and SLAM antibodies targeting this receptor may be disparate because of the differences in SLAM - binding sites on the virus particles (hemagglutinin) and antigen binding sites on the polyclonal antibodies. A previous study on the clustering of CD46 receptors induced either with measles vaccine strain (MeV-Vac) or antibodies showed that the valence of interactions between the virus and its receptor has a major influence on the cells response to these events (Crimeen-Irwin et al., 2003). Overall, the clustering induced results mimics the effects of MeV on macropinocytosis and associated increase in fluid-phase endocytosis, and these processes are inhibited by cf2642.

5.2.3. Indirect SLAM-receptor clustering with primary-secondary antibody combination

The objective behind using this method was to enable the observation of, what are postulated to be, changes associated with SLAM-receptor clustering by confocal microscopy. The non-availability of good directly labelled monoclonal antibodies against SLAM for confocal microscopy, restricts the use of direct SLAM clustering for IF assays. Thus an indirect method for clustering SLAM was used. VeroSLAM cells were briefly incubated (30 min) with mouse anti-SLAM monoclonal antibodies at 37ºC. This was then followed by incubation of cells with an anti-mouse secondary antibody that is conjugated with Alexa Fluor - 647. In a virus-free setting, these secondary antibodies mimics MeV particles that come into contact with cells during the initial stages of virus-cell interaction. The effect of SLAM clustering was then analyzed by microscopy at different time points post clustering w/o cf2642. An added advantage of using this methodology for IF experiments is that the fluorescence signal associated with SLAM, that is labelled by the Alexa Fluor -647 conjugated secondary antibody, is not lost upon fixation with PFA. This allows the use to unlabelled anti-SLAM primary antibodies for these experiments.

5.2.3.1. Calculation of protein concentration and dye:protein molar ratio for the Alexa fluor antibody used for SLAM clustering

The indirect clustering of SLAM receptors was done using a commercially available Alexa Fluor-647 conjugated secondary antibody which contains 5 mM sodium azide (NaN_3) as a preservative. Since the experiment involves

incubation of live cells with this antibody, the NaN_3 content was removed using centrifugal filtration (see methods section 2.2.16.1.1).

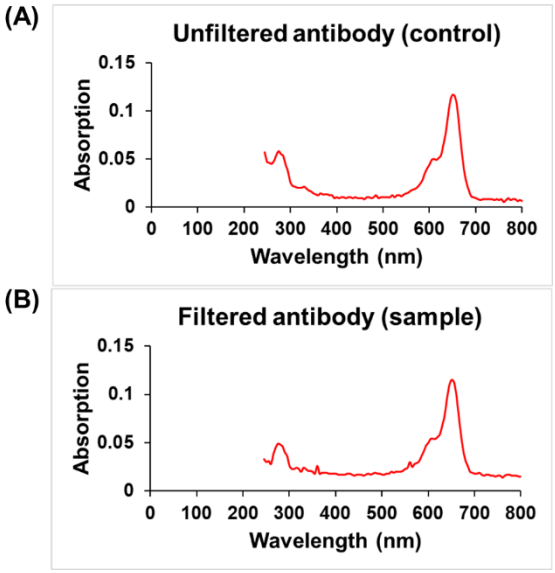

Fig 5.4 Absorption spectrum of chicken anti mouse Alexa Fluor-647 antibody solution. The commercially available chicken anti-mouse Alexa Fluor - 647 secondary antibody solution was purified by centrifugal filtration and absorbance measured at 280 to 650 nm using a Cary60 UV spectrophotometer. The values were compared with the unfiltered antibody (control). Figure shows the absorption spectrum for **(A)** Unfiltered antibody and **(B)** filtered antibody solutions.

Absorption spectra (Fig 5.4) and molar extinction coefficients were used to calculate the numbers of fluorophores in the antibody, dye:protein ratio (see methods section 2.2.16.1.2). The protein concentration for the unfiltered control and filtered antibody solutions were calculated to be 1.9 and 1.6 mg/mL respectively. Using these protein concentration values, the dye:protein molar ratio were found to be 2.0 for the unfiltered control and 1.8 for the filtered antibody.

5.2.3.2. Dose-dependent response of Alexa Fluor-647 conjugated secondary antibodies on SLAM internalization

During live MeV infection, cells may be exposed to different titres of live virus particles during the virus entry. Hence, to best mimic MeV infection in a non-infectious setting by SLAM clustering, the cells were exposed to increasing concentrations of secondary antibody. This was also used to determine the optimum secondary antibody concentration to be used for subsequent SLAM clustering experiments.

Briefly, live VeroSLAM cells were first incubated with 2 µg/mL anti-mouse SLAM antibody and then clustered with increasing concentrations of Alexa Fluor-647 secondary antibody at 37ºC in the presence or absence of 10µM cf2642. The cells were then fixed and incubated with LAMP1 antibodies directly labelled with the fluorophore FIT to label lysosomes. The fluorescence signal from directly labelled secondary antibodies (no primary) served as the label for SLAM receptors. The amount of internalized SLAM was then calculated using imagej (see methods section 2.2.16.1.4.2.1 for details).

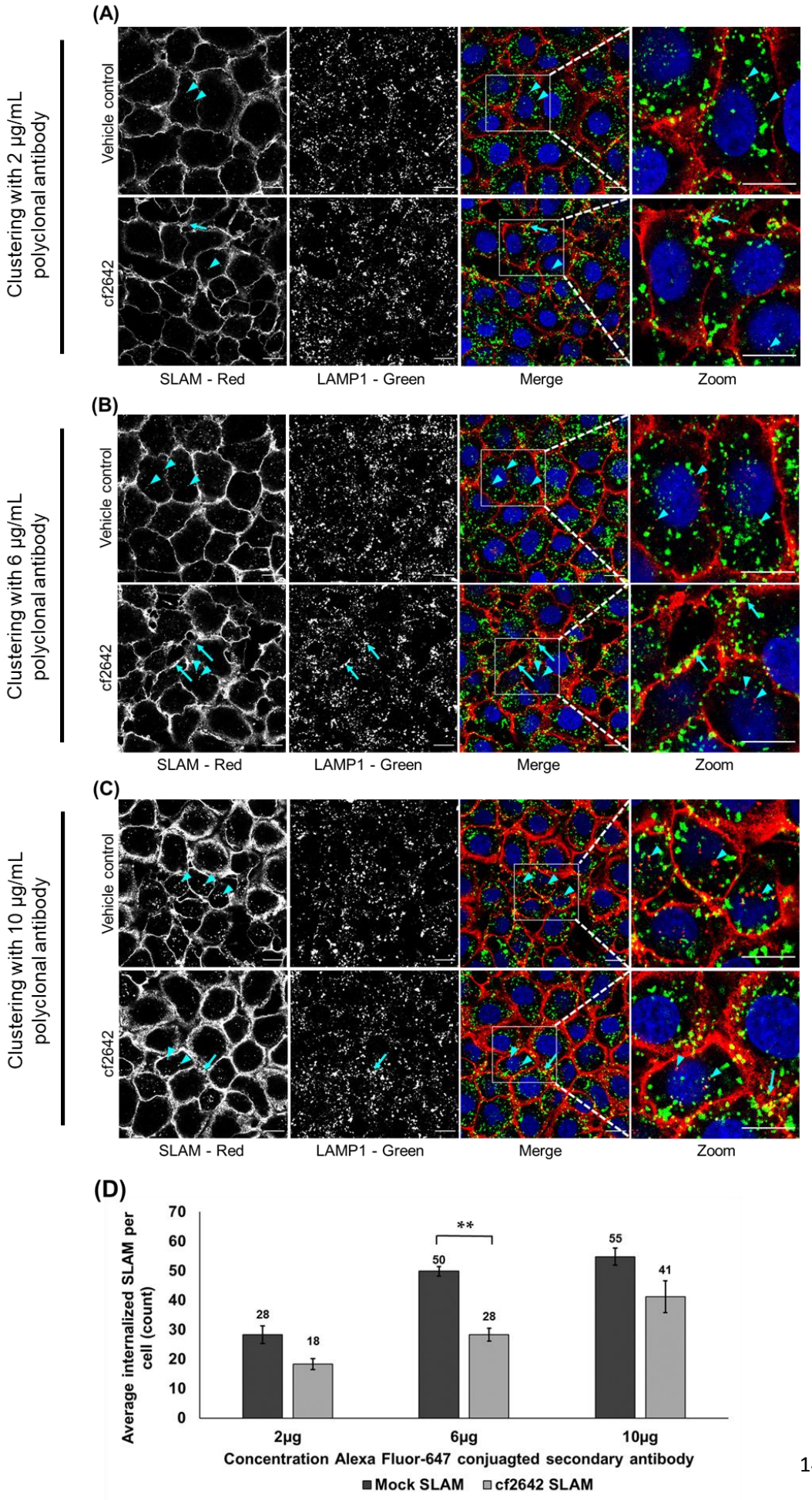
(A)
Clustering with 2 µg/mL polyclonal antibody
Vehicle control
cf2642
SLAM - Red
LAMP1 - Green
Merge
Zoom
(B)
Clustering with 6 µg/mL polyclonal antibody
Vehicle control
cf2642
SLAM - Red
LAMP1 - Green
Merge
Zoom
(C)
Clustering with 10 µg/mL polyclonal antibody
Vehicle control
cf2642
SLAM - Red
LAMP1 - Green
Merge
Zoom
(D)
Average internalized SLAM per cell (count)
70
60
50
40
30
20
10
0
**
28
18
50
28
55
41
2µg
6µg
10µg
Concentration Alexa Fluor-647 conjuagted secondary antibody
Mock SLAM
cf2642 SLAM

Fig 5.5. Effect of secondary antibody concentration on SLAM internalization in VeroSLAM cells. Cells were incubated for 30 min with monoclonal mouse anti-SLAM antibody and then incubated for 60 min with increasing concentrations of anti-mouse Alexa Fluor-647 conjugated secondary antibodies. After a 60 min chase, cells were fixed with 3% PFA and labelled with LAMP1-FITC antibody to label lysosomes. The single section images show incubations with **(A)** 2 µg/mL, **(B)** 6 µg/mL and **(C)**10µg/mL secondary antibody. **(D)** The average number of Internalized SLAM positive vesicles per cell were quantified using imagej by drawing ROIs for 30 cells per condition, and to include only the internal region of cells. Arrows indicate the aggregation of LAMP1 positive lysosomes in close proximity to the SLAM labelled plasma membrane in cf2642 treated cells. Arrowheads show internalised SLAM in punctate structures. Images are representative of three independent experiments. (Scale bar =20µm).

The data shown in Fig 5.5 indicates an increase in internalized SLAM positive vesicles, with increasing concentration of the Alexa Fluor-647 conjugated secondary antibody used for clustering. This was significantly reduced by half in the presence of cf2642 in cells clustered with 2 and 6 µg/mL secondary antibody (Fig 5.5D). The drug treated cells also showed the aggregation of LAMP1 positive lysosomes close the plasma membrane. A more pronounced labelling of SLAM was also observed with increasing concentrations of the secondary antibody. No significant cf2642 induced decreases in SLAM internalization was observed at 2 and 10µg/mL secondary antibody concentrations. The results indicate that the optimum concentration of secondary antibody to be used for indirect SLAM clustering was 6 µg/mL. No significant increases in internalization of SLAM was seen using higher concentration of antibody (10µg/mL), which could be because the antibody binding sites of SLAM receptors on the plasma membrane are completely occupied by these antibodies. Treatment with cf2642 caused the reduced internalization of SLAM and the tight grouping of LAMP1 labelled

lysosomes near the plasma membrane and this may be attributed to the effects of cf2642 on the plasma membrane. Lysosomal exocytosis and membrane resealing are known to occur in response to plasma membrane damage (Reddy et al., 2001, Tam et al., 2010). Whether cf2642 causes plasma membrane damage is not clear, but such effects do not affect cell viability at this concentration and at such short time points (see section 3.1 in Chapter 3.

5.2.4. Dextran-488 uptake induced by indirect SLAM-receptor clustering

Based on the dose response assay in section 5.6 above, all subsequent indirect SLAM-receptor clustering experiments were done using 6 µg/mL of the Alexa Fluor-647 conjugated secondary antibodies. The dextran uptake experiment by indirect SLAM clustering was done to test whether the results obtained with direct SLAM clustering in section 5.2 can be replicated using a combination of primary and secondary antibodies. If a similar trend in Dextran uptake can be obtained using this methodology, it gives more credence for the use of SLAM clustering as a non-virus based assay to mimic virus - cell interaction in vitro.

Indirect clustering of SLAM receptors was done by briefly incubating live VeroSLAM cells with monoclonal mouse anti-SLAM antibodies at 37ºC, followed by washing and incubating with Alexa Fluor - 647 conjugated polyclonal anti-mouse secondary antibodies on ice. This is followed by the addition of Dextran-488 at 5, 10 and 15 min time points w/o 10µM cf2642 as

done previously in sections 5.2 and 5.3 (see section 2.2.18.1.3 in methods and section 2.2.20.2.3 for details on flow cytometry analysis)

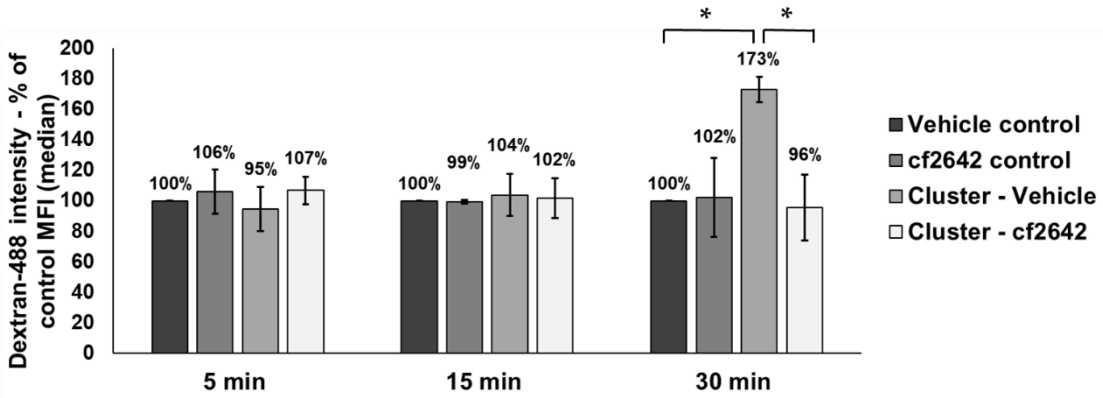

Fig 5.6.Indirect Clustering of SLAM receptors stimulates Dextran-488 uptake in VeroSLAM cells, and is inhibited by cf2642. Cells were first incubated with 2 µg/mL mouse anti-SLAM antibody for 30 min at 37ºC, washed and then incubated with 6 µg/mL polyclonal anti-mouse Alexa Fluor-647 antibody (cluster) for 60 min on ice. The cells were then moved to 37°C for the indicated time periods and 0.1 mg/mL Dextran-488 in the presence of 10µM cf2642 or vehicle (DMSO) was added during the last 5 min. Fluorescence intensity was analyzed by flow cytometry. The results were quantified and shown as percentage increase of Dextran-488 intensity normalized to the vehicle control. The vehicle control served as a measure of steady state Dextran-488 uptake. Student's t-test was performed to assess the P values; *p < 0.05. Error bars represent mean ± SE of three independent experiments.

A 73% increase in Dextran-488 uptake over the vehicle control, was seen in SLAM clustered cells at the 30 min time point (Fig 5.6) and this was significantly reduced in the presence of 10µM cf2642. Slight increases in Dextran-488 uptake was observed in the cf2642 controls and in clustered cells at 5 and 15 min time points. A 5% decrease in Dextran-488 uptake was seen in clustered cells at 5 min, but was not statistically significant. The results were similar to that of direct clustering wherein an increased dextran-488 uptake was observed at 30 min. In this case, the fluorescence intensity

of internalized dextran was less than that of direct clustering, which could be a consequence of differences in SLAM receptor-antibody interactions at the plasma membrane.

5.2.5. Effect of cf2642 on SLAM internalization and localization of lysosomes

The clustering of SLAM by MeV has been shown to cause the downregulation of these receptors at 24 - 48 hr post infection (Tanaka et al., 2002, Welstead et al., 2004). Since cf2642 was shown to causes a decrease in internalization of SLAM from the plasma membrane (section 5.7), the effect of cf2642 on extended clustering periods was studied. Any effects on the internalization and subsequent downregulation of SLAM may hinder MeV pathogenesis by affecting the ability of the virus to re-infect susceptible cells (Welstead et al., 2004).

Indirect clustering of SLAM was done as mentioned previously (section 5.7) and chased for either 1 or 5 hr after clustering with Alexa Fluor-647 conjugated secondary antibodies. The 2 and 6 hr clustering time periods mentioned below are defined based on the total incubation times after the initial 30 min incubation with mouse anti-SLAM antibody. Cells were then fixed and labelled with LAMP1-FITC antibody to label the lysosomes. The fluorescence signal from directly labelled secondary antibodies served as the label for SLAM receptors (see methods section 2.2.16.1.4.2.2).

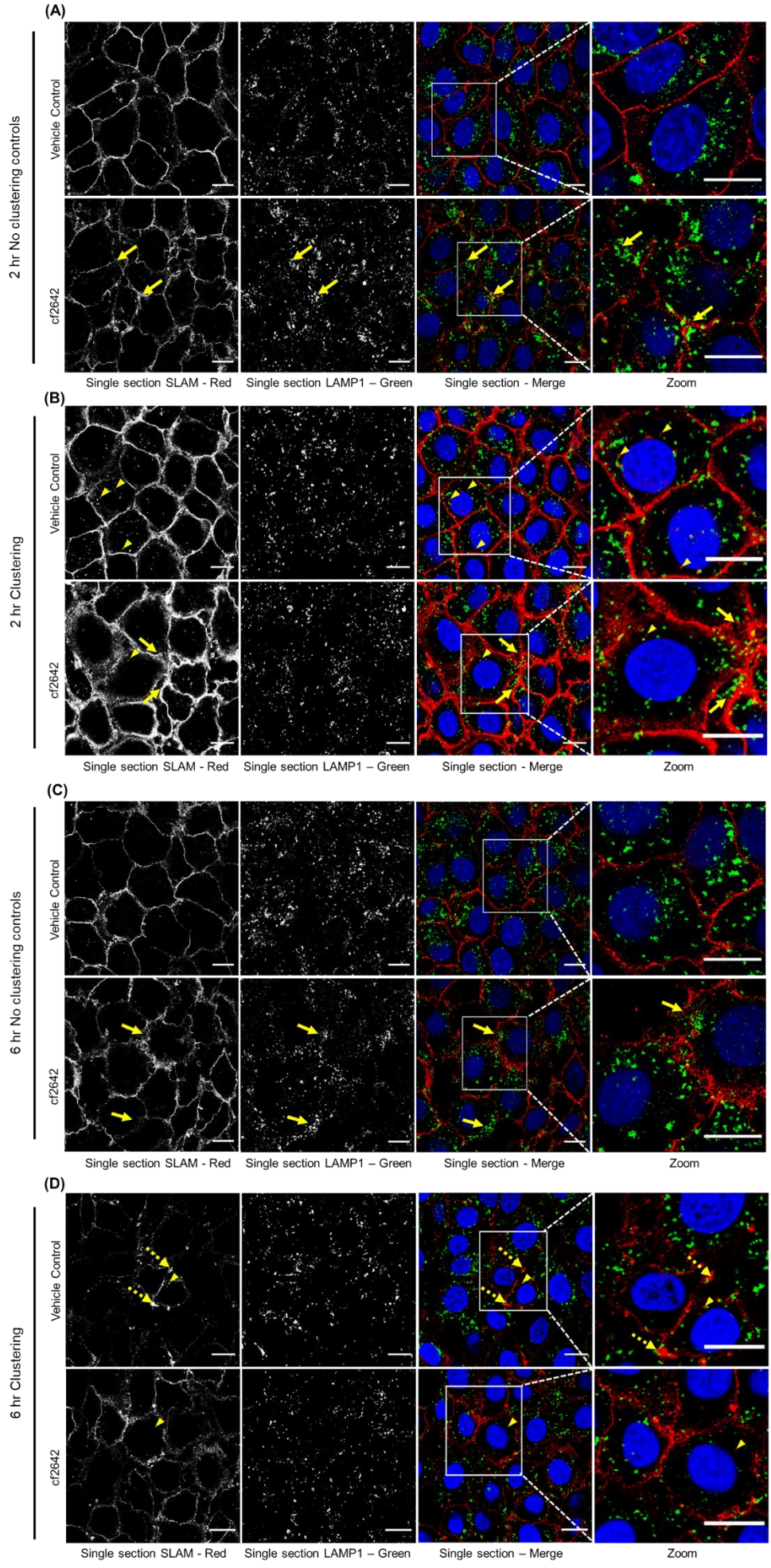
(A)
2 hr No clustering controls
Vehicle Control
cf2642
Single section SLAM - Red
Single section LAMP1 – Green
Single section - Merge
Zoom
(B)
2 hr Clustering
Vehicle Control
cf2642
Single section SLAM - Red
Single section LAMP1 – Green
Single section - Merge
Zoom
(C)
6 hr No clustering controls
Vehicle Control
cf2642
Single section SLAM - Red
Single section LAMP1 – Green
Single section - Merge
Zoom
(D)
6 hr Clustering
Vehicle Control
cf2642
Single section SLAM - Red
Single section LAMP1 – Green
Single section – Merge
Zoom

Fig 5.7 cf2642 causes reduced internalization of clustered SLAM receptors. Live VeroSLAM cells were incubated or not with mouse anti-SLAM antibodies for 30 min and clustered or not for 1 hr with chicken anti-mouse Alexa Fluor-64 conjugated secondary antibodies at 37ºCin the presence or absence of 10µM cf2642. Cells were then chased for 1 hr or 5 hr w/o 10µM cf2642 and immunolabelled with LAMP1-FITC antibody. **(B)** and **(D)** show cells after 2 hr (1 hr cluster + 1 hr chase) and 6 hr (1 hr cluster + 5 hr chase) SLAM clustering respectively. Steady state levels of SLAM without receptor clustering at 2 hr and 6 hr post treatment or not with cf2642 are shown in **(A)** and **(C)** respectively. Arrow heads indicate internalized SLAM positive vesicles. Arrows indicate the localization of LAMP1 labelled lysosomes near the plasma membrane and dashed arrows show small aggregates of SLAM labelling associated with the plasma membrane. Images are representative of three independent experiments. (Scale bar =20µm).

The 2 hr clustering of SLAM receptors resulted in internalization of SLAM positive vesicles and this was partially inhibited in the presence of 10µM cf2642 (Fig 5.7B). No such receptor internalization was observed in cells without clustering at both 2 and 6 hr time points, both in the presence or absence of cf2642 (Fig 5.7 A,C). Treatment with cf2642 resulted in the mislocalization of LAMP1 positive lysosomes to close proximity with the SLAM-labelled plasma membrane that was not observed in control cells. Cells subjected to 6 hr SLAM-receptor clustering did not show prominent plasma membrane SLAM labelling that was more apparent in the presence of cf2642 (Fig 5.7 D). The data indicate that extended clustering time periods resulted in almost complete loss of SLAM labelling from the plasma membrane. However, much of the SLAM labelling associated with the plasma membrane was retained in the presence of cf2642. This shows that the effect of cf2642 on SLAM internalization is not limited to the early time points post treatment. Controls without SLAM clustering showed uniform

labelling of the plasma membrane and no internalized vesicles, indicating that SLAM internalization is not a constitutive process and does not occur in the absence of clustering. It should be noted that the labelling methods used for the no-clustering controls was slightly different to that of the method used for clustered cells. In this case, cells were treated or not with cf2642 for the appropriate time periods, fixed and immunolabelled with SLAM and LAMP1. In the case of clustering, the cells were fixed and labelled only with LAMP1. Here, the SLAM labelling is associated with the fluorescence from the Alexa Fluor-647 conjugated secondary antibodies used for clustering. Interestingly, at 6 hr post clustering, the fluorescence signal from internalized SLAM vesicles was almost completely absent both in the presence and absence of drug.

5.2.6. Effect of cf2642 on SLAM internalization and localization of early endosomes

The above SLAM clustering experiments had shown the localization of lysosomes near the plasma membrane of cells in the presence of cf2642. To investigate whether this was specific to this organelle, cells treated in the same way were also labelled for EEA1, a marker of early endosomes. The methodology used for SLAM clustering was the same as before (section 5.7), but immunolabelling was done using EEA1 antibodies (see methods sections 2.2.16.1.4.2.2 and 2.2.3.2.3.4)

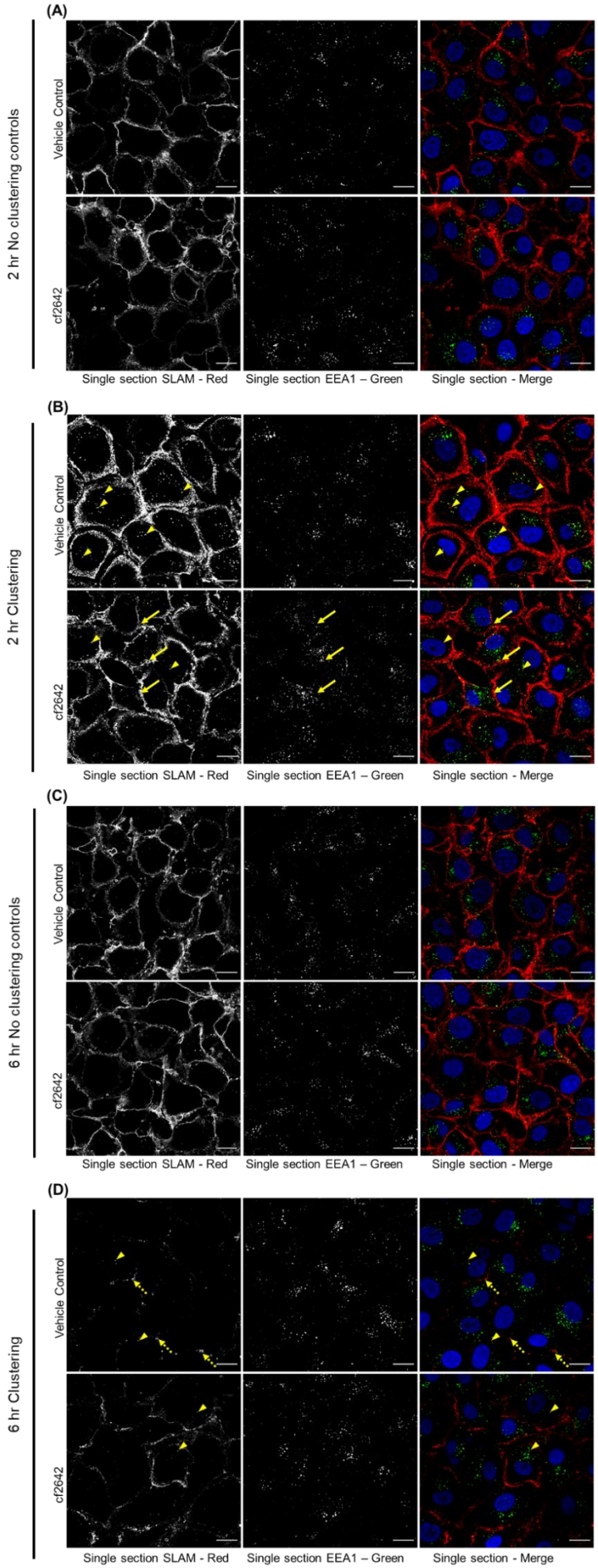
(A)
2 hr No clustering controls
Vehicle Control
cf2642
Single section SLAM - Red
Single section EEA1 – Green
Single section - Merge
(B)
2 hr Clustering
Vehicle Control
cf2642
Single section SLAM - Red
Single section EEA1 – Green
Single section - Merge
(C)
6 hr No clustering controls
Vehicle Control
cf2642
Single section SLAM - Red
Single section EEA1 – Green
Single section - Merge
(D)
6 hr Clustering
Vehicle Control
cf2642
Single section SLAM - Red
Single section EEA1 – Green
Single section - Merge

Fig 5.8 cf2642 causes scattering of early endosomes in cells with clustered SLAM receptors. Live VeroSLAM cells were incubated or not with mouse anti-SLAM antibodies for 30 min and clustered or not for 1 hr with chicken anti-mouse Alexa Fluor-64 conjugated secondary antibodies at 37ºCin the presence or absence of 10µM cf2642. Cells were then chased for 1 hr or 5 hr w/o 10µM cf2642, fixed with 3% PFA and immunolabelled with EEA1 antibody. **(B)** and **(D)** show cells after 2 hr and 6 hr SLAM clustering respectively. Steady state levels of SLAM without receptor clustering at 2.5 hr and 5.5 hr post treatment or not with cf2642 are shown in **(A)** and **(C)** respectively. Arrow heads indicate internalized SLAM positive vesicles. Arrows indicate the localization of EEA1 labelled early endosomes near plasma membrane and dashed arrows show small aggregates of SLAM labelling associated with the plasma membrane. Images are representative of two independent experiments. (Scale bar =20µm).

Internalization of SLAM positive vesicles was observed upon 2 hr receptor clustering and this was partially inhibited with 10µM cf2642. EEA1 labelled early endosomes were seen in close proximity with the plasma membrane in cf2642 treated cells with 2 hr SLAM clustering (Fig 5.8 B). Few internalized SLAM positive structures were seen in the cells without clustering, 6 hr post treatment w/o cf2642 (Fig 5.8 C). Cells with 6 hr SLAM-receptor clustering showed very few internalized SLAM positive vesicles, and most of the plasma membrane associated SLAM labelling was retained in the presence of cf2642. In the absence of cf2642, small aggregates or clumps of SLAM positive regions were observed in the plasma membrane (Fig 5.8 D). The similarity in localization of LAMP1 (section 5.8) and EEA1 positive vesicles near the plasma membrane refutes the earlier discussed possibility that this may be associated with plasma membrane damage (see section 5.6).

5.2.7. Method development - Indirect SLAM clustering

5.2.7.1. Clustering with unconjugated secondary antibodies

Previous experiments in section 5.8 and 5.9 showed only very few internalized SLAM positive vesicles at 6 hr post clustering. This may either be the result of downregulation and subsequent degradation of these vesicles in the lysosomes or it could be an artefact associated with the fluorescence tag of the directly conjugated clustering secondary antibodies used. Thus an alternate methodology for clustering of SLAM receptors was designed and investigated. VeroSLAM cells were incubated with monoclonal anti SLAM antibodies for 30 min on ice in the absence of cf2642 and then clustered using unconjugated goat anti mouse secondary antibodies for 1 hr w/0 cf2642. After suitable chase periods, cells were fixed and immunolabelled with anti-SLAM and LAMP1 antibodies (see methods section 2.2.16.1.4.2.3)

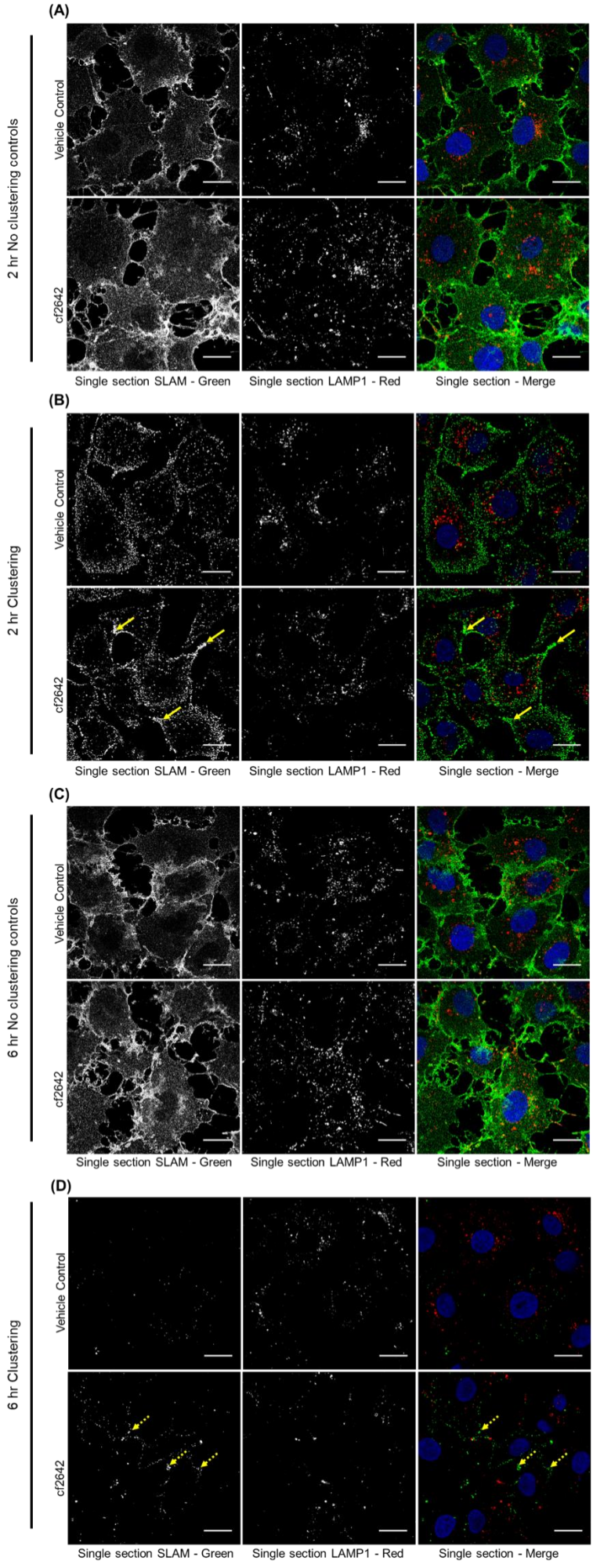
(A)
2 hr No clustering controls
Vehicle Control
cf2642
Single section SLAM - Green
Single section LAMP1 - Red
Single section - Merge
(B)
2 hr Clustering
Vehicle Control
cf2642
Single section SLAM - Green
Single section LAMP1 - Red
Single section - Merge
(C)
6 hr No clustering controls
Vehicle Control
cf2642
Single section SLAM - Green
Single section LAMP1 - Red
Single section - Merge
(D)
6 hr Clustering
Vehicle Control
cf2642
Single section SLAM - Green
Single section LAMP1 - Red
Single section - Merge

Fig 5.9 Indirect clustering with unconjugated secondary antibodies shows an altered labelling pattern of SLAM receptors. Live VeroSLAM cells were incubated or not with mouse anti-SLAM antibodies for 30 min on ice in the absence of cf2642 and clustered or not for 1 hr with goat anti-mouse secondary antibodies at 37ºCin the presence or absence of 10µM cf2642. Cells were then chased for 1 hr or 5 hr w/o 10µM cf2642, fixed with PFA and immunolabelled with LAMP1 and anti-goat Alexa Fluor-488 secondary antibodies to label the lysosomes and SLAM respectively. **(B)** and **(D)** show cells after 2 hr and 6 hr SLAM clustering respectively. Steady state levels of SLAM without receptor clustering at 2.5 hr and 5.5 hr post treatment or not with cf2642 are shown in **(A)** and **(C)** respectively. Arrows indicate localized areas of dense SLAM labelling in plasma membrane dashed arrows show small aggregates of SLAM labelling associated with the plasma membrane. Images are representative of three independent experiments. (Scale bar =20µm).

In the absence of the secondary antibody to induce clustering, SLAM labelling was observed predominantly on the plasma membrane with some evidence of cytoplasmic localisation (Fig 5.9 A and C). The phenotype was very different 2 hr post clustering where SLAM labelling was predominantly associated with vesicles scattered within the cytoplasm and more concentrated at the plasma membrane. A similar pattern was also observed in cf2642 treated cells, but with more prominent plasma membrane extensions (Fig 5.9 B). Cells incubated with the secondary antibody for 6 hr to induce clustering (Fig 5.9 D lower panel) showed almost no SLAM labelling on the plasma membrane that was still apparent in cf2642 incubated cells.The absence of uniform plasma membrane labeling of SLAM as seen previously could be due to the initial incubation of primary antibody on ice or the affinities between clustering and post fixation secondary antibodies. Even with this new method, the internalized SLAM vesicles were still not visible 6hr post clustering.

5.2.7.2. Indirect SLAM-receptor clustering in live cells

Since the use of unconjugated secondary antibodies did not improve the labelling of SLAM after 6 hr clustering, the protocol was repeated in live VeroSLAM cells. This can be used to determine whether the PFA fixation of cells at 6 hr post clustering has any effect on the fluorescence signal from Alexa Fluor-647 conjugated secondary antibodies. Cells were first pulse chased with Dextran-488 to label late endosomes/lysosomes and the indirect clustering of SLAM was done for 2 or 6 hr using Alexa Fluor-647 labelled secondary antibodies, followed by live imaging. (see methods section 2.2.16.1.4.2.4)

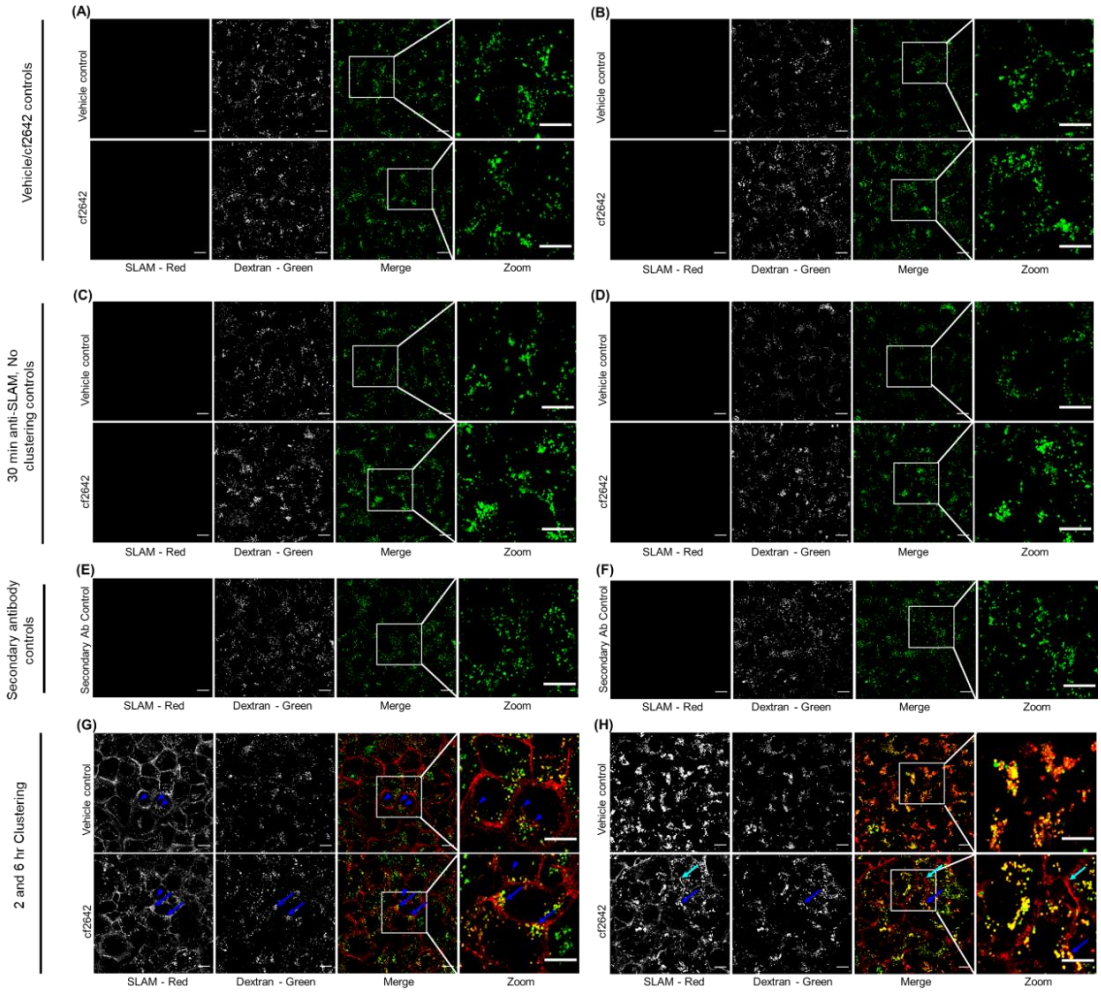

Fig 5.10. SLAM clustering in live cells reveals localization of these receptors 6 hr post clustering. Live VeroSLAM cells were pulsed with 0.2 mg/mL Dextran-488 for 2 hr and chased for 18 hr. Cells were then incubated or not with mouse anti-SLAM antibodies for 30 min at 37ºCin the presence or absence of cf2642, clustered or not for 1 hr with polyclonal Alexa Fluor-647 conjugated chicken anti-mouse secondary antibodies and chased for 1 or 5 hr w/o 10µM cf2642. Live images were captured at the respective time points. **(A)** and **(B)** show controls incubated or not with cf2642 for 2.5 hr and 6.5 hr respectively. The no-clustering controls were incubated for 30 min with mouse anti-SLAM antibodies w/o cf2642, washed and incubated or not with cf2642 for either **(C)** 1.5 or **(D)** 5.5 hr. **(E)** and **(F)** show secondary antibody controls pertaining to the 2 and 6 hr clustering time points respectively. **(G)** shows cells with 2 hr clustering and **(H)** shows clustering for 6 hr. Images show SLAM in red and late endosomes/lysosomes in green. Arrow heads indicate internalized SLAM positive vesicles and blue arrows show the localization of late endosomes/lysosomes near the plasma membrane. Cyan arrow heads show co-localization of internalized SLAM positive vesicles and Dextran-488 labelled late endosomes/lysosomes. Cyan arrows show SLAM labelled plasma membrane retained in the presence of cf2642. Images are representative of three independent experiments. (Scale bar =20µm).

The vehicle and cf2642 controls at both 2.5 and 6.5 hr post treatment showed cells with uniform localization of the Dextran-488 labelled late endosomes/lysosomes (Fig 5.10.0 A-B). No-clustering controls treated with cf2642 showed cells with late endosomes/lysosomes localized in tight groups, compared to the more dispersed positioning seen in vehicle controls (Fig 5.10 C-D). SLAM clustering for 2 hr caused decreased internalization of SLAM positive vesicles in the presence of cf2642. Also, the Dextran labelled late endosomes/lysosomes were positioned near the plasma membrane and co-localized with the internalized SLAM positive vesicles. No differences in the plasma membrane labelling was observed between the vehicle and cf2642 treated cells at this time point (Fig 5.10 E-F). When clustered for 6 hr in the absence of cf2642, the SLAM labelling associated

with plasma membrane was completely lost and the internalized SLAM positive vesicles were co-localized with the Dextran-488 labelled late endosomes and lysosomes. However, in the presence of cf2642, much of the SLAM labelling associated with plasma membrane remained and far less co-localization with the late endosomes/lysosomes was seen (Fig 5.10 G-H). Also, as seen with the 2 hr clustering, the late endosome/lysosomes in cf2642 incubated cells were positioned in close proximity with the plasma membrane. The retainment of SLAM labelling of plasma membrane 6 hr post clustering in the presence of cf2642 confirms previous findings observed in fixed cells. The overall decrease in co-localization between SLAM and Dextran-488 positive lysosomes in the presence of cf2642 is another indication of the reduced uptake of SLAM. The reduced internalization of SLAM even at 2 hr post treatment indicates cell-targeting effects of cf2642 at early time points post treatment. This could have a direct impact of MeV entry and interaction of virus particles with the SLAM receptors.

5.2.8. Effect of cf2642 on transferrin uptake

The effect of cf2642 on the internalization of cargo has been previously tested using fluorescence labelled dextran conjugates, but in this case, their uptake occurs via macropinocytosis and short incubations with cf2642 was not done (see section 4.3 in Chapter 4). Since receptor internalization has been shown to occur via CME(Le Roy and Wrana, 2005), and to test the effect of cf2642 on the uptake of cargo via this pathway, transferrin experiments were performed. (see methods section 2.2.17)

Transferrin is iron-binding glycoprotein that act as a shuttle for the delivery of iron to cells. As an iron bound protein it binds to transferrin receptors on cell surfaces and the receptor complex is internalized as a constitutive process via CME to early endosomes. On the endocytic pathway a reduction in pH causes the release of iron into the endosomal lumen and then into the cytosol for use. The transferrin receptor-ligand complex, is then recycled back to the cell surface via recycling endosomes, ready for another round of iron uptake (Mayle et al., 2012).

For transferrin uptake analysis VeroSLAM cells were first starved in serum free medium to deplete bovine transferrin form the system and incubated with Alexa Fluor-488- transferrin (Tf-488) and cell mask for 30 min at 4ºC; the latter is a commercial probe used to label the plasma membrane (Hagn et al., 2012). Cells were then chased w/o cf2642 for up to 30 min and images were captured every 10 min by confocal microscopy.

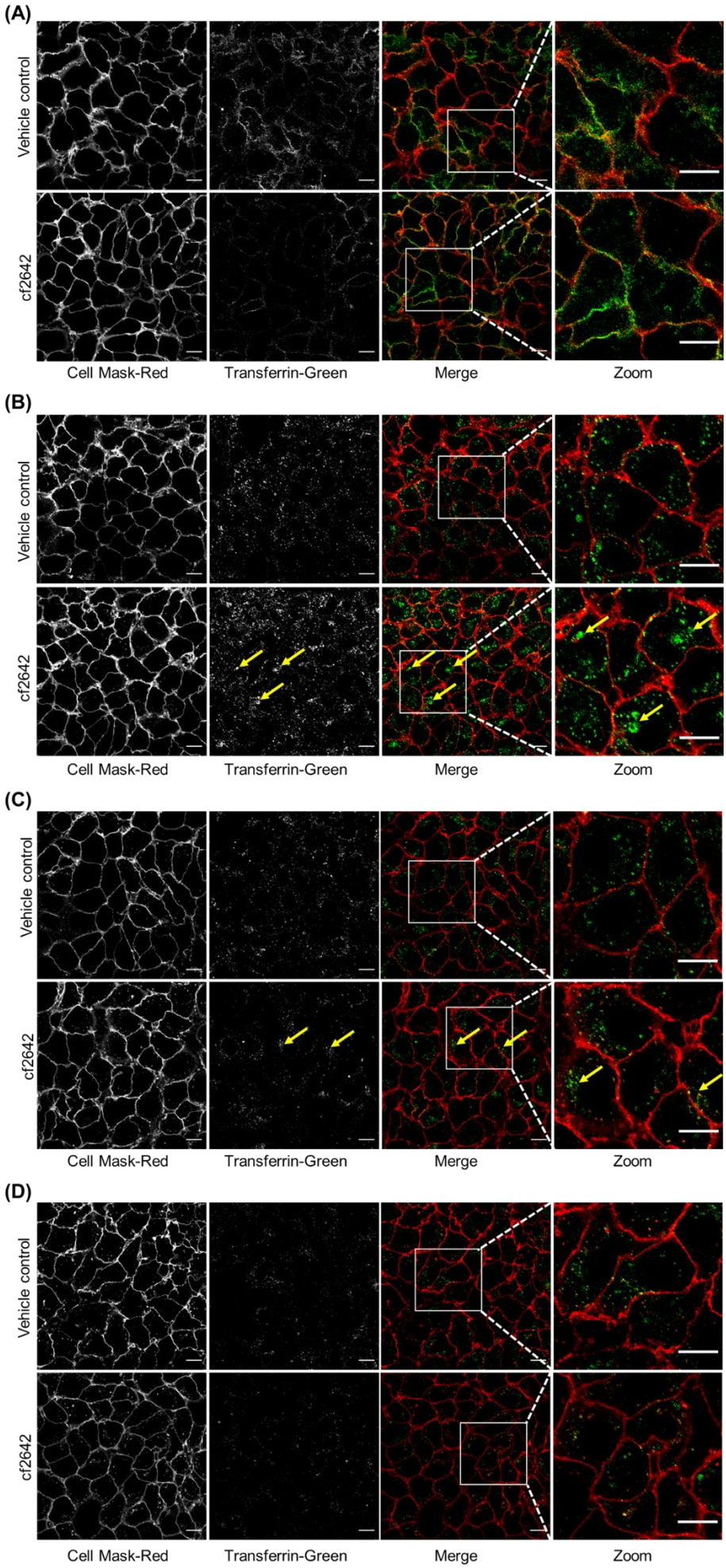
(A)
Vehicle control
cf2642
Cell Mask-Red
Transferrin-Green
Merge
Zoom
(B)
Vehicle control
cf2642
Cell Mask-Red
Transferrin-Green
Merge
Zoom
(C)
Vehicle control
cf2642
Cell Mask-Red
Transferrin-Green
Merge
Zoom
(D)
Vehicle control
cf2642
Cell Mask-Red
Transferrin-Green
Merge
Zoom

Fig 5.11. cf2642 causes the peripheral localization of transferrin loaded recycling endosomes. VeroSLAM cells were serum starved for 30 min in the absence of cf2642 and then incubated with Tf-488 and cell mask for 30 min on ice. Cells were then chased at 37ºC for up to 30 min in the presence or absence of 10µM cf2642 and live images were captured at 10 min intervals. Data shows images captured at **(A)** 2 min, **(B)** 10 min, **(C)** 20 min and **(D)** 30 min time points. The cell mask labelled plasma membrane is shown in red and transferrin in green. Arrows show the peripheral localization of transferrin-488 labelled vesicles. Images are representative of two independent experiments. (Scale bar =20µm).

At the 2 min time point, transferrin labelled vesicles were mostly associated with the plasma membrane but the labelling by this protein appeared to be lower in the presence of cf2642 (Fig 5.11 A). After a 10 min chase, cf2642 treated cells showed transferrin positive structures as small puncta but also grouped together, this compared with the more dispersed peripheral localization seen in the absence of drug. Small numbers of internalized cell mask positive structures were also observed in the presence of cf2642, compared to the vehicle control (Fig 5.11 B). On account of recycling, the total number of Tf-488 positive structures in the presence or absence of cf2642 steadily decreased over time and at 30 min post chase, cells showed increased presence of cell mask positive vesicles (Fig 5.11 C-D).The results demonstrate that cf2642 may alter the endocytic traffic of Tf-488, shown by the polarisation of Tf-488 vesicles as opposed to the peripheral localization of these vesicles in the absence of drug. Since there was no retention of the internalized transferrin at 30 min, it shows that the drug does not affect the normal cellular processes involved in transferrin recycling.

5.2.9. Effect of cf2642 on macropinocytosis

5.2.9.1. Effect of cf2642 on SLAM-receptor clustering mediated macropinocytosis

Previous experiments have shown that both direct and indirect clustering of SLAM receptors results in the increased uptake of Dextran-488 after 30 min (sections 5.2 and 5.3.3). Since this was significantly reduced in the presence of cf2642, it indicates that the drug possibly affects a cellular pathway like macropinocytosis, that has been shown to be involved in dextran uptake, predominantly in growth factor activated cells. MeV has been shown to utilize this endocytic pathway as an alternate means of cellular entry (Delpeut et al., 2017) and hence the effect of cf2642 on macropinocytosis was studied. Focus here was given to the arrangement of actin that mediates the cell ruffling and uptake associated with this process; subsequent experiments also investigated whether the MeV also affected the actin cytoskeleton.

VeroSLAM cells were first incubated with mouse anti-SLAM antibodies and then incubated for 1 hr using polyclonal chicken anti mouse antibodies (clustering) w/o cf2642. After a further 30 or 60 min chase w/o cf2642, cells were fixed and actin filaments were labelled with rhodamine phalloidin (see methods section 2.2.16.1.4.3)

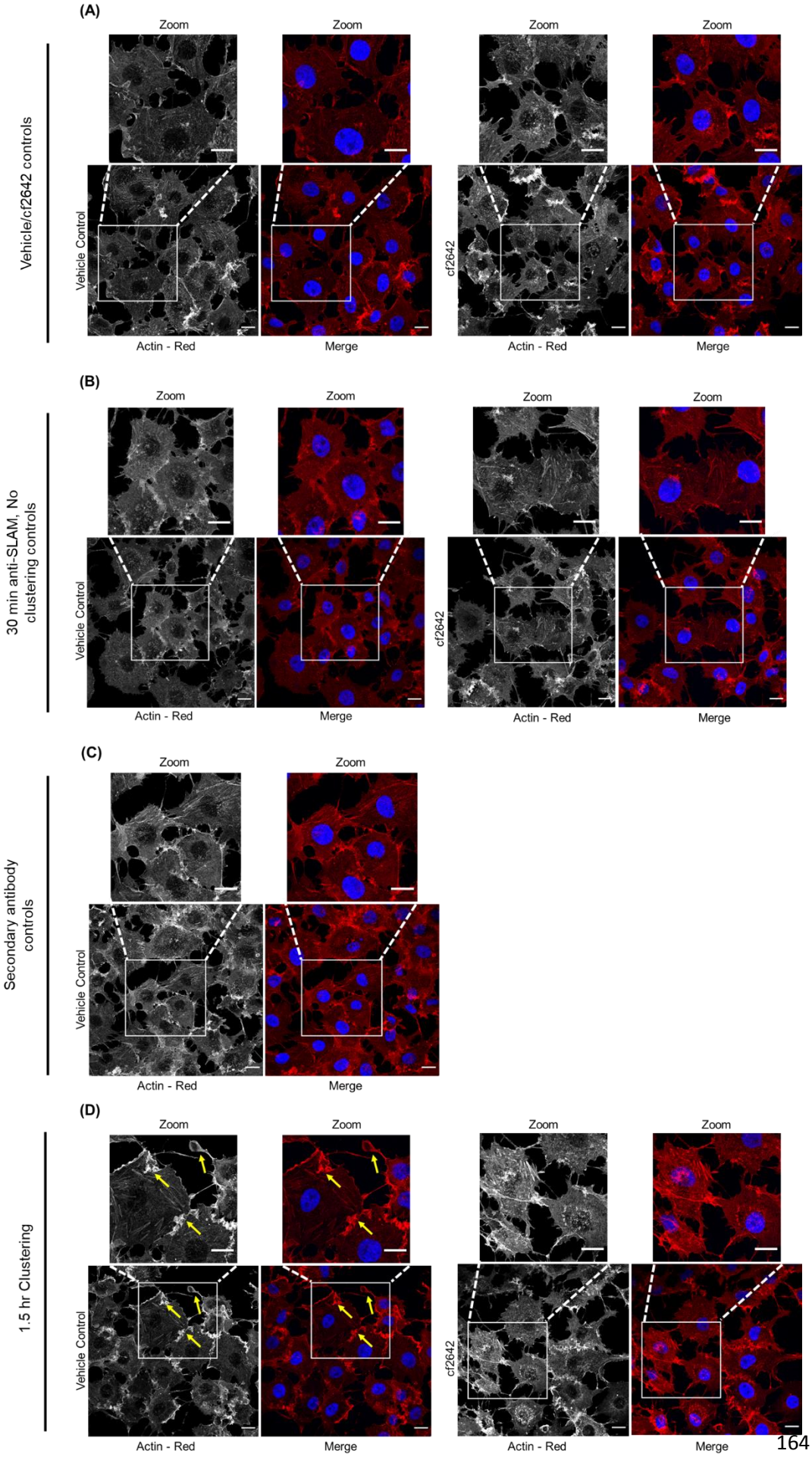
(A)
Zoom
Zoom
Zoom
Zoom
Vehicle/cf2642 controls
Vehicle Control
cf2642
Actin - Red
Merge
Actin - Red
Merge
(B)
Zoom
Zoom
Zoom
Zoom
30 min anti-SLAM, No clustering controls
Vehicle Control
cf2642
Actin - Red
Merge
Actin - Red
Merge
(C)
Zoom
Zoom
Secondary antibody controls
Vehicle Control
Actin - Red
Merge
(D)
Zoom
Zoom
Zoom
Zoom
1.5 hr Clustering
Vehicle Control
cf2642
Actin - Red
Merge
Actin - Red
Merge

Fig 5.12 Crosslinking of SLAM receptors for 1.5 hr results in membrane blebbing. VeroSLAM cells were incubated or not with mouse anti-SLAM antibodies w/o 10µM cf2642 for 30 min at 37ºC and clustered or not with chicken anti mouse Alexa Fluor - 647 antibodies in the presence of absence of cf2642 for 1 hr. After a 30 min chase, cells were fixed, permeabilized and labelled with rhodamine phalloidin and Hoechst to label actin filaments and nucleus respectively. Cells incubated only with vehicle control or cf2642 are shown in **(A)**, and **(B)** shows no-clustering controls where cells were incubated with primary antibody but not clustered. **(C)** shows the secondary antibody controls and **(D)** shows cells with SLAM-clustering w/o cf2642. Arrows indicate membrane blebs caused by actin protrusions. Images are representative of three independent experiments. (Scale bar =20µm).

The vehicle, cf2642 controls, no-cluster (primary alone) and secondary antibody controls showed complete labelling of the actin cytoskeleton and very little indications of extensive actin protrusions or ruffles (Fig 5.12 A-C). Cells with crosslinked SLAM receptors showed the formation of actin ruffles as indicated by yellow arrows; actin protrusions were also observed to emanate from these cells. This effect was inhibited by cf2642 manifest as the control actin phenotype (Fig 5.12 D) (see discussion below).

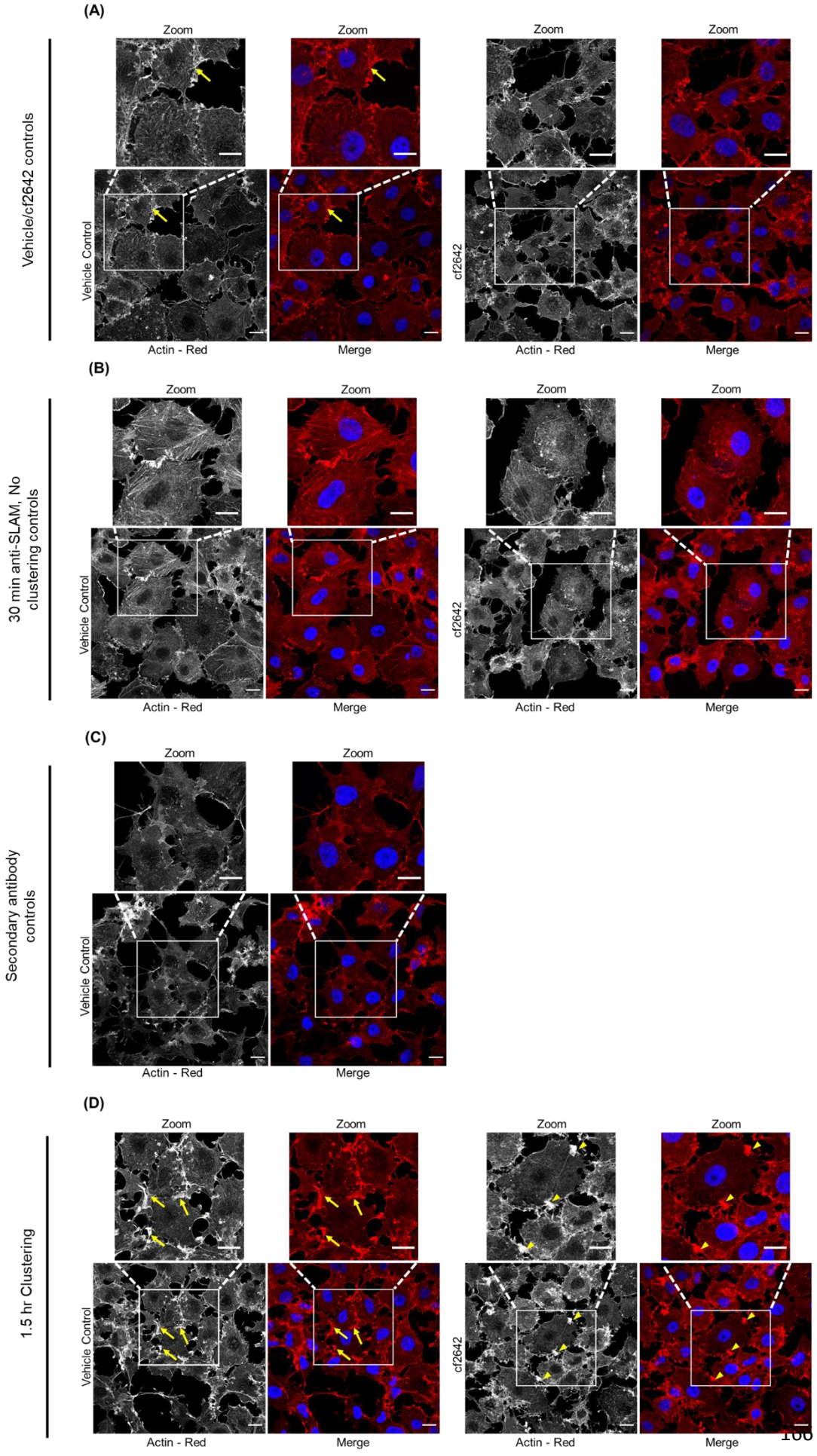
(A)
Zoom
Zoom
Zoom
Zoom
Vehicle/cf2642 controls
Vehicle Control
cf2642
Actin - Red
Merge
Actin - Red
Merge
(B)
Zoom
Zoom
Zoom
Zoom
30 min anti-SLAM, No clustering controls
Vehicle Control
cf2642
Actin - Red
Merge
Actin - Red
Merge
(C)
Zoom
Zoom
Secondary antibody controls
Vehicle Control
Actin - Red
Merge
(D)
Zoom
Zoom
Zoom
Zoom
1.5 hr Clustering
Vehicle Control
cf2642
Actin - Red
Merge
Actin - Red
Merge

Fig 5.13 Crosslinking of SLAM receptors for 2 hr results in extensive membrane bleb formation. VeroSLAM cells were incubated or not with mouse anti-SLAM antibodies w/o 10µM cf2642 for 30 min at 37ºC and clustered or not with chicken anti mouse Alexa Fluor - 647 antibodies in the presence of absence of cf2642 for 1 hr. After a 60 min chase, cells were fixed, permeabilized and labelled with rhodamine phalloidin and Hoechst to label actin filaments and nucleus respectively. Cells incubated only with vehicle control or cf2642 are shown in **(A)**, and **(B)** shows no-clustering controls where cells were incubated with primary antibody but not clustered. **(C)** shows the secondary antibody controls and **(D)** shows cells with SLAM-clustering w/o cf2642. Arrows indicate membrane blebs caused by actin protrusions. Arrowheads indicate aggregates of actin labelling. Images are representative of three independent experiments. (Scale bar =20µm).

The experiment in Fig 5.13 used the same antibody times points as used for the flow cytometry analysis shown in Fig 5.12. Experiments were then performed whereby the period after secondary antibody (clustering) incubation was increased from 30 to 60 min. This was to investigate whether more prominent effects could be see via this extended period. Fig 5.13 show in the presence or absence of cf2642 and in the absence of secondary antibody (no clustering), some actin labelling, identified as small folds protruding from the cell surface. (Fig 5.13 A,C). Extensive formation of ruffles and actin protrusions were seen in almost all cells clustered with the secondary antibody. This effect was almost completely reversed in the presence of cf2642 and these cells showed the presence of small patches on the cell surface with dense labelling of actin (Fig 5.13 D).

Actin labelling results in Fig 5.12 and 5.13 showed the presence of ruffles and actin protrusions at the same time point as the Dextran uptake experiments, which confirms that this was due to the induction of macropinocytosis. However, a more pronounced induction of actin protrusions, along with cell shrinkage was observed after a further 30 min

chase (Fig 5.13), indicating that SLAM clustering induced macropinocytosis was an ongoing process and lasts for at least 2 hr post clustering. In either case, cf2642 inhibited these changes in the actin cytoskeleton, thereby supporting the previous data on inhibition of clustering induced dextran uptake.

5.2.9.2. Effect of cf2642 on MeV induced SLAM clustering

Previous experiments have shown that MeV interaction with VeroSLAM cells results in the increased uptake of Dextran (section 5.2). Here, the effect of virus on the actin cytoskeleton was tested by infecting VeroSLAM cells with MeV for a short period in the presence or absence of cf2642. (see methods section 2.2.19)

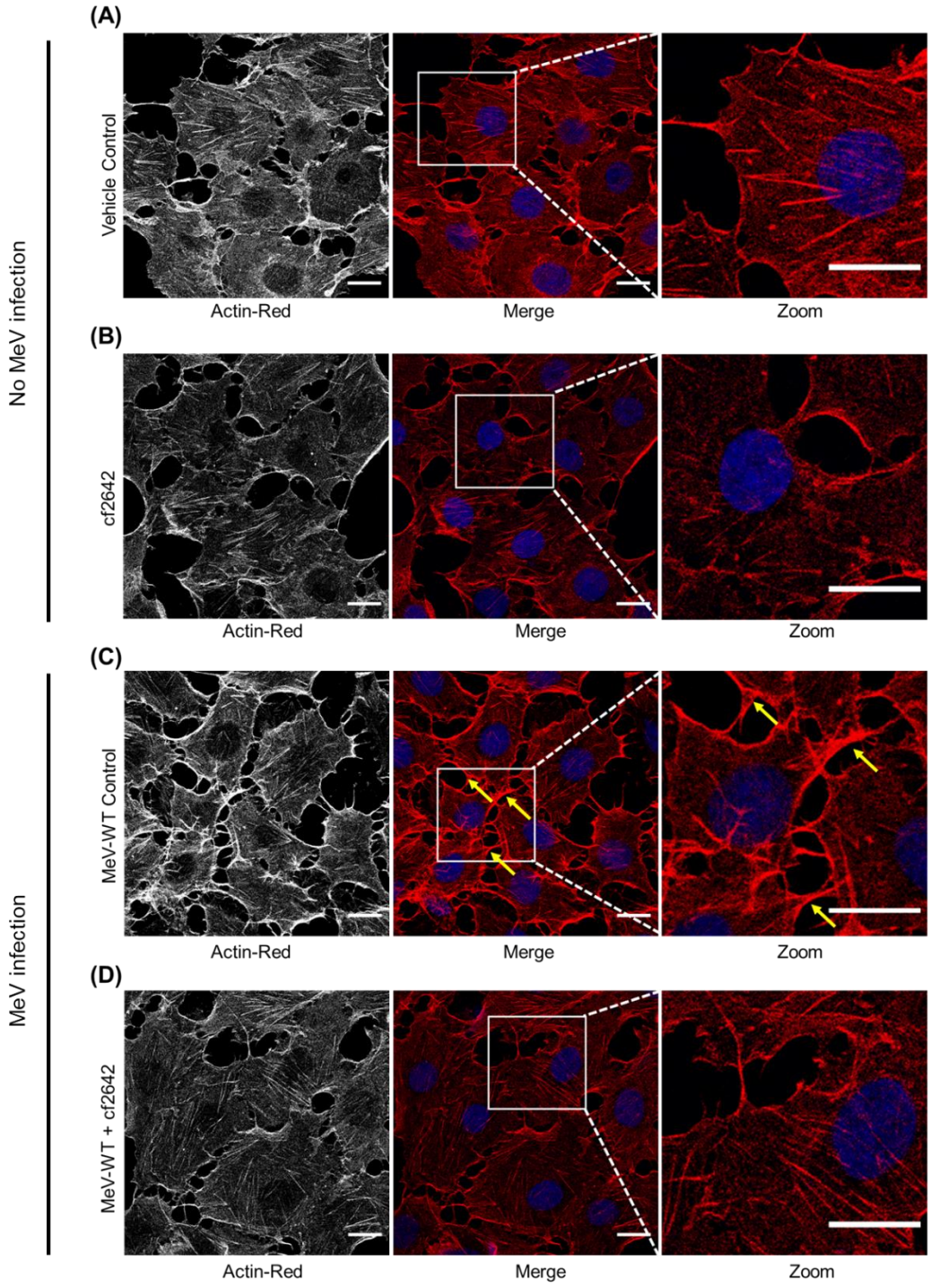

Fig 5.14 MeV infection in VeroSLAM cells results in actin cytoskeleton changes which is reversed in the presence of cf2642. Cells grown over glass coverslips were infected **(C-D)** or not **(A-B)** with MeV (MOI-10) in the presence of 10µM cf2642 or vehicle (DMSO) and incubated for 30 min at 37ºC. The cells were fixed, labelled using Alexa Fluor 647 Phalloidin and DAPI to visualize actin and nuclei respectively and analyzed by confocal microscopy. Single section images show actin labelling (grey scale) and also as merged images with nucleus labelling (blue). Yellow arrows indicate actin driven membrane protrusions in the MeV control. (scale bar = 20µm)

Figure 5.14 shows the usual labelling of actin in cells showing prominence close to the plasma membrane and on filaments. MeV caused a significant change in this localisation noting the appearance of numerous actin positive protrusions emanating from the plasma membrane. As a result, the virus infected cells appeared to be smaller than control cells. In the presence of cf2642, cells were of normal size and lacked any of the actin protrusions that were present in the MeV controls (Fig 5.14 C-D). cf2642 on its own, did not appear to have any effect on the actin arrangement (Fig 5.14 A-B). The effect of cf2642 on MeV induced changes in actin morphology shows the effect of the drug on virus induced macropinocytosis at these early time points. A 30 min incubation period with MeV was used in accordance with a previous report showing MeV (MOI-1) induced differences in actin morphology at this time point (Delpeut et al., 2017). An MOI of 10 was used in this experiment, taking into account the relatively high MOI used previously for the Dextran uptake experiment. The data suggests that MeV when used at MOIs between 10 and 100 induces changes in actin morphology and this may occur soon after virus infection. The virus induced Dextran-488 uptake that was observed at 15 min may perhaps be the time point at which MeV causes maximum effects on cell plasma membranes, culminating in virus entry via macropinocytosis. In reality MOIs of >10 are unlikely to occur in nature but taken together, the results suggest an effect of cf2642 on cell membranes occurs as early as 5 min post treatment and the MoA of cf2642 against measles may be attributed this cell-targeting activity of the drug. It still remains to be determined if the effects are limited

to the plasma membrane or whether the drug also has an effect on internal membranes that are critical for the virus life cycle- discussed below.

5.2.10. cf2642 MoA studies

5.2.10.1. Measles entry/spread assay sheds light on the MoA of cf2642

Previous data in this chapter has revealed that MeV stimulates Dextran uptake and that the virus induces macropinocytosis in VeroSLAM cells at early time points post infection. Here, in the same experiment, the MoA of cf2642 was studied by testing its possible effect on virus entry as opposed to virus spread. VeroSLAM cells were first infected with MeV expressing green fluorescence protein (MeV-GFP) for 2 hr either in the presence or absence of 10µM cf2642. The cells were then washed and further incubated with 10µM cf2642 or not for 24 hr, this time without adding any fresh virus to the cells. (see methods section 2.2.20.1.2 and section 2.2.20.2.3 for details on flow cytometry analysis)

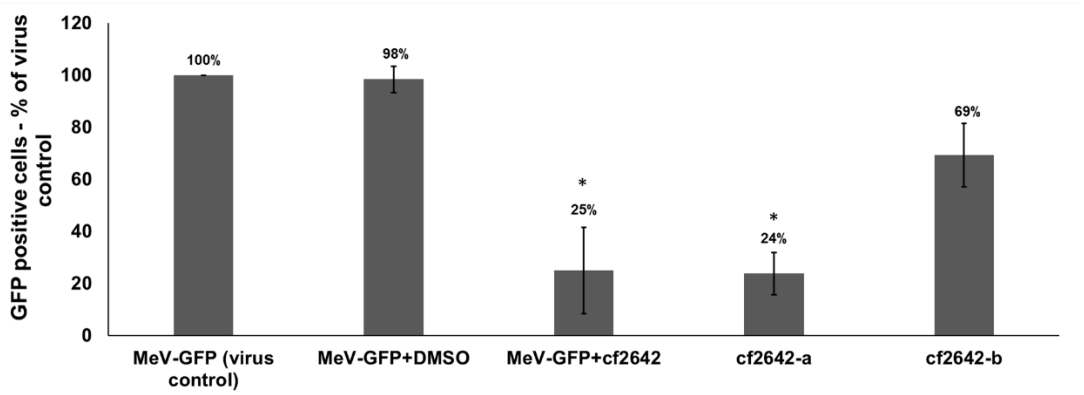

Fig 5.15 cf2642 inhibits MeV-EGFP spread. VeroSLAM cells were infected with MeV-GFP at MOI 0.5 for 2 hr in the absence or presence of 10µM cf2642, washed and further incubated with 10µM cf2642 or not for 24 hr and analyzed by flow cytometry. The results show the percentage of GFP positive cells normalized to virus control. To study the effects on MeV-GFP entry or spread, cf2642 was added either after the 2 hr viral incubation step (cf2642-a) or immediately prior to the initial 2 hr incubation with virus (cf2642-b). The percentage of GFP positive cells was measured by flow cytometry analysis and normalized to the untreated virus control. Error bars represent mean ± SE of three independent experiments. Student's t test was performed to assess the p values; *< p,0.05.

Vehicle (DMSO) had only negligible effects in the GFP signal (Fig 5.15). MeV-GFP infection in the presence of cf2642 caused a significant 75% decrease in cellular GFP fluorescence. There was a significant (approx.-75%) decrease in fluorescencewhen the drug was incubated with cells throughout the experimental virus period or when added 2 hr post viral treatment.However, only a 31% decrease in cell fluorescence was observed when cf2642 was added only during the 2hr virus incubation step and this reduction in fluorescence was not statistically significant (Fig 5.15). The rationale behind adding the drug at different stages of the experiment was to test which stage of the virus infection cycle, whether entry or spread, was being inhibited. When the cells are infected during the first 2 hr in the presence or absence of cf2642 (cf2642-b), the virus has the opportunity to

attach to cells and initiate virus entry. If cf2642 does inhibit virus entry, there will not be any infection occurring during the subsequent 24 hr incubation step and therefore no/less GFP signal by flow cytometry analysis. Next, when the cells are washed and treated with cf2642 during the 24 hr incubation step (cf2642-a), the cells that have already entered the cells initially will have a change to propagate. But if the drug inhibits spread, then the GFP signal associated with this will be less or absent. In the presence of cf2642, significant (76%) decrease in GFP positive cells was observed when the infected cells were treated during the 24 hr incubation step (cf2642-a), indicating that the drug affected virus spread. The 31% decrease associated with the cf2642-b condition was not statistically significant, and hence it can only be speculated that cf2642 partially affects MeV entry. This effect of cf2642 on virus spread may be a result of the drug's effects on internal membranes which in turn inhibits virus-induced syncytia formation. The formation of syncytia by fusion of infected and non-infected cells is vital for the lateral spread of MeV particles and hence, any effects on this process will irreversibly affect the virus life cycle (Rima and Duprex, 2011b, Plemper et al., 2011a). Another possibility could be that cf2642 affects the virus envelope during entry stages, thereby resulting in less efficient uptake and/or improper assembly and replication of MeV particles.

5.2.10.2. Time of addition (ToA) assay

The ToA assay was done to determine how long the addition of cf2642 can be postponed before it loses its antiviral activity; the assay has been used to

gain insights into the mechanism of action of antiviral compounds. (Daelemans et al., 2011) For instance, a drug which targets the viral genome will have an effect only when added during the early time points post infection. When added at later time points, the drug will no longer be able to affect virus replication. VeroSLAM cells were first infected with MeV-GFP and cf2642 was added at various time points pre and post infection, for up to 12 hr. After a further 12 hr incubation, the percentage of GFP positive cells was analyzed by flow cytometry. The following conditions were used:

1. *Blank - Cells without virus or drugs/DMSO*
2. *Vehicle (DMSO) control*
3. *T0 - 30 min (a) (30 min pre-treatment with 10μM cf2642, cells washed 2x and infected with MeV-GFP without cf2642)*
4. *T0 - 30 min (b) (30 min pre-treatment with 10μM cf2642, cells washed 2x and infected with MeV-GFP with 10μM cf2642)*
5. *Virus control (T0) - MeV-GFP infection, no cf2642 treatment*
6. *Virus + cf2642 - MeV-GFP infection and cf2642 treatment done together*
7. *T0 + 30 min (MeV-GFP infection, cf2642 treatment done 30 min post infection)*
8. *T0 + 2hr (MeV-GFP infection, cf2642 treatment done 2 hr post infection)*
9. *T0 + 4hr (MeV-GFP infection, cf2642 treatment done 4 hr post infection)*
10. *T0 + 6hr (MeV-GFP infection, cf2642 treatment done 6 hr post infection)*
11. *T0 + 8hr (MeV-GFP infection, cf2642 treatment done 8 hr post infection)*
12. *T0 + 10hr (MeV-GFP infection, cf2642 treatment done 2 hr post infection)*
13. *T0 + 12hr (MeV-GFP infection, cf2642 treatment done 2 hr post infection)*

(see section 2.2.20.1.1 for methodology and section 2.2.20.2.3 for details on flow cytometry analysis)

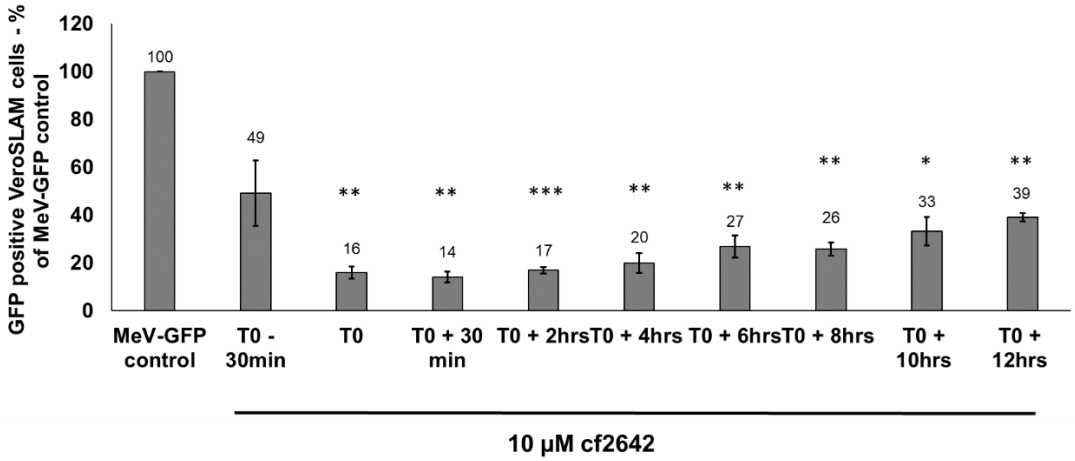

Fig 5.16 cf2642 time of addition (ToA) assay indicates sustained anti MeV activity. VeroSLAM cells were infected with MeV-GFP at MOI 0.5 and 10µM cf2642 was added either 30 min prior to infection (T0-30 min), at the same time as infection (T0) or after various time points up to 12 hr post infection, as indicated. Cells were incubated for a further 12 hr and analyzed by flow cytometry. The results are representative of three independent experiments and are shown as percentage of EGFP positive cells normalized to the untreated virus control. Error bars represent mean ± SE of three independent experiments. Student's t test was performed to assess the p values; *< p,0.05, **<p,0.01, ***<p,0.001.

The maximum activity of 10µM cf2642 against MeV-GFP was observed at the T0 min and T0+30 min time points when cf2642 treatment was performed either at the same time as virus infection or 30 min post infection respectively (Fig 5.16). Upon the addition of drug 30 min prior to infection of cells (T0 - 30 min), only a 50% decrease in virus associated GFP signal was observed, but this was not statistically significant. The GFP signal positively correlated with the time of addition of the drug that when added 12 hrs post infection still inhibited the fluorescence signal by 61%. Since a significant inhibition of MeV-GFP even when cf2642 was added 12 hr post infection, it

indicates that a cellular component that was required for MeV during its entire life cycle was being affected. This also supports the data from virus entry/spread assay wherein cf2642 was shown to only partially affect virus entry. If virus entry was being inhibited, the addition of cf2642 at or after 2 hr post infection would not have resulted virus inhibition.

5.2.11. Impedance assay

As part of MoA studies, the response of cells to MeV infection and cf2642 treatment was studied using the RTCA xCELLigence instrument which uses non-invasive electrical impedance measurements to monitor changes in cell behaviour in terms of proliferation, morphology and adherence in real time (Pennington and Van de Walle, 2017). Cells are made to grown in specialized tissue culture plates containing inter-digitated gold electrodes on its base. When a low frequency alternating current is applied, the cells impede the flow of ionic current across the monolayer, which is in turn read as cell impedance. As the cells grow over time, the ionic flow around or between the cells decreases, thereby increasing cell impedance (Abassi et al., 2004, Xing et al., 2006). The impedance of electron flow by the cells is reported as a unit less parameter called the Cell Index. The response of cells to infection by cell-fusion inducing viruses has been reported earlier and shown to produce characteristic cell index profiles (Watterson et al., 2016).

Briefly, VeroSLAM cells were seeded in 96-well impedance measurements plates and 24 hr post seeding, infected with MeV in the presence or absence of increasing concentrations of cf2642. Impedance measurements

were taken at various time points post infection. (see methods section 2.2.20.1.4).

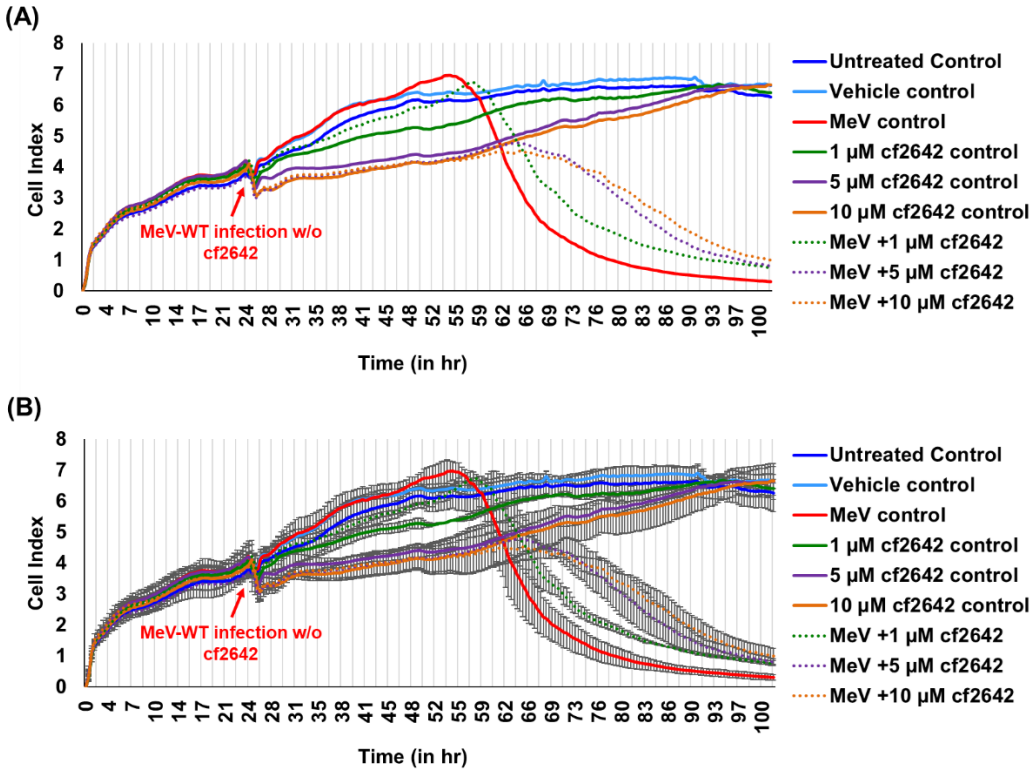

Fig 5.17 Impedance assay shows the anti-viral activity of cf2642 in real time. VeroSLAM cells were seeded in duplicates in 16 well impedance measurement plates and 24 hr later, infected with MeV (MOI 0.5) in the presence or absence of increasing concentrations of cf2642 as indicated. Impedance measurements were taken in real time at every 15 min intervals during 0-24 hr incubation of cells post seeding, 1 min intervals during 24 to 27 hr post infection and again at 15 min intervals during 27 to 100 hr. Measurements were plotted against cell index and time. (A) shows ell index plot from 0 to 10 hr and (B) shows the same cell index plot with error bars representing standard error from two independent experiments.

The data depicts the increase in the cell index for all conditions during 0 to 24 hr post seeding of cells and in the absence of virus (Fig 5.17). After a small dip at the virus addition time point, the cell index continued to increase for both the controls, and 1µM cf2642 control. The increase in cell index was

slightly reduced in cells treated with 5 and 10µM cf2642. The impedance of MeV control cells increased and at a similar rate to non-infected cells but then declined after 30 hr post infection. MeV infected cells in the presence of cf2642 showed a reduced cell index during the first 66 hours and then a reduced rate of decline in cell index for the rest of the experiment. The rapid increase in cell impedance upon infection with MeV translates to the increase in surface area occupied by infected cells due to formation of syncytia. A similar profile was previously reported for Respiratory syncytial virus (RSV), which is a Class-1 fusion inducing virus like MeV(Watterson et al., 2016). The subsequent decline in impedance was most likely due to cell death and the resulting detachment of cells from the electrode surface. This is well documented when this assay is used test anti vital compounds against other viruses but time did not allow for parallel experiments using microscopy that would have clearly shown this cell death and detachment that resulted in the decline in cell index. The observation that loss of impedance measurements was inhibited in the presence of both 5 and 10µM cf2642, strongly suggests inhibition of virus induced syncytia formation. Evidence for this was already provided in chapter 3, section 3.2.2).

5.3. Summary

An understanding of the different stages of a virus life cycle is vital in the design, development and testing of different antiviral compounds. Initial experiments towards elucidating the MoA of cf2642 were to investigate whether receptor clustering could mimic early MeV-induced effects on cells

in a non-infectious context. The aim was to test the effects of cf2642 on macropinocytosis. Several experiments in this chapter highlighted that cf2642 was having effects on cells in the absence of virus. Focus was placed on endocytosis and the data show that the drug was able to affect the localisation of early and late endocytic structures. A major challenge was to associate these changes to effects on viral life cycle. For this, MeV experiments were performed together with the developments of assays mimicking the demonstrated effects of the virus on the SLAM receptor. The increased Dextran-488 uptake seen with both SLAM-receptor clustering and MeV infection was completely abrogated by only a 5 min incubation with 10µM cf2642 and moreover, actin labelling studies confirmed this was likely to be due to the inhibition macropinocytosis induced membrane ruffles and actin protrusions by the drug. Live and fixed cell imaging revealed that internalization of SLAM receptor was partially inhibited in the presence of cf2642. The possible implication of this during live MeV infection could be that cf2642 affects virus entry or early events occurring during infection of cells. The MeV entry/spread assay clearly showed that the MoA of cf2642 was associated with the inhibition of virus spread and only partially affected entry. This was also supported by the ToA data where in it was shown that cf2642 affects a cellular process used by the virus during its entire life cycle. The anti-MeV activity of cf2642 was further supported by the results from impedance assay, where the increased cell index associated with MeV infection was abrogated in the presence of 5 and 10µM c2642. Overall, the data from this chapter show that the antiviral activity of cf2642 against MeV is attributed to its effects on intracellular membranous compartments utilized

by the virus during its life cycle. The effects of cf2642 on MeV entry was not conclusive and further studies are required to ascertain whether the drug affects virus entry via macropinocytosis.

Chapter 6 - General Discussion

Measles outbreaks continue to occur in both developed and developing nations of the world in spite of the availability of an effective vaccine against this disease (Fischer, 2018, Sundaram et al., 2019, Mensah et al., 2019). Due to the unavailability of an effective antiviral against measles, the control measures during such outbreaks are limited to quarantine of infected individuals and supportive therapy. In such a scenario, the availability of an effective antiviral that can be administered as an immediate post-exposure prophylaxis measure to non-immunized individuals and their immediate contacts can significantly reduce the spread of infection during measles outbreaks. Moreover, the long incubation period of measles prior to the onset of clinical symptoms offers a large window for such treatment measures (Plemper and Snyder, 2009). This supports the urgent need for research towards development of an effective antiviral against this disease (McCune and Reynolds, 2015).

Ever since the synthesis of cf2642 by Prof. Chris McGuigan's group at the Cardiff University School of Pharmacy, there has been considerable interest in elucidating the MoA of this drug. Initial studies revealed the antiviral activity cf2642 against both measles and VACVand suggested that a common cellular target might be affected (Farleigh, 2014). Since these studies were focussed on the anti-viral activity of cf2642 against VACV, the primary objective of this project was to understand the effects of this drug on measles virus. Such an approach has a distinct advantage that the findings from these two studies can be bridged together, thus providing conclusive

evidence in relation to the common cellular target that renders cf2642 effective against these two different viruses. As noted, measles also represents a current clinical problem whereas smallpox has been eradicated.

VeroSLAM cells were used for the most part of this research since they express the SLAM/CD150 receptor used by MeV to gain cell entry (Lin and Richardson, 2016). Earlier PhD studies on this drug at Cardiff University suggested that there may be a cellular target for this drug that would explain the fact that there was variation in toxicity profiles when different cell lines were investigated as measles hosts, including B95A. (Farleigh, 2014). This was confirmed in this new study in HeLa and VeroSLAM models, where the latter was found to be more sensitive to the drug. The antiviral activity of cf2642 against MeV was shown earlier in B95a cells by the inhibition of virus induced syncytia (Farleigh, 2014). Similar results were observed using VeroSLAM cells and this gave us confidence that we could use these cells as a model for the measles virus and clustering studies in this thesis. In the VeroSLAM cells, a dose-dependent effect of cf2642 against MeV was shown using both virus-plaque and impedance assays. In the latter, an increased cell index caused by the formation of MeV induced syncytia was effectively inhibited by higher concentrations of the drug. The antiviral effects of cf2642 shown by these two different biological assays gives more credence to the concept that this drug is an effective agent against MeV.

The ability of MeV to induce autophagy led to experiments investigating whether the drug had any effects on this cellular process. The inhibition of this virus induced autophagy by cf2642 provided evidence of a cellular

target for the drug. Previous studies have shown that inhibition of MeV induced autophagy affects virus spread (Richetta et al., 2013). This was confirmed by results from the MeV-GFP entry/spread assay in Chapter 5 wherein c2642 was shown to inhibit virus spread and only partially affect virus entry into VeroSLAM cells.

Endocytic profiling and dextran uptake studies were performed in an effort to better understand the cell-targeting effects of cf2642 in both HeLa and VeroSLAM cells. Two major findings were discovered from these experiments. Firstly, cf2642 does not affect the endocytic uptake of both dextran and transferrin, and subsequent trafficking for the former through early to late endosomes and then to terminal lysosomes. Secondly, there was very strong evidence to show that the subcellular localisation of endocytic structures in live and fixed cells was affected by the drug. This was mostly manifest as a scattering of organelles as opposed to them being more polarized, possibly organised, in untreated cells. The reason for this is still unknown but does not seem to be due to disruption of the actin or tubulin (data not shown) cytoskeleton that hold these organelles in place in the cytoplasm. Of note here is that disruption of actin has been shown to affect the measles life cycle (Dietzel et al., 2013). New recent evidence suggests that endocytosis may be used by this virus for uptake into cells and it remains to be determined if this mislocalisation of endocytic structures somehow contributes to the effects of cf2642. A limitation of the study is that intermediate filaments were not studied; these cellular structures have been poorly explored in comparison to actin and microtubules but have been

implicated in controlling virus life cycles (Sripada and Dayaraj, 2010, Hertel, 2011).

Previous studies have revealed the absence of cf2642-induced cytotoxicity when the medium was changed after 16 hr treatment with the drug, and this was attributed to the rescue of cells from the fact that the drug increases the acidity of the extracellular medium (Farleigh, 2014). This effect merits further study including the possibility that the drug could activate the many processes by which cells pump out protons from the cytosol into the cell exterior (Ruffin et al., 2014). Interesting candidates are Sodium Hydrogen exchangers such as NHE1 that regulate intracellular pH by pumping protons, in exchange for sodium, into the extracellular space. Drugs such as amiloride can inhibit these pumps and it would be interesting to see how this would affect the cf2642 induced acidification process. These agents, through inhibition of macropinocytosis, can inhibit the uptake of a number of different viruses including measles (Casey et al., 2010, Masereel et al., 2003, Delpeut et al., 2017). Early experiments performed with one addition of drug and no recovery period, showed that 10μM cf2642 induced toxicity. However, the later dextran uptake experiments performed in Chapter 4 with the same cf2642, did not affect the cells. This may be attributed to the additional washing of cells after 12 hr treatment in these experiments thus reducing the possible effects of high acidity in the extracellular medium. Also, the cytotoxicity of cf2642 mediated by low extracellular pH is more likely the result of the induction of apoptosis rather that necrosis, as shown by the LDH release assay (Chan et al., 2013a).

An important and novel finding that resulted from this research project is the successful use of SLAM-receptor clustering to mimic the early effects of MeV in a non-infectious setting. Being able to replicate the effects of MeV on clustering of SLAM-receptors during the early stages of infection (Fig 6.1), enables one to better understand virus-host interactions and also to screen the in vitro effects of cf2642 in the absence of live virus to investigate whether they have an effect on this process and the viral dynamics on the plasma membrane.

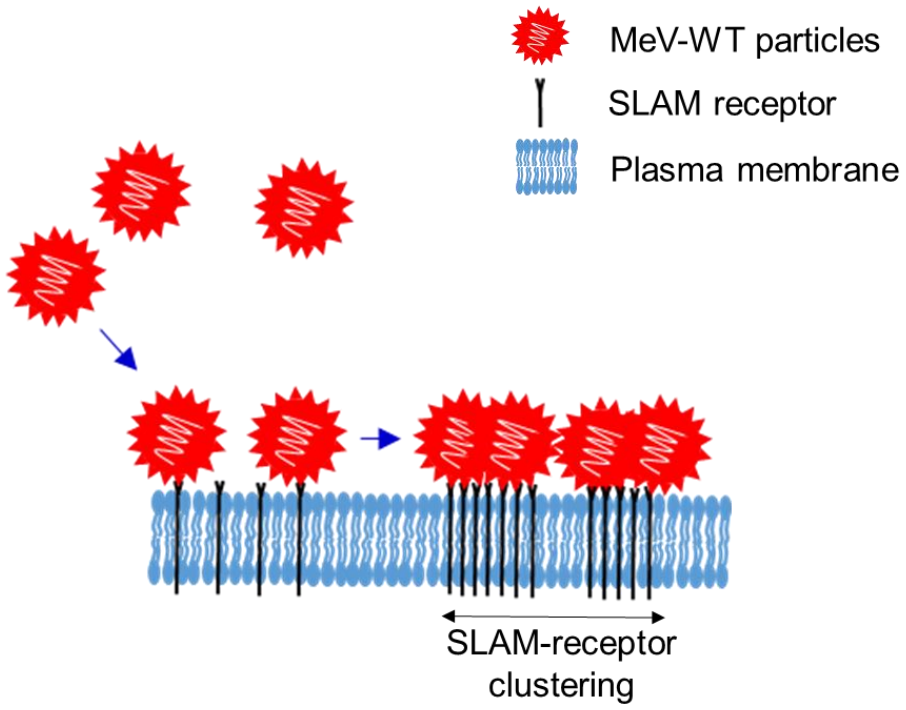

Fig 6.1 Illustration of the early effects of MeV interaction with cells. During the early stages of virus-cell interaction, MeV particles first interact with the SLAM receptors on the plasma membrane and subsequently causes the clustering of these receptors, thereby leading to virus entry via macropinocytosis.

The inhibition of both SLAM-receptor clustering and MeV induced uptake of Dextran-488 by only a 5 min incubation with cf2642 exemplifies the early

effects of this drug on cells; most probably at the level of the plasma membrane, but as mentioned, there is also the interesting possibility that the drug could also affect the virus envelope (Chapter 5). Confocal microscopy analysis clearly showed the stimulatory effects of MeV and also SLAM clustering on macropinocytosis manifest in both cases as prominent actin protrusions and blebs. The abrogation of these effects in the presence of cf2642 further supports the inhibition of Dextran-488 uptake by macropinocytosis. Moreover, macropinocytosis is also exploited by other enveloped viruses including adenovirus, Ebolavirus, influenza A, VACV and Nipah virus (Mercer and Helenius, 2009). This thesis showed that cf2642 is an inhibitor of MeV/SLAM receptor induced macropinocytosis suggesting a novel MoA against MeV, VACVand possibly other enveloped viruses that warrant further study.

It is clear that cf2642 has effects on cells beyond the remit of interfering with them as hosts for MeV entry and replication.

The drug possesses a hydrophobic modality to allow greater penetration across the plasma membrane, but it is unknown if this affects the structural integrity of any membrane that it encounters such that it is not so amenable to exploitation by viruses. This could include the plasma membrane and internal membrane structures that measles and other viruses make use of for their own gains. The putative effects of cf2642 on these membrane systems, and possibly the viral envelope suggest that much further analysis is warranted to investigate the potential of this drug as a broad spectrum antiviral targeting the entry and spread of other enveloped viruses.

Future work

1. Further studies on the effects of cf2642 on MeV can be done by investigating the localisation of virus (e.g. MeV expressing gfp) traffic through endocytic compartments (early endosomes to lysosomes) in the presence or absence of drug. These could be based on microscopy methods utilising some of the probes used here and GFP-tagged variants of Rabs and other proteins labelling distinct endocytic stations (Vercauteren et al., 2011).

List of publication and presentations

Publication

1. Sanjay G. Patel, Edward J. Sayers, Lin He, Rohan Narayan, Thomas L. Williams, Emily M. Mills, Rudolf K. Allemann, Louis Y. P. Luk, Arwyn T. Jones & Yu-Hsuan Tsai. Cell-penetrating peptide sequence and modification dependent uptake and subcellular distribution of green florescent protein in different cell lines. *Scientific Reports* Volume 2019, 9, 6298.

Posters and presentations

1. Studies on the antiviral mechanism of L-dideoxy Bicyclic Pyrimidine Nucleoside Analogue cf2642 - Poster presentation, Postgraduate Research day: 28-04-2017.
2. MoA studies on the lead L-ddBCNA antiviral cf2642 - Poster Presentation, NRN postgraduate conference: 11-09-2017.
3. Biological evaluation of a novel cell targeting L-ddBCNA antiviral against MeV - Oral presentation, NRN conference, 4th Annual Drug Discovery Congress: 29-09-2017.
4. Biological evaluation of a novel cell targeting L-ddBCNA antiviral against measles virus - Medical Biodefence Conference (MDBC) in the Bundeswehr Institute for Microbiology, Munich, Germany: 28-10-2018
5. Biological evaluation of a novel cell targeting L-ddBCNA antiviral against measles virus - Poster presentation, American Society for Virology (ASV) annual meeting: 19-07-2018. *Note: Unable to attend the conference due*

to US Visa issues. The poster was presented by Dr. Joachim Bugert on my behalf.

References

1. World Heath Organization. Measles fact sheet https://www.who.int/news-room/fact-sheets/detail/measles (Accessed on 01 February, 2019).
2. Abassi, Y. A., Jackson, J. A., Zhu, J., Oconnell, J., Wang, X. & Xu, X. 2004. Label-free, real-time monitoring of IgE-mediated mast cell activation on microelectronic cell sensor arrays. *Journal of immunological methods,* 292**,** 195-205.
3. Alya Dabbagh, R. L. L., Claudia Steulet; Laure Dumolard, Mick N. Mulders, Katrina Kretsinger, James P. Alexander, Paul A. Rota, James L. Goodson 2018. Progress Toward Regional Measles Elimination — Worldwide, 2000–2017. *Morbidity and Mortality Weekly Report (MMWR),* 67**,** 1323–1329.
4. Andrei, G., Snoeck, R., Goubau, P., Desmyter, J. & De Clercq, E. 1992. Comparative activity of various compounds against clinical strains of herpes simplex virus. *European Journal of Clinical Microbiology and Infectious Diseases,* 11**,** 143-151.
5. Andrei, G., Snoeck, R., Reymen, D., Liesnard, C., Goubau, P., Desmyter, J. & De Clercq, E. 1995. Comparative activity of selected antiviral compounds against clinical isolates of varicella-zoster virus. *European Journal of Clinical Microbiology and Infectious Diseases,* 14**,** 318-329.
6. Axe, E. L., Walker, S. A., Manifava, M., Chandra, P., Roderick, H. L., Habermann, A., Griffiths, G. & Ktistakis, N. T. 2008. Autophagosome formation from membrane compartments enriched in phosphatidylinositol

3-phosphate and dynamically connected to the endoplasmic reticulum. *The Journal of cell biology,* 182**,** 685-701.

7. Baravalle, G., Schober, D., Huber, M., Bayer, N., Murphy, R. F. & Fuchs, R. 2005. Transferrin recycling and dextran transport to lysosomes is differentially affected by bafilomycin, nocodazole, and low temperature. *Cell Tissue Res,* 320**,** 99-113.
8. Bellini, W. J. & Helfand, R. F. 2003. The challenges and strategies for laboratory diagnosis of measles in an international setting. *J Infect Dis,* 187 Suppl 1**,** S283-90.
9. Berger, S. B., Romero, X., Ma, C., Wang, G., Faubion, W. A., Liao, G., Compeer, E., Keszei, M., Rameh, L. & Wang, N. 2010a. SLAM is a microbial sensor that regulates bacterial phagosome functions in macrophages. *Nature immunology,* 11**,** 920-927.
10. Berger, S. B., Romero, X., Ma, C. Y., Wang, G. X., Faubion, W. A., Liao, G. X., Compeer, E., Keszei, M., Rameh, L., Wang, N. H., Boes, M., Regueiro, J. R., Reinecker, H. C. & Terhorst, C. 2010b. SLAM is a microbial sensor that regulates bacterial phagosome functions in macrophages. *Nature Immunology,* 11**,** 920-U70.
11. Bhella, D., Ralph, A. & Yeo, R. P. 2004. Conformational flexibility in recombinant measles virus nucleocapsids visualised by cryo-negative stain electron microscopy and real-space helical reconstruction. *Journal of molecular biology,* 340**,** 319-331.
12. Brimacombe, C. L., Grove, J., Meredith, L. W., Hu, K., Syder, A. J., Flores, M. V., Timpe, J. M., Krieger, S. E., Baumert, T. F. &

Tellinghuisen, T. L. 2011. Neutralizing antibody-resistant hepatitis C virus cell-to-cell transmission. *Journal of virology,* 85**,** 596-605.

13. Calain, P. & Roux, L. 1993. The rule of six, a basic feature for efficient replication of Sendai virus defective interfering RNA. *Journal of virology,* 67**,** 4822-4830.
14. Carlsson, A. E. 2018. Membrane bending by actin polymerization. *Curr Opin Cell Biol,* 50**,** 1-7.
15. Casey, J. R., Grinstein, S. & Orlowski, J. 2010. Sensors and regulators of intracellular pH. *Nature reviews Molecular cell biology,* 11**,** 50.
16. Chan, F. K.-M., Moriwaki, K. & De Rosa, M. J. 2013a. Detection of necrosis by release of lactate dehydrogenase activity. *Immune Homeostasis.* Springer.
17. Chan, F. K., Moriwaki, K. & De Rosa, M. J. 2013b. Detection of necrosis by release of lactate dehydrogenase activity. *Methods Mol Biol,* 979**,** 65-70.
18. Chazotte, B. 2008. Labeling the Golgi Apparatus with BODIPY-FL-Ceramide (C5-DMB-ceramide) for Imaging. *CSH Protoc,* 2008**,** pdb.prot4931.
19. Crimeen-Irwin, B., Ellis, S., Christiansen, D., Ludford-Menting, M. J., Milland, J., Lanteri, M., Loveland, B. E., Gerlier, D. & Russell, S. M. 2003. Ligand binding determines whether CD46 is internalized by clathrin-coated pits or macropinocytosis. *Journal of Biological Chemistry,* 278**,** 46927-46937.

20. Daelemans, D., Pauwels, R., De Clercq, E. & Pannecouque, C. 2011. A time-of–drug addition approach to target identification of antiviral compounds. *Nature protocols,* 6**,** 925.
21. De Clercq, E. 2004. Discovery and development of BVDU (brivudin) as a therapeutic for the treatment of herpes zoster. *Biochem Pharmacol,* 68**,** 2301-15.
22. De Clercq, E., Balzarini, J., Torrence, P., Mertes, M., Schmidt, C., Shugar, D., Barr, P., Jones, A., Verhelst, G. & Walker, R. 1981. Thymidylate synthetase as target enzyme for the inhibitory activity of 5-substituted 2'-deoxyuridines on mouse leukemia L1210 cell growth. *Molecular Pharmacology,* 19**,** 321-330.
23. De Clercq, E. & Li, G. 2016. Approved antiviral drugs over the past 50 years. *Clinical microbiology reviews,* 29**,** 695-747.
24. De Vries, R. D., Mesman, A. W., Geijtenbeek, T. B., Duprex, W. P. & De Swart, R. L. 2012. The pathogenesis of measles. *Curr Opin Virol,* 2**,** 248-55.
25. De Witte, L., Abt, M., Schneider-Schaulies, S., Van Kooyk, Y. & Geijtenbeek, T. B. 2006. Measles virus targets DC-SIGN to enhance dendritic cell infection. *Journal of virology,* 80**,** 3477-3486.
26. Delpeut, S., Sisson, G., Black, K. M. & Richardson, C. D. 2017. Measles Virus Enters Breast and Colon Cancer Cell Lines through a PVRL4-Mediated Macropinocytosis Pathway. *Journal of Virology,* 91**,** e02191-16.

27. Desouza, M., Gunning, P. W. & Stehn, J. R. 2012. The actin cytoskeleton as a sensor and mediator of apoptosis. *Bioarchitecture,* 2**,** 75-87.
28. Dietzel, E., Kolesnikova, L. & Maisner, A. 2013. Actin filaments disruption and stabilization affect measles virus maturation by different mechanisms. *Virology journal,* 10**,** 249.
29. Doherty, G. J. & Mcmahon, H. T. 2009. Mechanisms of endocytosis. *Annual review of biochemistry,* 78**,** 857-902.
30. Dong, X. & Levine, B. 2013. Autophagy and viruses: adversaries or allies? *J Innate Immun,* 5**,** 480-93.
31. Dorig, R. E., Marcil, A., Chopra, A. & Richardson, C. D. 1993. The Human Cd46 Molecule Is a Receptor for Measles-Virus (Edmonston Strain). *Cell,* 75**,** 295-305.
32. Dudley, M. Z., Salmon, D. A., Halsey, N. A., Orenstein, W. A., Limaye, R. J., O'leary, S. T. & Omer, S. B. 2018. Do Vaccines Cause Autism? *The Clinician's Vaccine Safety Resource Guide.* Springer.
33. Dutta, D. & Donaldson, J. G. 2012. Search for inhibitors of endocytosis: Intended specificity and unintended consequences. *Cellular logistics,* 2**,** 203-208.
34. Erlenhoefer, C., Wurzer, W. J., Löffler, S., Schneider-Schaulies, S., Ter Meulen, V. & Schneider-Schaulies, J. 2001. CD150 (SLAM) is a receptor for measles virus but is not involved in viral contact-mediated proliferation inhibition. *Journal of virology,* 75**,** 4499-4505.
35. Eskelinen, E. L. 2006. Roles of LAMP-1 and LAMP-2 in lysosome biogenesis and autophagy. *Mol Aspects Med,* 27**,** 495-502.

36. Falcone, S., Cocucci, E., Podini, P., Kirchhausen, T., Clementi, E. & Meldolesi, J. 2006. Macropinocytosis: regulated coordination of endocytic and exocytic membrane traffic events. *J Cell Sci,* 119**,** 4758-4769.
37. Farleigh, L. 2014. Cardiff University PhD Thesis - Development of a new class of antivirals active against pox and measles viruses.
38. Farrugia, A. & Quinti, I. 2018. Herd immunity and primary immune deficiencies. *Vaccine*.
39. Fischer, P. R. 2018. Measles From Coast to Coast: Risks, Costs, and Potential Interventions. *Infectious Disease Alert,* 37.
40. Frecha, C., Levy, C., Costa, C., Negre, D., Amirache, F., Buckland, R., Russell, S. J., Cosset, F. L. & Verhoeyen, E. 2011. Measles virus glycoprotein-pseudotyped lentiviral vector-mediated gene transfer into quiescent lymphocytes requires binding to both SLAM and CD46 entry receptors. *J Virol,* 85**,** 5975-85.
41. Fulton, B. O., Sachs, D., Beaty, S. M., Won, S. T., Lee, B., Palese, P. & Heaton, N. S. 2015. Mutational analysis of measles virus suggests constraints on antigenic variation of the glycoproteins. *Cell reports,* 11**,** 1331-1338.
42. Gans, H., Maldonado, Y. A. & Kaplan, S. L. 2018. Measles: Clinical manifestations, diagnosis, treatment, and prevention. *Uptodate. Consultation: April,* 12.
43. Goncalves-Carneiro, D., Mckeating, J. A. & Bailey, D. 2017. The Measles Virus Receptor SLAMF1 Can Mediate Particle Endocytosis. *Journal of Virology,* 91.

44. Gregoire, I. P., Richetta, C., Meyniel-Schicklin, L., Borel, S., Pradezynski, F., Diaz, O., Deloire, A., Azocar, O., Baguet, J., Le Breton, M., Mangeot, P. E., Navratil, V., Joubert, P. E., Flacher, M., Vidalain, P. O., Andre, P., Lotteau, V., Biard-Piechaczyk, M., Rabourdin-Combe, C. & Faure, M. 2011. IRGM is a common target of RNA viruses that subvert the autophagy network. *PLoS Pathog,* 7**,** e1002422.
45. Griffin, D. E. 2007. Measles virus . In D.M. Knipe and P.M. Howley. *Fields Virology. Philadelphia, PA: Lippincott Williams and Wilkins.***,** 1551–1586.
46. Griffin, D. E. 2010. Measles virus-induced suppression of immune responses. *Immunol Rev,* 236**,** 176-89.
47. Hagn, M., Sontheimer, K., Dahlke, K., Brueggemann, S., Kaltenmeier, C., Beyer, T., Hofmann, S., Lunov, O., Barth, T. F. & Fabricius, D. 2012. Human B cells differentiate into granzyme B-secreting cytotoxic B lymphocytes upon incomplete T-cell help. *Immunology and cell biology,* 90**,** 457-467.
48. Harrison, M. S., Sakaguchi, T. & Schmitt, A. P. 2010. Paramyxovirus assembly and budding: building particles that transmit infections. *The international journal of biochemistry & cell biology,* 42**,** 1416-1429.
49. Hashimoto, K., Ono, N., Tatsuo, H., Minagawa, H., Takeda, M., Takeuchi, K. & Yanagi, Y. 2002. SLAM (CD150)-independent measles virus entry as revealed by recombinant virus expressing green fluorescent protein. *Journal of virology,* 76**,** 6743-6749.

50. He, L., Sayers, E., Watson, P. & Jones, A. 2018. Contrasting roles for actin in the cellular uptake of cell penetrating peptide conjugates. *Scientific reports,* 8.
51. Hertel, L. 2011. Herpesviruses and intermediate filaments: close encounters with the third type. *Viruses,* 3**,** 1015-1040.
52. Heuser, J. 1989. Changes in lysosome shape and distribution correlated with changes in cytoplasmic pH. *J Cell Biol,* 108**,** 855-64.
53. Hoeller, D., Volarevic, S. & Dikic, I. 2005. Compartmentalization of growth factor receptor signalling. *Current opinion in cell biology,* 17**,** 107-111.
54. Hopkins Tanne, J. 2019. Measles: two US outbreaks are blamed on low vaccination rates. *BMJ,* 364**,** l312.
55. Hu, W., Gray, N. W. & Brimijoin, S. 2009. Amyloid-beta alters trafficking of internalized acetylcholinesterase and dextran. *International journal of physiology, pathophysiology and pharmacology,* 1**,** 15.
56. Huang, J., Canadien, V., Lam, G. Y., Steinberg, B. E., Dinauer, M. C., Magalhaes, M. A., Glogauer, M., Grinstein, S. & Brumell, J. H. 2009. Activation of antibacterial autophagy by NADPH oxidases. *Proceedings of the National Academy of Sciences,* 106**,** 6226-6231.
57. Humphries Iv, W. H., Szymanski, C. J. & Payne, C. K. 2011. Endo-lysosomal vesicles positive for Rab7 and LAMP1 are terminal vesicles for the transport of dextran. *PloS one,* 6**,** e26626.
58. Hviid, A., Hansen, J. V., Frisch, M. & Melbye, M. 2019. Measles, mumps, rubella vaccination and autism: A nationwide cohort study. *Annals of Internal Medicine,* 170**,** 513-520.

59. Jones, A. T. 2007. Macropinocytosis: searching for an endocytic identity and role in the uptake of cell penetrating peptides. *Journal of cellular and molecular medicine,* 11**,** 670-684.
60. Jordheim, L. P., Durantel, D., Zoulim, F. & Dumontet, C. 2013. Advances in the development of nucleoside and nucleotide analogues for cancer and viral diseases. *Nat Rev Drug Discov,* 12**,** 447-64.
61. Kaksonen, M. & Roux, A. 2018. Mechanisms of clathrin-mediated endocytosis. *Nat Rev Mol Cell Biol,* 19**,** 313-326.
62. Kendig, D. M. & Tarloff, J. B. 2007. Inactivation of lactate dehydrogenase by several chemicals: implications for in vitro toxicology studies. *Toxicology in vitro : an international journal published in association with BIBRA,* 21**,** 125-132.
63. Kerr, M. C. & Teasdale, R. D. 2009. Defining macropinocytosis. *Traffic,* 10**,** 364-371.
64. Kim, J., Kundu, M., Viollet, B. & Guan, K.-L. 2011. AMPK and mTOR regulate autophagy through direct phosphorylation of Ulk1. *Nature cell biology,* 13**,** 132-141.
65. Klionsky, D. J. 2007. Autophagy: from phenomenology to molecular understanding in less than a decade. *Nature reviews Molecular cell biology,* 8**,** 931-937.
66. Klionsky, D. J. 2012. Look people,“Atg” is an abbreviation for “autophagy-related.” That’s it. *Autophagy,* 8**,** 1281-1282.
67. Krumm, S. A., Yan, D., Hovingh, E. S., Evers, T. J., Enkirch, T., Reddy, G. P., Sun, A., Saindane, M. T., Arrendale, R. F., Painter, G., Liotta, D. C., Natchus, M. G., Von Messling, V. & Plemper, R. K. 2014. An orally

available, small-molecule polymerase inhibitor shows efficacy against a lethal morbillivirus infection in a large animal model. *Sci Transl Med,* 6**,** 232ra52.

68. Kudchodkar, S. B. & Levine, B. 2009. Viruses and autophagy. *Rev Med Virol,* 19**,** 359-78.
69. Kumari, S., Swetha, M. & Mayor, S. 2010. Endocytosis unplugged: multiple ways to enter the cell. *Cell research,* 20**,** 256-275.
70. Laemmli, U. K. 1970. Cleavage of structural proteins during the assembly of the head of bacteriophage T4. *Nature,* 227**,** 680-5.
71. Laksono, B., De Vries, R., Mcquaid, S., Duprex, W. & De Swart, R. 2016. Measles virus host invasion and pathogenesis. *Viruses,* 8**,** 210.
72. Lamb, R. P., Gd. 2006. Paramyxoviridae: the viruses and their replication. *In: Knipe, DM.; Howley,PM., editors. Fields Virology. Philadelphia: Lippincott, Williams and Wilkins***,** 1449-96.
73. Le Roy, C. & Wrana, J. L. 2005. Clathrin-and non-clathrin-mediated endocytic regulation of cell signalling. *Nature reviews Molecular cell biology,* 6**,** 112.
74. Lemon, K., De Vries, R. D., Mesman, A. W., Mcquaid, S., Van Amerongen, G., Yüksel, S., Ludlow, M., Rennick, L. J., Kuiken, T. & Rima, B. K. 2011. Early target cells of measles virus after aerosol infection of non-human primates. *PLoS pathogens,* 7**,** e1001263.
75. Li, G., Zhang, J., Sun, Y., Wang, H. & Wang, Y. 2009. The evolutionarily dynamic IFN-inducible GTPase proteins play conserved immune functions in vertebrates and cephalochordates. *Molecular biology and evolution,* 26**,** 1619-1630.

76. Lin, L.-T. & Richardson, C. 2016. The host cell receptors for measles virus and their interaction with the viral hemagglutinin (H) protein. *Viruses,* 8**,** 250.
77. Loos, B., Du Toit, A. & Hofmeyr, J. H. 2014. Defining and measuring autophagosome flux-concept and reality. *Autophagy,* 10**,** 2087-96.
78. Ludlow, M., Rennick, L. J., Sarlang, S., Skibinski, G., Mcquaid, S., Moore, T., De Swart, R. L. & Duprex, W. P. 2010. Wild-type measles virus infection of primary epithelial cells occurs via the basolateral surface without syncytium formation or release of infectious virus. *Journal of General Virology,* 91**,** 971-979.
79. Luo, M. 2012. Influenza virus entry. *Adv Exp Med Biol,* 726**,** 201-21.
80. Macaya-Ruiz, A., Raspall-Chaure, M., Tallada-Serra, M., Pasqual-López, I. & Roig-Quilis, M. 2006. Subacute sclerosing panencephalitis: combined treatment with interferon alpha and intraventricular ribavirin. *Revista de neurologia,* 42**,** 277-281.
81. Manisha Patel, M. a. D. L., Msph1; Susan B. Redd1; Nakia S. Clemmons, Mph1; Rebecca J. Mcnall, Phd1; Amanda C. Cohn, Md2; Paul A. Gastañaduy, Md1 2019. Increase in Measles Cases — United States, January 1–April 26, 2019. *Morbidity and Mortality Weekly Report (MMWR),* 68**,** 402–404.
82. Marsh, M. & Mcmahon, H. 1999. The structural era of endocytosis. *Science,* 285**,** 215-220.
83. Masereel, B., Pochet, L. & Laeckmann, D. 2003. An overview of inhibitors of Na+/H+ exchanger. *European journal of medicinal chemistry,* 38**,** 547-554.

84. Mathieu, C., Huey, D., Jurgens, E., Welsch, J. C., Devito, I., Talekar, A., Horvat, B., Niewiesk, S., Moscona, A. & Porotto, M. 2015. Prevention of measles virus infection by intranasal delivery of fusion inhibitor peptides. *J Virol,* 89**,** 1143-55.
85. Mayle, K. M., Le, A. M. & Kamei, D. T. 2012. The intracellular trafficking pathway of transferrin. *Biochimica et Biophysica Acta (BBA)-General Subjects,* 1820**,** 264-281.
86. Mccune, J. S. & Reynolds, K. S. 2015. Developing and Using Therapeutics for Emerging Infections. *Clinical Pharmacology & Therapeutics,* 98**,** 346-351.
87. Mcguigan, C., Brancale, A., Barucki, H., Srinivasan, S., Jones, G., Pathirana, R., Carangio, A., Blewett, S., Luoni, G. & Bidet, O. 2001. Furano pyrimidines as novel potent and selective anti-VZV agents. *Antiviral Chemistry and Chemotherapy,* 12**,** 77-89.
88. Mcguigan, C., Hinsinger, K., Farleigh, L., Pathirana, R. N. & Bugert, J. J. 2013. Novel antiviral activity of l-dideoxy bicyclic nucleoside analogues versus vaccinia and measles viruses in vitro. *J Med Chem,* 56**,** 1311-22.
89. Mcguigan, C., Pathirana, R. N., Snoeck, R., Andrei, G., De Clercq, E. & Balzarini, J. 2004. Discovery of a new family of inhibitors of human cytomegalovirus (HCMV) based upon lipophilic alkyl furano pyrimidine dideoxy nucleosides: action via a novel non-nucleosidic mechanism. *Journal of medicinal chemistry,* 47**,** 1847-1851.
90. Mcguigan, C., Yarnold, C. J., Jones, G., Velázquez, S., Barucki, H., Brancale, A., Andrei, G., Snoeck, R., De Clercq, E. & Balzarini, J. 1999. Potent and selective inhibition of varicella-zoster virus (VZV) by

nucleoside analogues with an unusual bicyclic base. *Journal of medicinal chemistry,* 42**,** 4479-4484.

91. Meiffren, G., Joubert, P.-E., Grégoire, I. P., Codogno, P., Rabourdin-Combe, C. & Faure, M. 2010. Pathogen recognition by the cell surface receptor CD46 induces autophagy. *Autophagy,* 6**,** 299-300.
92. Mensah, K., Heraud, J., Takahashi, S., Winter, A., Metcalf, C. & Wesolowski, A. 2019. Seasonal gaps in measles vaccination coverage in Madagascar. *Vaccine*.
93. Mercer, J. & Helenius, A. 2009. Virus entry by macropinocytosis. *Nature cell biology,* 11**,** 510.
94. Mills, I. G., Jones, A. T. & Clague, M. J. 1999. Regulation of endosome fusion. *Molecular membrane biology,* 16**,** 73-79.
95. Mizushima, N., Yoshimori, T. & Levine, B. 2010. Methods in mammalian autophagy research. *Cell,* 140**,** 313-26.
96. Mooren, O. L., Galletta, B. J. & Cooper, J. A. 2012. Roles for actin assembly in endocytosis. *Annu Rev Biochem,* 81**,** 661-86.
97. Moss, W. J. & Griffin, D. E. 2012. Measles. *The Lancet,* 379**,** 153-164.
98. Mühlebach, M. D., Mateo, M., Sinn, P. L., Prüfer, S., Uhlig, K. M., Leonard, V. H., Navaratnarajah, C. K., Frenzke, M., Wong, X. X. & Sawatsky, B. 2011. Adherens junction protein nectin-4 is the epithelial receptor for measles virus. *Nature,* 480**,** 530.
99. Navaratnarajah, C. K., Oezguen, N., Rupp, L., Kay, L., Leonard, V. H. J., Braun, W. & Cattaneo, R. 2011. The heads of the measles virus attachment protein move to transmit the fusion-triggering signal. *Nature structural & molecular biology,* 18**,** 128-134.

100. Ni, H.-M., Bockus, A., Wozniak, A. L., Jones, K., Weinman, S., Yin, X.-M. & Ding, W.-X. 2011. Dissecting the dynamic turnover of GFP-LC3 in the autolysosome. *Autophagy,* 7**,** 188-204.

101. Noyce, R. S. & Richardson, C. D. 2012a. Nectin 4 is the epithelial cell receptor for measles virus. *Trends in microbiology,* 20**,** 429-439.

102. Noyce, R. S. & Richardson, C. D. 2012b. Nectin 4 is the epithelial cell receptor for measles virus. *Trends Microbiol,* 20**,** 429-39.

103. Orenstein, W. A. & Gay, N. J. 2004. The theory of measles elimination: implications for the design of elimination strategies. *The Journal of infectious diseases,* 189**,** S27-S35.

104. Parzych, K. R. & Klionsky, D. J. 2014. An overview of autophagy: morphology, mechanism, and regulation. *Antioxid Redox Signal,* 20**,** 460-73.

105. Pennington, M. R. & Van De Walle, G. R. 2017. Electric cell-substrate impedance sensing to monitor viral growth and study cellular responses to infection with alphaherpesviruses in real time. *mSphere,* 2**,** e00039-17.

106. Petkova, D. S., Viret, C. & Faure, M. 2013. IRGM in autophagy and viral infections. *Frontiers in immunology,* 3**,** 426.

107. Pfeffer, S. R. 2017. Rab GTPases: master regulators that establish the secretory and endocytic pathways. *Molecular Biology of the Cell,* 28**,** 712-715.

108. Plemper, R. K., Brindley, M. A. & Iorio, R. M. 2011a. Structural and mechanistic studies of measles virus illuminate paramyxovirus entry. *PLoS pathogens,* 7**,** e1002058.

109. Plemper, R. K., Brindley, M. A. & Iorio, R. M. 2011b. Structural and mechanistic studies of measles virus illuminate paramyxovirus entry. *PLoS Pathog,* 7**,** e1002058.

110. Plemper, R. K. & Snyder, J. P. 2009. Measles control–Can measles virus inhibitors make a difference? *Current opinion in investigational drugs (London, England: 2000),* 10**,** 811-820.

111. Prusoff, W. H. 1959. Synthesis and biological activities of iododeoxyuridine, an analog of thymidine. *Biochimica et biophysica acta,* 32**,** 295-296.

112. Racaniello, V. 2011. Virology. An exit strategy for measles virus. *Science,* 334**,** 1650-1.

113. Ramshesh, V. K. & Lemasters, J. J. 2012. Imaging of mitochondrial pH using SNARF-1. *Methods Mol Biol,* 810**,** 243-8.

114. Ravikumar, B., Sarkar, S., Davies, J. E., Futter, M., Garcia-Arencibia, M., Green-Thompson, Z. W., Jimenez-Sanchez, M., Korolchuk, V. I., Lichtenberg, M. & Luo, S. 2010. Regulation of mammalian autophagy in physiology and pathophysiology. *Physiological reviews,* 90**,** 1383-1435.

115. Reddy, A., Caler, E. V. & Andrews, N. W. 2001. Plasma membrane repair is mediated by Ca2+-regulated exocytosis of lysosomes. *Cell,* 106**,** 157-169.

116. Reed, L. J. & Muench, H. 1938. A simple method of estimating fifty per cent endpoints. *American journal of epidemiology,* 27**,** 493-497.

117. Richetta, C. & Faure, M. 2013. Autophagy in antiviral innate immunity. *Cell Microbiol,* 15**,** 368-76.

118. Richetta, C., Gregoire, I. P., Verlhac, P., Azocar, O., Baguet, J., Flacher, M., Tangy, F., Rabourdin-Combe, C. & Faure, M. 2013. Sustained autophagy contributes to measles virus infectivity. *PLoS Pathog,* 9**,** e1003599.

119. Riley-Vargas, R. C., Gill, D. B., Kemper, C., Liszewski, M. K. & Atkinson, J. P. 2004. CD46: expanding beyond complement regulation. *Trends in immunology,* 25**,** 496-503.

120. Rima, B. & Duprex, W. 2009. The measles virus replication cycle. *Measles.* Springer.

121. Rima, B. K. & Duprex, W. P. 2006. Morbilliviruses and human disease. *J Pathol,* 208**,** 199-214.

122. Rima, B. K. & Duprex, W. P. 2011a. Measles Virus.

123. Rima, B. K. & Duprex, W. P. 2011b. New concepts in measles virus replication: getting in and out in vivo and modulating the host cell environment. *Virus Res,* 162**,** 47-62.

124. Rothberg, K. G., Heuser, J. E., Donzell, W. C., Ying, Y.-S., Glenney, J. R. & Anderson, R. G. 1992. Caveolin, a protein component of caveolae membrane coats. *Cell,* 68**,** 673-682.

125. Rozières, A., Viret, C. & Faure, M. 2017. Autophagy in Measles Virus Infection. *Viruses,* 9**,** 359.

126. Ruffin, V. A., Salameh, A. I., Boron, W. F. & Parker, M. D. 2014. Intracellular pH regulation by acid-base transporters in mammalian neurons. *Frontiers in physiology,* 5**,** 43.

127. S.J Flint, V. R. R., Glen F. Rall, Anna-Marie Skalka, Lynn W. Enquist 2008. *Principles of virology, Attachment and Entry*.

128. Sanjuán, R., Nebot, M. R., Chirico, N., Mansky, L. M. & Belshaw, R. 2010. Viral mutation rates. *Journal of virology,* 84**,** 9733-9748.

129. Santiago, C., Celma, M. L., Stehle, T. & Casasnovas, J. M. 2010. Structure of the measles virus hemagglutinin bound to the CD46 receptor. *Nature structural & molecular biology,* 17**,** 124.

130. Schwegmann, A. & Brombacher, F. 2008. Host-directed drug targeting of factors hijacked by pathogens. *Sci. Signal.,* 1**,** re8-re8.

131. Shaffer, J. A., Bellini, W. J. & Rota, P. A. 2003. The C protein of measles virus inhibits the type I interferon response. *Virology,* 315**,** 389-397.

132. Sidorenko, S. P. & Clark, E. A. 2003. The dual-function CD150 receptor subfamily: the viral attraction. *Nature immunology,* 4**,** 19-24.

133. Sintes, J. & Engel, P. 2011. SLAM (CD150) is a multitasking immunoreceptor: from cosignalling to bacterial recognition. *Immunology and cell biology,* 89**,** 161.

134. Smythe, E. & Ayscough, K. R. 2006. Actin regulation in endocytosis. *J Cell Sci,* 119**,** 4589-4598.

135. Sripada, S. & Dayaraj, C. 2010. Viral interactions with intermediate filaments: Paths less explored. *Cell Health and Cytoskeleton,* 2**,** 1-7.

136. Stenmark, H., Aasland, R., Toh, B.-H. & D'arrigo, A. 1996. Endosomal localization of the autoantigen EEA1 is mediated by a zinc-binding FYVE finger. *Journal of Biological Chemistry,* 271**,** 24048-24054.

137. Sundaram, M. E., Guterman, L. B. & Omer, S. B. 2019. The True Cost of Measles Outbreaks During the Postelimination Era. *Jama*.

138. Tam, C., Idone, V., Devlin, C., Fernandes, M. C., Flannery, A., He, X., Schuchman, E., Tabas, I. & Andrews, N. W. 2010. Exocytosis of acid sphingomyelinase by wounded cells promotes endocytosis and plasma membrane repair. *The Journal of cell biology,* 189**,** 1027-1038.

139. Tanaka, K., Minagawa, H., Xie, M.-F. & Yanagi, Y. 2002. The measles virus hemagglutinin downregulates the cellular receptor SLAM (CD150). *Archives of virology,* 147**,** 195-203.

140. Tatsuo, H., Ono, N., Tanaka, K. & Yanagi, Y. 2000. SLAM (CDw150) is a cellular receptor for measles virus. *Nature,* 406**,** 893.

141. Taylor, B., Miller, E., Farrington, C., Petropoulos, M.-C., Favot-Mayaud, I., Li, J. & Waight, P. A. 1999. Autism and measles, mumps, and rubella vaccine: no epidemiological evidence for a causal association. *The Lancet,* 353**,** 2026-2029.

142. Vale-Costa, S. & Amorim, M. 2016. Recycling endosomes and viral infection. *Viruses,* 8**,** 64.

143. Van Der Vlist, M., De Witte, L., De Vries, R. D., Litjens, M., De Jong, M. A., Fluitsma, D., De Swart, R. L. & Geijtenbeek, T. B. 2011. Human Langerhans cells capture measles virus through Langerin and present viral antigens to CD4+ T cells but are incapable of cross-presentation. *European journal of immunology,* 41**,** 2619-2631.

144. Varshosaz, J. 2012. Dextran conjugates in drug delivery. *Expert Opinion on Drug Delivery,* 9**,** 509-523.

145. Veillette, A., Dong, Z. & Latour, S. 2007. Consequence of the SLAM-SAP signaling pathway in innate-like and conventional lymphocytes. *Immunity,* 27**,** 698-710.

146. Vercauteren, D., Deschout, H., Remaut, K., Engbersen, J. F. J., Jones, A. T., Demeester, J., De Smedt, S. C. & Braeckmans, K. 2011. Dynamic Colocalization Microscopy To Characterize Intracellular Trafficking of Nanomedicines. *ACS Nano,* 5**,** 7874-7884.

147. Wakefield, A. J., Murch, S. H., Anthony, A., Linnell, J., Casson, D. M., Malik, M., Berelowitz, M., Dhillon, A. P., Thomson, M. A. & Harvey, P. 1998. RETRACTED: Ileal-lymphoid-nodular hyperplasia, non-specific colitis, and pervasive developmental disorder in children. Elsevier.

148. Wang, X., Grunz-Borgmann, E. A. & Parrish, A. R. 2014. Loss of α (E)-catenin potentiates cisplatin-induced nephrotoxicity via increasing apoptosis in renal tubular epithelial cells. *Toxicological Sciences,* 141**,** 254-262.

149. Watterson, D., Robinson, J., Chappell, K. J., Butler, M. S., Edwards, D. J., Fry, S. R., Bermingham, I. M., Cooper, M. A. & Young, P. R. 2016. A generic screening platform for inhibitors of virus induced cell fusion using cellular electrical impedance. *Scientific reports,* 6**,** 22791.

150. Weiss, K., Salzig, D., Mühlebach, M., Cichutek, K., Pörtner, R. & Czermak, P. 2012. Key parameters of measles virus production for oncolytic virotherapy. *American Journal of Biochemistry and Biotechnology,* 8**,** 81-98.

151. Welstead, G. G., Hsu, E. C., Iorio, C., Bolotin, S. & Richardson, C. D. 2004. Mechanism of CD150 (SLAM) down regulation from the host cell surface by measles virus hemagglutinin protein.

152. Whelan, S., Barr, J. & Wertz, G. 2004. Transcription and replication of nonsegmented negative-strand RNA viruses. *Biology of Negative Strand RNA Viruses: The Power of Reverse Genetics.* Springer.

153. Xie, Z. & Klionsky, D. J. 2007. Autophagosome formation: core machinery and adaptations. *Nature cell biology,* 9**,** 1102-1109.

154. Xing, J. Z., Zhu, L., Gabos, S. & Xie, L. 2006. Microelectronic cell sensor assay for detection of cytotoxicity and prediction of acute toxicity. *Toxicology in vitro,* 20**,** 995-1004.

155. Yan, D., Krumm, S. A., Sun, A., Steinhauer, D. A., Luo, M., Moore, M. L. & Plemper, R. K. 2013. Dual myxovirus screen identifies a small-molecule agonist of the host antiviral response. *Journal of virology***,** JVI. 01425-13.

156. Yanagi, Y., Takeda, M. & Ohno, S. 2006. Measles virus: cellular receptors, tropism and pathogenesis. *J Gen Virol,* 87**,** 2767-79.

157. Yang, Y. P., Hu, L. F., Zheng, H. F., Mao, C. J., Hu, W. D., Xiong, K. P., Wang, F. & Liu, C. F. 2013. Application and interpretation of current autophagy inhibitors and activators. *Acta Pharmacol Sin,* 34**,** 625-35.

158. Yoshii, S. R. & Mizushima, N. 2017. Monitoring and measuring autophagy. *International journal of molecular sciences,* 18**,** 1865.

159. Zhou, Y., Su, J. M., Samuel, C. E. & Ma, D. 2019. Measles Virus Forms Inclusion Bodies with Properties of Liquid Organelles. *Journal of virology***,** JVI. 00948-19.

Appendix A: Macro for quantification of internalized SLAM positive vesicles

```
macro "Background subtraction [F5]" {
 print(" RFP-GFP-LC3 Colocalization macro, Dan Shiwarski and Ruben Dagda 10/19/10");
wait(100);
open();
run("Split Channels");
run("Window/Level...");
run("Enhance Contrast", "saturated=0.35");
setMinAndMax(25, 96);
saveAs("Tiff", "D:\\Blue.tif");
close();
run("Window/Level...");
run("Enhance Contrast", "saturated=0.35");
setMinAndMax(25, 96);
saveAs("Tiff", "D:\\Green.tif");
close();
run("Enhance Contrast", "saturated=0.35");
setMinAndMax(25, 96);
saveAs("Tiff", "D:\\Red.tif");
close();
open("D:\\Green.tif");
run("Subtract Background...", "rolling=14");
open("D:\\Red.tif")
run("Subtract Background...", "rolling=14");
open("D:\\Green.tif");
//run("Threshold...");
setAutoThreshold("RenyiEntropy");
setAutoThreshold("RenyiEntropy dark");
run("Convert to Mask");
open("D:\\Red.tif");
setAutoThreshold("RenyiEntropy");
//run("Threshold...");
setAutoThreshold("RenyiEntropy dark");
run("Convert to Mask");
    run("Merge Channels...", "red=Red.tif green=Green.tif blue=*None* gray=*None* create");
 run("Stack to RGB");
 run("Split Channels");
  selectWindow("Composite (RGB) (blue)");
  close();
  run("Coloc 2"); "channel_1=[Composite (RGB) (red)] channel_2=[Composite (RGB)(green)]
  ratio=30 threshold_channel_1=15 threshold_channel_2=15 display=255");
  selectWindow("Composite");
 run("Make Binary");
 run("Analyze Particles...", "size=3-1000 circularity=0.00-1.00 show=Outlines display summarize");
 selectWindow("Composite (RGB) (green)");
  run("Make Binary");
  run("Analyze Particles...", "size=3-1000 pixel circularity=0.00-1.00  show=Outlines display summarize");
  selectWindow("Composite (RGB) (red)");
  run("Make Binary");
  run("Analyze Particles...", "size=3-1000 pixel circularity=0.00-1.00 show=Outlines display summarize");
  s = getString("Do you want to analyze and count nuclei? [y/n+comment]","n");
   if (fromCharCode(charCodeAt(s,0)) == "n") exit;   // end of program, updated on May 15-
    2010
 else { open();
 selectWindow("Blue.tif");
//run("Threshold...");
macro "Count Nuclei [F10]"{
run("Make Binary");
run("Analyze Particles...", "size=15-1000000 pixel circularity=0.00-1.00 show=Outlines display summarize");
}
 macro "Close All Windows [F4]"
{
  while (nImages>0)
 { selectImage(nImages); close();
 }
```

Appendix B: Macro for quantification of red and green fluorescence intensities

```
imageTitle = getTitle();

if(isOpen("ROI Manager"))
{
                selectWindow("ROI Manager");
                run("Close");
}

setBatchMode(true);
//Setting up the nucleus mask
run("Split Channels");
selectWindow("C1-" + imageTitle);
setAutoThreshold("Li dark");
setOption("BlackBackground", false);
run("Make Binary");
run("Fill Holes");
run("Erode");run("Erode");run("Erode");
run("Dilate");run("Dilate");run("Dilate");
roiManager("Deselect");
run("Analyze Particles...", "exclude clear add");


//measure green and red intensity in the nucleus
for(j=0; j<6; j++)
{
                counts=roiManager("count");
                for(i=0; i<counts; i++)
                {
                  roiManager("Select", i);
                  run("Enlarge...", "enlarge=[j]");
                  roiManager("Update");
                }

                for(i=0; i<counts; i++)
                {
                  selectWindow("C2-" + imageTitle);  //red
                  roiManager("Select", i);
                                getStatistics(redArea,redMean);

                                selectWindow("C3-" + imageTitle);  //green
                  roiManager("Select", i);
                  getStatistics(greenArea,greenMean);

                  setResult("Cell:", ((counts*j)+i), (i+1));
                  setResult("Enlarge:",((counts*j)+i), j);
                  setResult("Area(Green):",((counts*j)+i), greenArea);
                  setResult("Int(Green):",((counts*j)+i), greenMean);
                  setResult("Area(Red):",((counts*j)+i), redArea);
                  setResult("Int(Red):",((counts*j)+i), redMean);

                }

}

updateResults;
setBatchMode(false);
```

Appendix C: Products and suppliers

Biorad (Hemel Hempstead, UK):

- Precision plus protein dual colour standards (161-0374)
- Clarity, Western ECL substrate (170-5060)
- 12% Mini-PROTEAN® TGX™ Precast Protein Gels, 10-well, 30 µl (# 4561043)

DAKO (Ely, UK):

- Fluorescence mounting medium (S3023)

Fisher Scientific (Loughborough, UK):

- Coverslips No. 1 circle 16mm diameter (12313138)
- PVDF membrane (10344661)
- SuperSignal West Femto Chemiluminescent Substrate (34094)
- 40% acrylamide/Bis (10376643)
- Thermo Scientific™ Pierce™ LDH Cytotoxicity Assay Kit (88953)

Life Technologies (Paisley, UK):

- DMEM (61965)
- DMEM (11880)
- Earle's Balanced Salt Solution (24010043)
- FBS (16000-044)
- 0.05% Trypsin EDTA (25300062)
- Hoechst 33342 (H3570)
- Rhodamine Phalloidin (R415)
- Dextran, Alexa Fluor 647; 10,000 MW, Anionic, Fixable (11570266)
- Dextran, Alexa Fluor 488; 10,000 MW, Anionic, Fixable (11530266)
- CellMask™ Plasma Membrane Stain (C10046)
- Transferrin from Human Serum, Alexa Fluor™ 488 Conjugate (T13342)
- Alexa Fluor 647 Phalloidin (A22287)
- DAPI (D1306)

MatTek Corporation

- 35mm glass bottom dishes, 1.5 thickness, 10mm diameter (P35G-1.5-10-C)

Promega (Loughborough, UK)

- CellTitre Blue viability assay (G8080)

Roche Diagnostics (Burgess Hill, UK):

- Complete Protease Inhibitor Cocktail Tablets (11836153001)

Sigma Aldrich (Poole, UK):

- Triton X-100 ()
- BSA (A7906)
- Ponceau S solution (P7170)
- Tween 20 (P1379)
- Rapamycin (R8781)
- Wortmannin (W3144)
- Chloroquine diphosphate salt (C6628)
- Methyl Cellulose (M0387)
- Crystal Violet (C3886)
- LookOut Mycoplasma PCR Detection Kit (MP0035)
- JumpStart™ Taq DNA Polymerase (D9307)
- Ethidium Bromide (E1510)

Millipore:

- Amicon Ultra-0.5 Centrifugal Filter Unit (UFC505024)